U.S. Department of Labor

Mine Safety and Health Administration
1100 Wilson Boulevard
Arlington, Virginia 22209-3939

December 7, 2007

MEMORANDUM FOR: THE FILE

FROM: LINDA F. ZEILER
Acting Director of Technical Support

SUBJECT: U.S. Army Corp of Engineers Draft Report: "CFD Study and Structural Analysis of the Sago Mine Accident"

The original intent of the Computational Fluid Dynamics (CFD) study performed under contract for the Mine Safety and Health Administration's (MSHA) Technical Support Directorate (Technical Support) by the U.S. Army Corps of Engineers (USACE) was to use a sophisticated computer simulation as a way to mathematically model the methane explosion at the Sago Mine and potentially establish the seal overpressures. The report was not finalized for the following reasons:

- From the outset, Technical Support recognized that the contract for the CFD study may be pioneering and had initially hoped, as stated in the contract, that "...the study may serve as a basis for future agency decisions. MSHA will have a comprehensive scientific study that may serve as the platform for future mine regulation concerning the design, construction, testing, and maintenance of seals..." However, Technical Support did not fully realize at the onset the difficulty of accurately modeling the explosive atmosphere. The results of the computer simulations are highly dependent on knowing the concentration and distribution of methane in the sealed area. At the time when the scope of the study was planned, the lack of detailed information on these parameters was not appreciated.

- Although MSHA's Sago Mine investigation team gathered as much information as possible by conducting methane liberation studies and by contracting with Sandia Laboratories to evaluate the possible ignition sources, the detailed information needed to complete the CFD model and create an accurate simulation was simply not available.

- The study consisted of only three mathematical simulations of explosions in the sealed area. The first two analyses were conducted using 9.5% methane distributed throughout the whole sealed area. This is a worst-case condition, and is extremely unlikely to occur. Methane can be introduced into a sealed area from the surrounding strata at over 90% concentration. Therefore, the actual concentration of methane within any particular area varies, and can be further affected by other factors such as changes in elevation, differences in atmospheric density, and exchanges of air that would make it virtually impossible for a uniform percentage of methane to exist throughout a sealed area.

- The third and final run was made with 8% methane mixture up to elevation 1408 and 17% methane above this level. This was to be the most realistic analysis, but again, this distribution of methane was a simplification for the modeling and extremely unlikely to occur. More importantly, factual observations from the mine did not match the model results. The third run of the model predicted "the loads on the seals ranged from 51 psi at seal 8 to 225 psi at seal 1". The MSHA Sago investigation team conducted an extensive review of the damage in the underground portions of the mine. All of the seals were destroyed, but the extent of the debris from the seals indicated a higher pressure occurred near seals 5 through 10 than in the area from seals 1 through 5. Furthermore, the third run of the model indicated a pressure of at least 21 psi at the location of one of the victims, while an evaluation of the conditions indicated a pressure of approximately 5 psi. These comparisons again brought the practical applicability of results of the study into question.

- The USACE made every effort to complete the study as it was designed, and eventually submitted a draft report for review. Technical Support decided not to publish the study because the critical information necessary to develop an accurate simulation was not available, and therefore, any results could not be relied upon for decision-making. Much of the data provided to the USACE for the three simulations described in the draft report was speculative, involving:

    - Uncertainty of quantity of methane in sealed area.
    - Uncertainty of distribution of methane in sealed area.
    - Uncertainty of composition of the atmosphere other than methane in the sealed area.
    - Uncertainty of the level of energy of the ignition source.
    - Uncertainty of the conditions required for the explosion to transition to a detonation.

It should be noted that the USACE cited limitations in the draft report as well, for example:

"There are many unknowns associated with the Sago Mine explosion."

"The concentration and location of this methane in the sealed area could dramatically affect the blast loads on the seals."

"It is not possible to say with assurance at this time, that any particular configuration of methane concentration and location was present at the time of the explosion. Further analysis could establish the range of possible configurations and their effects on the seals."

"The conditions under which a combustible concentration of methane-air can transition to a detonation are not well understood. A series of experiments in a simulated or actual mine should be conducted in order to further understand these phenomena."

The bottom line is that it turned out that vital pieces of information that the USACE needed in order for the study to truly simulate the conditions that existed in Sago Mine when the explosion occurred could not be known and therefore could not be provided. MSHA would like to monitor the atmosphere and collect data in a recently sealed area of an underground coal mine in order to learn more about how methane diffuses in a sealed area; a better understanding of this type of information is needed for mathematical modeling to be more representative of actual conditions.

Therefore, with regard to the Sago investigation, Technical Support believes that the full-scale testing of seals at Lake Lynn, following the Sago accident, provided more relevant information, and for rulemaking purposes on the issue of seal overpressures, the NIOSH report "Explosion Pressure Design Criteria for New Seals in U.S. Coal Mines" provided MSHA the most up-to-date scientific reference material.

Geotechnical and Structures Laboratory

ERDC/GSL TR-06-X

Final Draft

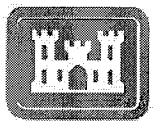

US Army Corps of Engineers®
Engineer Research and Development Center

CFD Study and Structural Analysis of the Sago Mine Accident

G. W. McMahon, J. Robert Britt, James L. O'Daniel,
L. Kim Davis, and Robert E. Walker

May, 2007

ERDC/GSL TR-06-X
June 2006

CFD Study and Structural Analysis of the Sago Mine Accident

Gordon W. McMahon, James L. O'Daniel, L. Kim Davis, and Robert E. Walker

Geotechnical and Structures Laboratory
U.S. Army Engineer Research and Development Center
3909 Halls Ferry Road
Vicksburg, MS 39180-6199

J. Robert Britt

SAIC

Final Draft report

Prepared for U.S. Department of Labor, Mine Safety and Health Administration, Pittsburgh Safety and Health Technology Center

Contents

Figures and Tables

Figures

Tables

Preface

The study reported herein was performed by personnel of the Structural Engineering Branch, Geosciences and Structures Division, Geotechnical and Structures Laboratory (GSL), U. S. Army Engineer Research and Development Station (ERDC) at the Waterways Experiment Station, Vicksburg, MS, during the period 28 August, 2006 and 4 April, 2007. The study was conducted for the Department of Labor, Mine Safety Health Administration, Pittsburgh Safety and Health Technology Center, under Interagency Agreement IA-AR600012. Mssers Terrence Taylor and Richard Allwes were the technical monitors for MSHA.

Dr. Will McMahon was the team leader for this study. Dr. McMahon, Mr. J. Robert Britt, Dr. Jim O'Daniel, Mr. Kim Davis, and Mr. Robert Walker authored this report. Mr. J. Robert Britt, SAIC, was responsible for the CDF Study, under contract to ERDC. Dr. James L. O'Daniel was the lead analyst for the structural calculations. Mr. R. E. Walker provided material models for both the CFD Study and the Structural Study in addition to the SDOF models for the structural calculations. Mr. Thomas Rendine and Mr. Dale Ranta, SAIC, developed the 3-D stereolithograph (STL) files for the Sago Mine including detailed elevation contours of the Second Left Mains. Dr. Michael Stephens and Mr. Kevin George of the ERDC HPC Scientific Visualization Center developed the 3-D STL model of Run 3, and processed the spatial data into animations and still frames used in this report. Professor C.William Kaufman, University of Michigan and consultant to SAIC, provided valuable insight into methane explosions in mines and tunnels. Ms. D.B. Rowland assisted in the preparation of this report.

The work reported herein was performed under the supervision of Mr. Steve Shore, Chief of the Structural Engineering Branch.

During the period of the preparation of this report, Dr. Robert L. Hall was the Chief, Geosciences and Structural Division, Dr. David W. Pittman was Director, GSL, Dr. James R. Houston was Director of ERDC, and COL Richard Jenkins was the ERDC Commander.

Unit Conversion Factors

Multiply	By	To Obtain
feet	0.3048	meters
grains	0.06480	grams
inches	2.54	centimeters
pounds	0.454	kilograms
pounds (force) per square inch	0.006895	megapascals

1 Executive Summary

Methane gas slowly seeps out of coal seams, so underground coal mines must be ventilated to maintain a safe working atmosphere. When a large section of a coal mine is abandoned, it is often sealed off to avoid the cost of ventilation. Methane gas is flammable and, if triggered by a spark, will burn when mixed in a critical level of concentration with air. If certain conditions are present, the burn rate can accelerate, and even possibly transition to a detonation. The mine seals are therefore intended to contain a possible explosion in the sealed area, as well as to prevent gas intrusion into the ventilated areas.

It became clear that mine seals could be subjected to blast loads well above those expected under current safety standards when the seals, constructed of light-weight concrete blocks and mortar, were completely blown away by the methane explosion accident in the Sago Mine in January 2006, resulting in a number of casualties to miners beyond the sealed area. The study reported here was funded by the Mine Safety and Health Administration of the U.S. Department of Labor to aid in establishing realistic standards for mine seal designs by (a) investigating the possible blast loads that were produced in the Sago accident, and (b) analyzing the structural response of the Sago seals and other items damaged by the blast.

A highly advanced, computational fluid dynamics (CFD) computer code was used to simulate the methane burn and explosion in the sealed area of the Sago Mine. The code was first validated by calculating blast levels that matched measurements made by the National Institute for Occupational Safety and Health (NIOSH) in methane explosion experiments at a test mine. In the code run modeling the Sago mine, the simulation propagated the burn and blast throughout the sealed area to the locations of the ten mine seals, and then into the working area of the mine after the seals failed. The three-dimensional calculation provided graphic depictions of the multiple reflections and collisions of blast waves as they traveled through the complex of entries and cross-cuts, sometimes producing a number of pressure fronts that arrived successively at a given point from different directions. Time histories of pressure, particle velocity and density, from which dynamic pressures are calculated, were also produced at many locations throughout the mine.

ERDC also performed both finite element (FE) and dynamic single-degree-of-freedom (SDOF) analyses of the response of the seals to different levels of blast

loads. Similar calculations were performed to reproduce observed damage to rock bolt plates and belt hangers in the Sago Mine and to determine the structural capacity of those components.

The good correlation between the CFD calculations and the NIOSH experiments showed that such codes can predict complex blast phenomena in underground systems. The simulation of the Sago accident indicated that the blast pressures exceeded the current criteria for mine seal designs, and confirmed the indications of successive blast wave impacts from multiple directions. The results of the FE models demonstrated the utility of this technique for evaluating the capability of mine seal designs to resist and survive blast loads, while the SDOF calculations showed that this simple approach can quickly provide reasonable predictions of the failure levels of mine seals and other structural items.

In summary, the study demonstrated the potential value of these computational techniques as aids in the development and evaluation of new seal designs to provide effective protection against accidental methane explosions in underground coal mines. The study results indicated the following conclusions:

- FE models of seals showed that shear strength was the dominant factor in the seal failures. Little to no arching action from bending was observed. The FE analysis of the LLEM Sago seals provided validation of the models.

- Foam concrete block seals like those in Sago mine have been tested to withstand blast loads of 20 psi. The analysis showed that at higher loadings, there is an abrupt shear failure around the seal perimeter. This is due both to the low strength of the block material and the lack of any shear reinforcing where the seals abut the mine walls.

- The results of the analysis show that the belt hangers attached directly to the roof respond primarily to the directional dynamic pressure environment, not the overpressure. They began to fail in bending when subjected to a dynamic pressure (i. e., the blast "flow", or drag pressure) of about 150 psi normal to the face of the hanger.

- Rock bolts with belt hangers attached to their ends also respond primarily to the dynamic pressure environment and can be permanently bent at much lower dynamic pressures. The length of the bolt extending below the roof surface is a factor in the response of the bolts. Considering all the bolts surveyed in the mine after the accident, the dynamic pressures required to bend them to their observed level ranged from 10psi to 120 psi.

- Spider plates and pie plates used with rock bolts to support the roof begin to deform under dynamic pressure when the peak overpressure at the plate location reaches about 30 psi. The damage sustained by these items is dependent on many variables, including the roughness of the tunnel ceiling in the general area, the orientation of the pan, whether there is a gap between the back of the pan and the rock surface, and the uncertainty of the blast loading conditions at the exact point of the plate location. The plates can be bent on multiple sides by blast waves arriving successively from different directions. This complex blast wave effect was observed at many plate locations in the CFD calculations.

- Runs 1 and 2 of the CFD study were designed to investigate a "worst case" situation, in which a methane concentration of 9.5% completely filled the sealed area. The results of these runs indicated that an initial methane burn would transition to a detonation at some intermediate distance between the ignition point and the seals. However, these conditions have not been validated against an actual full-scale methane mine explosion event.

- In order to define the maximum blast loadings on the seals, Run 1 assumed that the seals were non-responding. This run indicated that the confined volume pressure behind the seals would have reached the theoretical maximum value of 120 psi static pressure. The reflected shock pressures, however, which indicate the load that a non-responding seal would experience, were much higher.

- Run 2 contained a limited structural response model that allowed the Sago seals to fail, and then calculated the blast environment in the Second Left Parallel beyond the seal locations. The static pressures in this case were lower than in Run 1, due to the reduction of the blast confinement as the seals failed. Run 2 calculations showed that the blast pressure loads on the seals ranged from 156 psi at Seal 3 to 629 psi at Seal 8.

- Run 3 was designed to determine the explosion environment from an 8% concentration of methane dispersed in a volume less than the full volume behind the seals. The volume chosen was based on methane liberation studies and ventilation studies, following the accident. The results of this calculation indicated that the loads on the seals ranged from 51 psi at seal 8 to 225 psi at seal 1.

- There are many unknowns associated with the SAGO mine explosion. MSHA determined the likely amount of methane that was present behind the seals, including the amount that was consumed during the event. The concentration and location of this methane in the sealed area could dramatically affect the blast loads on the seals. The Run 3 calculations represent only one possible configuration of methane concentration and location (8% methane initiated near Spad 4010 and contained in slightly more than half of the volume in the sealed area). It is not possible to say with assurance, at this time, that any particular configuration of methane concentration and location was present at the time of the explosion. Further analysis could establish the range of possible configurations and their effects on the seals.

2 Introduction

Research Requirement

Methane is a naturally-occurring gas that slowly seeps out of exposed seams of coal. Although it is flammable, it is quickly diluted and dispersed in air under normal circumstances. In the confinement of underground coal mines, however, the gas can accumulate in significant concentrations if not flushed away by a ventilation system. In addition to being flammable, methane can also become explosive when mixed with air in concentrations between approximately 5 and 15 percent (Reference 1). Safety regulations mandated by the Mine Safety and Health Administration (MSHA) set forth specific requirements for ventilation and other precautions to protect personnel in the U.S. mining industry from methane hazards, in accordance with Title 30, Part 75.335 of the U.S. Code of Federal Regulations (CFR).

Although coal seams are usually relatively shallow in thickness, they can extend horizontally over many square miles. Consequently, underground coal mines can be very extensive, with excavations running for miles in different directions to follow the seams. Maintaining ventilation over such large areas to the level required by safety regulations can become quite difficult and expensive, especially when portions of the mine have played out, and are no longer actively mined. It has therefore become a common practice to seal off these abandoned areas, for both safety and economic reasons. The sealing off of an abandoned area of a mine (called a "gob") can produce a new risk, however. Over a period of time, the seeping methane can build up within the sealed area to the level of concentration that can explode, if ignited by a flame or a spark.

Until recently, the seals used to close off the abandoned areas have often been simple walls constructed of light-weight concrete blocks, extending from floor to ceiling across the width of a tunnel. Since the main purpose of the seals was to prevent leakage of methane into the working area of the mine, the CFR and MSHA regulations only required such walls to resist an applied pressure of 20 psi. In January 2006, however, a methane gas explosion in a sealed area of the Sago Mine in West Virginia blew out seals built to this standard, resulting in a number of deaths of miners in a nearby active area of the mine. In view of the catastrophic failure of the seals in the Sago Mine incident, and considering data gathered from experiments involving deliberate explosions of methane in small underground test areas, the MSHA criterion for a seal wall resistance was recently increased to the 50 psi level (that is also now required by several other countries).

The National Institute for Occupational Safety and Health (NIOSH) has conducted full-scale tests of mine seals at their Lake Lynn Experimental Mine (LLEM) test facility near Pittsburgh, PA. Reference 2 describes tests that were designed to evaluate the explosion resistance of new seal designs for rapid deployment in mine emergencies. The LLEM has a complex of drifts and crosscuts that replicate those in actual coal mines, such as the Sago Mine. The seals were subjected to blast loads from the explosion of a critical methane/air mixture in a chamber at the end of a drift. The test seals were located in cross-cuts from about 5 to 70 meters away. The gas mixture was contained in the chamber by a diaphragm hung across the entrance.

Although the tests described in Reference 2 provided excellent data on the performance of full-scale seals in a realistic coal mine environment, the loadings applied to the seals were limited to the 20 psi (138 kpa) level used, at that time (2004), as the blast load criterion. The small volume of the methane/air mixture, and the distance of the gas chamber from the test seals, gave no indications of the loading levels that could be generated in an actual mine accident, where the gas may fill an entire sealed volume, all the way up to the face of the seals.

In order to establish realistic requirements for the resistance of mine seals to methane blast loads, it is essential to know what those loads might be in a reasonable "worst case" situation; i.e., when a large volume of the gob is filled with a critical methane/air mixture. It is also important to know whether certain features of the blast environment might enhance the blast load applied to the seals. Such features might include, for example, piles of mine debris, timber cribs used to provide additional support to the tunnel crown, irregularities in the tunnel profiles, and the presence of mined-out pits, sudden reductions in the tunnel height, and constrictions in the tunnel diameter. The surfaces of these features may produce reflections, constrictions, and expansions of the moving blast wave that could possibly result in significant increases in the loads applied to the seals. In addition, the multiple tunnels, pillars, bays, and cross-cuts in a mine could contribute to turbulence in the moving blast wave that might enhance the peak pressures or impulse levels.

To experimentally study these effects by reproducing them in a full-scale mine environment would be prohibitively expensive. However, the field of computational fluid dynamics (CFD) has advanced in recent years to the point that explosion events can be accurately modeled mathematically, even in complex environments such as an underground coal mine. The U.S. Army Engineer Research and Development Center (ERDC) has many years of experience in the investigation of explosion blast effects, both experimentally and by the use of

advance computer models. ERDC was therefore tasked by MSHA to establish credible levels of blast loads from methane explosions in coal mines by using state-or-the-art CFD programs to model the Sago Mine incident, and to correlate the calculated loads with damage effects observed in the Sago Mine. The results of the study are intended to provide a scientific reference in support of the Sago Mine Investigation Team's assessment of the Sago explosion and the subsequent failure of the seals.

Details of this tasking are provided in the Interagency Agreement between the Mine Safety and Health Administration and the U.S. Army Corps of Engineers, and the accompanying Statement of Work (Reference 3).

Objectives

The overall purpose of this study was to develop and demonstrate a computer-based method of predicting the blast environment in underground coal mines from methane gas explosions. The specific objectives were to use CFD models to:

- Establish the possible pressure-time histories in the Sago Mine that could have been produced by the January 2006 methane gas explosion that occurred in the sealed Second Left Mains
- Account for the effects on the blast propagation of specific features of the mine, such as non-uniformities in the tunnel and pillar geometries, debris piles, berms, cribs, stoppings, sudden changes in tunnel height or depth, etc.
- Account for failure of the seals and the effect on blast propagation into the nearby unsealed area of the mine
- Calculate the blast loads required to produce the damage effects observed in the mine, such as damage to blast seals, timber cribs, rock bolt plates (spider plates and pie pans), and belt hangers, as well as debris transport distances
- Compare the calculated blast levels to those required to produce the damage observed at different locations in the mine, and in the experiments conducted at the Lake Lynn Experimental Mine, as a means of validating the accuracy of the CFD models

3 Background and Approach

Description of the Explosion

In order to perform the CFD calculations, it was necessary to assume a location for initiation of the methane in the Second Left Mains, and the amount of methane that was involved in the explosion event. MSHA conducted a survey to address these issues by examining the mine for clues. The origin of the event was based on indications of the direction of the blast flow from bent belt hangers and rock bolt plates, scattering of debris, and other evidence. From signs of charring on the tunnel surfaces, it was possible to ascertain the distances in different directions from the origin that burning of the methane gas mixture apparently occurred.

The explosion occurred in the sealed area 22 days after sealing. Based on measurements of the rate of methane liberation in the mine, it was estimated that the sealed area contained about 347,000 cu. ft. of methane at the time of the event (Reference 4). It was estimated that approximately 205,000 cu. ft. of methane remained in the Second Left Mains after the event, leaving approximately 142,000 cu. ft. to have been involved in the explosion.

[Note: It should be mentioned here that, prior to the initiation of this study, there was some question as to whether the use of the term "explosion" in regard to the Sago Mine accident was entirely appropriate. In many instances, large volumes of methane have been known to simply burn, without detonating. Therefore one of the secondary objectives of the study was to utilize the CFD calculations to determine if, in fact, an initial burn could have transitioned into a detonation under the conditions existing at the Sago Mine. This issue will be addressed later in this report, but for convenience, use of the terms "explosion" and "detonation" will be continued here. The word "explosion" refers to a violent burn but may not necessarily transition to the higher levels of pressure in a "detonation"]

It was further assumed that a higher methane concentration would be lighter than a lower concentration and therefore would rise to the higher elevations near the seals. Based on the detailed survey of the Second Left Mains, the volumes of the tunnels and crosscuts in the sealed area were known. MSHA therefore concluded that methane/air mixture assumed to be consumed in the explosion could be accommodated by the mine volume lying below the 1408-ft elevation, with the volume above that elevation representing a higher concentration of inert methane/air mixture.

The final piece of information needed was the methane/air concentration level. As mentioned in Chapter 2, the critical values of this ratio range between 5 and 15 percent. MSHA determined that the CFD calculations should assume a methane/air concentration level of 8 percent contained in the volume below elevation 1408.

Information Provided by MSHA

This study could not have been performed without the extensive amount of necessary information and data provided by MSHA. Much of this information was obtained by special investigations conducted by MSHA in the months following the January 2006 accident at the Sago Mine. Other information was developed in a series of explosive tests funded by MSHA and conducted by NIOSH at their LLEM facility in Pennsylvania. The following sections list most of the categories of information provided, with additional details given at appropriate locations within this report.

Mine Surveys

An initial step in the CFD calculations reported in Chapter 4 is the construction of a three-dimensional geometric model of the mine area involved in the simulation (the Second Left Mains and the Second Left Parallel). To provide a basis for this, MSHA provided a digital copy of a 3-D contour mine survey of the sealed area (Reference 5). The mine map contained contours of the sealed area at one-foot intervals. The survey was sufficient to capture the changes in the tunnel width and height along the entries and cross-cuts, including voids from rockfalls or secondary mining below floor levels, piles of debris, and other changes in the tunnel configurations.

Damage Surveys

MSHA conducted extensive and detailed surveys of damaged items in the Sago mine after the explosion, with the idea in mind that they could provide clues as to magnitude and direction of propagation of the blast wave. These included belt hangers, rock bolts and their roof plates, cribbing, seal debris, and other items. Each item was given an identification number, its location was plotted on a map of the mine, the type and degree of damage was recorded, and, in many cases, the item was photographed.

Material Properties

In some of the initial CFD calculations, the tunnel boundaries and the seals were assumed to be infinitely strong, non-yielding materials. This allowed impacting blast waves to be perfectly reflected, giving a "worst case" situation with regard to the intensity of the reflected blast. To represent a more realistic case in later calculations, however, these materials were allowed to yield under a blast load in the calculations in a manner consistent with their actual strength properties, which reduced the intensity of the reflections. Limited material properties were available for the Omega block material. These included the unconfined compression strength, tensile strength, direct shear strength, density, and porosity (References 6 and 7). These data were not sufficient for the complete material descriptions required in structural analysis, so additional data were used to describe the omega material. Development of the material models used in the analysis is covered in more detail in Section 6.

LLEM Experiments

In order to aid the Sago investigation team, a series of experiments named the 2006 Seal Tests were performed by the National Institute for Occupational Safety and Health (NIOSH) at their Lake Lynn Experimental Mine (LLEM) in Pennsylvania (Reference 8). The purpose of the experiments was to investigate the blast effects produced in mine tunnels and crosscuts by deliberate initiations of critical methane/air mixtures, and the level of damage sustained by seals similar in construction to those that were destroyed in the Sago Mine accident and other more robust designs.

The LLEM contains of a number of tunnels and cross-cuts that are similar in size and configuration to those in the Sago Mine, but in limestone, rather than a coal bed. Since the Sago seals failed so catastrophically, it was surmised that the blast load applied to them by during the accident must have far exceeded the 20-psi standard to which the seals had been designed. To verify this conclusion, a series of methane blast tests were conducted at the LLEM against seals identical to those in the Sago Mine. The pressure-time histories along the tunnel were recorded, along with the damage to the seals. This information was provided to ERDC to use as a basis for evaluating the accuracy of blast pressures calculated for the LLEM tests using the CFD code.

A total of six tests were conducted, as described in Table 1. For all tests, a critical methane/air mixture of 9.5% was confined in an area at the end of a tunnel similar in cross-section to those at the Sago Mine. The methane volumes were increased with successive tests to provide a range of blast loads on the seals. Airblast gages

were used to record the pressure histories along the blast travel path down the tunnel.

Three types of 40-inch thick Omega block seals were tested: a "Sago"-type design, a "proper" design, and a "hybrid" design. In addition, a solid concrete block seal was tested. In most of the tests, all of the seals were installed in crosscuts near their intersections with the charge tunnel, except for the Sago seal, which was placed across the tunnel at a distance of 320 feet from the methane charge. This is illustrated in the layout for Test 6, shown in Figure 1.

Table 1. Summary of 2006 Seal Tests at the Lake Lynn Experimental Mine (from Ref7)

Date	LLEM test #	Seals		Max. Pressure psi	Result
		locations	type		
4/15/2006	501	X-2	'proper' 40" Omega	23	survived
		X-3	'hybrid' 40" Omega	25	survived
6/15/2006	502	X-2	'proper' 40" Omega, 2001 design	22	survived
		X-3	'hybrid' 40" Omega	39	failed
		C-320ft	'proper' 40" Omega, 2001 design	51	failed
8/4/2006	503	X-2	'proper' 40" Omega, 2001 design	13	survived
		X-3	'Sago-like' 40" Omega	16	survived
		C-320ft	'Sago-like' 40" Omega	17	survived
8/16/2006	504	X-2	'proper' 40" Omega, 2001 design	15	survived
		X-3	'Sago-like' 40" Omega	18	survived
		C-320ft	'Sago-like' 40" Omega	21	survived
8/23/2006	505	X-2	'proper' 40" Omega, 2001 design	26	survived
		X-3	'Sago-like' 40" Omega	35	failed
		C-320ft	'Sago-like' 40" Omega	57	failed
10/19/2006	506	X-2	'proper' 40" Omega, 2001 design	51	survived
		X-3	solid-block[1]	49	survived
		C-320ft[5]	'Sago-like' 40" Omega[2]	93	failed

[1]Mitchell-Barrett solid-concrete-block seal (w/Type S mortar & no wedges).
[2]Sago 40-inch thick Omega block seal using the block from the Sago Mine.
Note: a Mitchell-Barrett solid-concrete-block seal (w/BlocBond mortar & no wedges) was installed in X-1 for all tests.
Note: maximum pressures were at 15-point smoothing or ~100 Hz or ~10 msec average

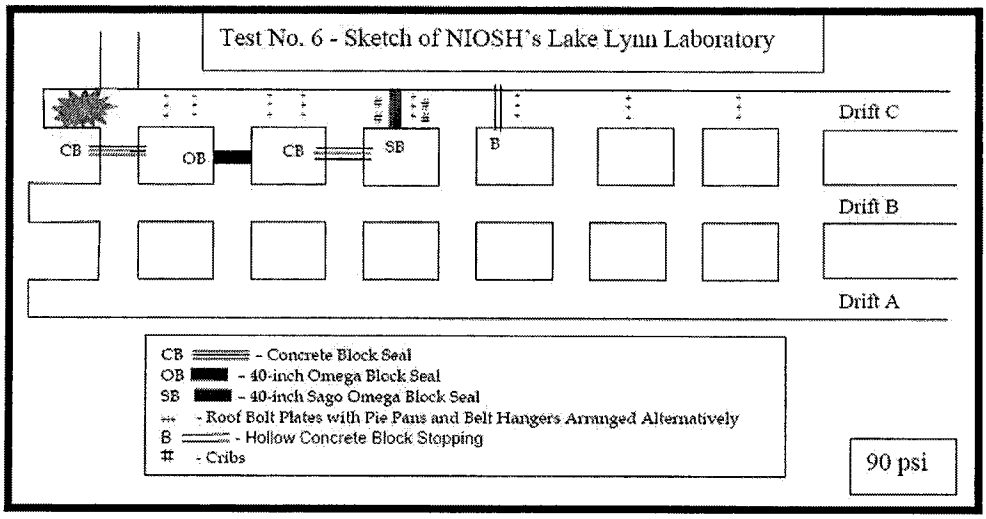

Figure 1. Sketch of layout for Test No. 6 at the LLEM (from Ref 7)

The Sago Mine

Description of the Mine.

The Sago Mine is an underground coal mine located near Buckhannon, WV. The bituminous coal is part of the Pittsburgh Bed. The principal seam is 4 to 7 feet thick, and is excavated using the room-and-pillar mining method. Figure 2 shows a layout of the Sago Mine. The explosion accident of January 2006 occurred in an area called the Second Left Mains, which is located at the north end of two mile-long strip of excavation called the 2 North Mains. Figure 3 shows, in more detail, the Second Left Mains and the adjacent area, the Second Left Parallel.

The mine walls and ceiling are relatively rough from the cutting made by the excavator machine, or from later rock falls. Rock rubble is scattered over the floors of the tunnels and crosscuts, and in small piles in some locations. Where the tunnel ceilings seemed to be weak, timber cribbing was placed to provide additional support. Cribs were also placed on each side of the seals to prevent any settlement of the ceiling from cracking the concrete blocks in the seals. At some locations, the floor or ceiling of a tunnel or crosscut makes a sudden change in elevation. For the ceilings, these are usually places where a rockfall occurred. For the floors, they are locations where the coal seam dipped below the main floor level, and the excavators dug sloping pits to recover the coal there.

The intersections of tunnels and crosscuts usually require additional ceiling support. In the Sago mine, rockbolts are emplaced to reinforce the overhead rock,

with metal plates bolted against the rock surface at the bottom ends of the bolts. The two kinds of plates used in the Sago Mine are called "pie pans" and "spider plates", because of their shapes. Both are made of sheet metal. The pie pans are about 18 inches in diameter, and the spider plates are about 18 inches square. Short steel angle irons welded to the bottom ends of rock bolts are also located at points along some of the tunnels. These are "belt hangers" that were used to suspend the conveyor belts which carried the coal out, when those areas were being actively mined.

Description of the Seals.

The locations of the seals for the Second Left Mains area are shown in Figure 3. The seals were constructed of light-weight concrete blocks, known by their trade name as "Omega" blocks. The individual Omega blocks are about 24 inches long by 16 inches wide by eight inches thick. They are normally mortared into place over the full width and height of the tunnel or cross-cut, with a coat of mortar placed over the front and back faces of the wall to seal off any small openings between the blocks.

Figure 4 shows the construction of a seal wall using Omega blocks in accordance with the specifications used in the Sago Mine (Reference 9). Each course consisted of two rows of blocks, with those in one row being laid side-to-side, and those in the other row laid end-to-end. The pattern was reversed in alternate courses in

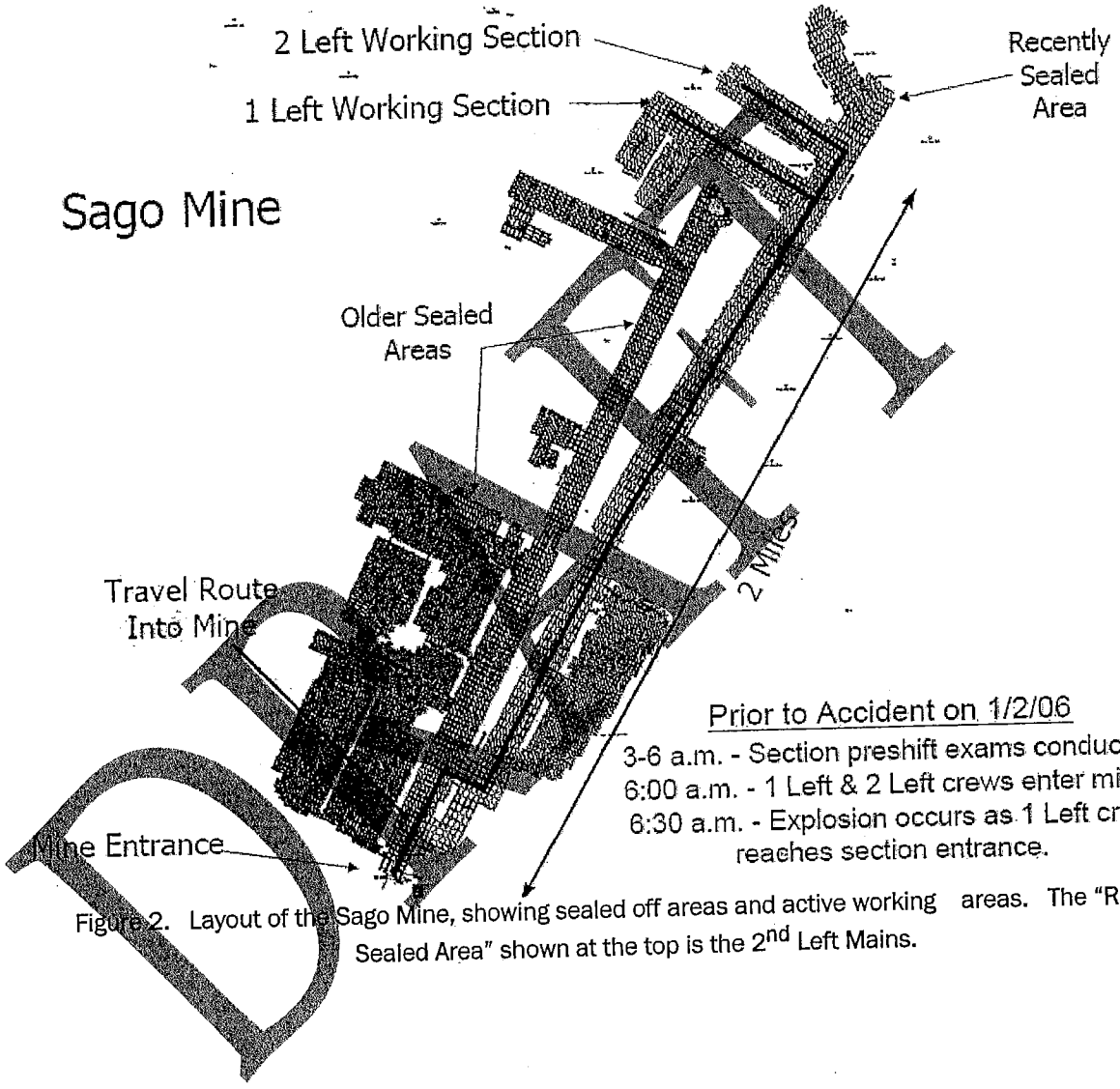

Figure 2. Layout of the Sago Mine, showing sealed off areas and active working areas. The "Recently Sealed Area" shown at the top is the 2nd Left Mains.

order to stagger the joints, so that all joints between blocks in one course were covered by the blocks in the next course. All joints were a minimum of ¼-inch thick, and were mortared using an approved mortar sealant.

The walls were not hitched (i.e., they were not keyed into recesses in the tunnel walls). When necessary, the blocks in the top course were sawed to reduce their thickness, so that the gap between the blocks and the tunnel crown was less than two inches. Three rows of wood planks were then laid on the top course, and

wedges were driven on one-foot centers or less between the planks and the tunnel crown. All gaps between the wedges were filled with sealant.

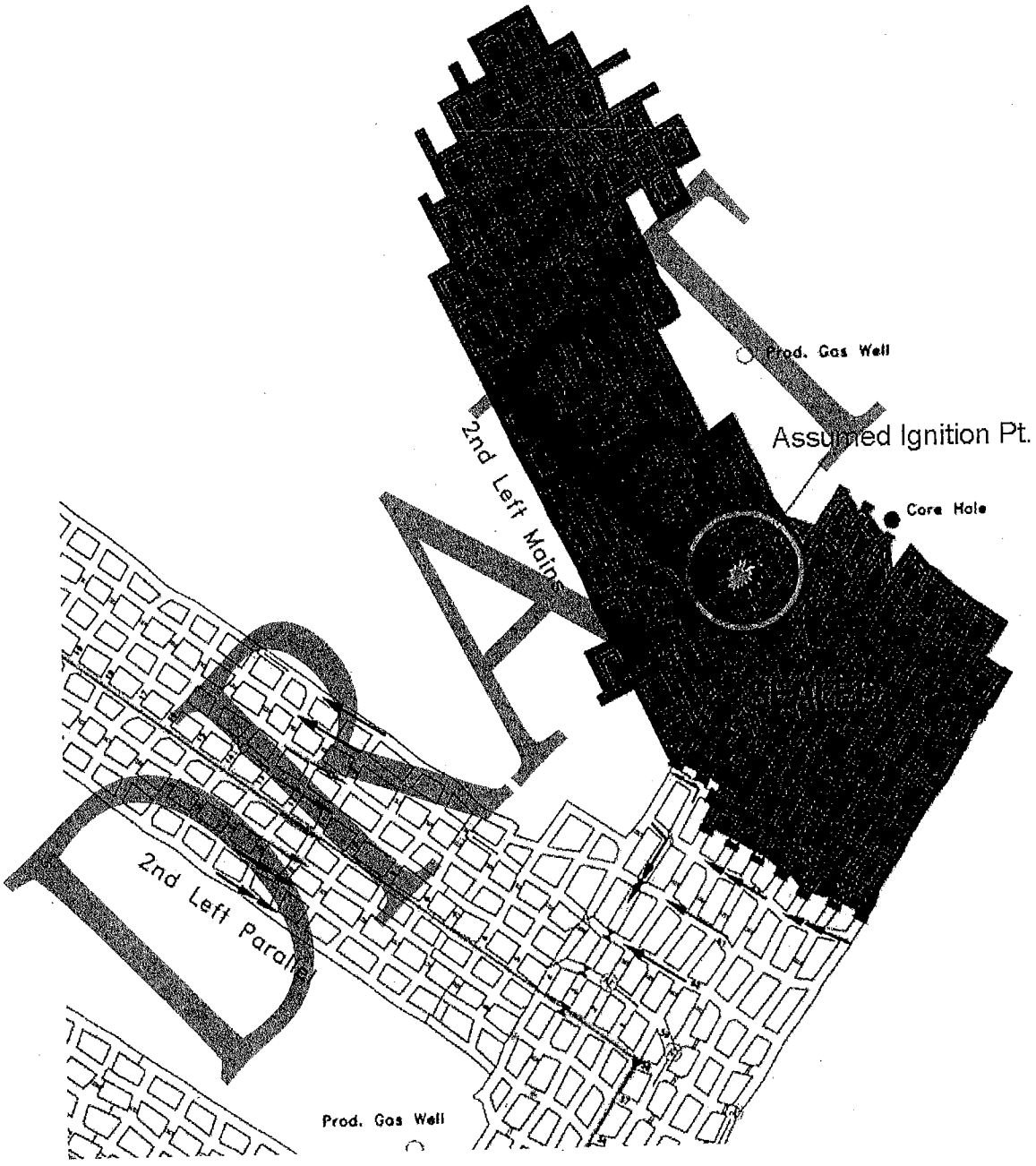

Figure 3. Close-up view of the 2nd Left Mains. The red marks across the tunnels, between the shaded (sealed) area and the unshaded (active working) area indicate the locations of the walls used to seal off the methane gas in the sealed area. The arrows show the path of ventilation air in the working area.

The January 2006 Accident.

On January 2, 2006, an explosion occurred in the Second Left Mains. The blast completely blew out the seals in all ten tunnels leading into the sealed area, and penetrated deep into the unsealed working area. One miner was killed by the blast beyond the seal locations, and sixteen escaped. Twelve miners were trapped in the Second Left Parallel, but only one survived long enough to be rescued. The others were overcome by the toxic gases produced by the explosion before rescuers could reach them.

In the months following the accident, several investigations were made into the cause of the explosion, the damage produced by the blast, the rescue operations, and other aspects of the incident. Reference 10, for example, is a preliminary report of a study commissioned by the governor of West Virginia. The investigations indicated that the explosion of the methane in the Second Left Mains may have been triggered by a lightning strike on the surface. How the lightning found a path into the Second Left Mains is unknown, at this time, however.

The investigations carefully documented all evidence of damage from the explosion in an attempt to pinpoint the initiation point, the volume of methane involved, and the progression of the blast wave through the array of tunnels and crosscuts to the seal locations. The documentations included damage to spider plates, pie pans, belt hanger rods, cribbing, cables, and other items, as well the distribution of debris from the tunnel walls and ceiling, cribbing, and the seals themselves.

In addition, a detailed survey was made of the entire Second Left Mains area to provide cross-sections of the tunnels and cross cuts along their lengths. This was done to determine both the total volume of the area, and the changes in volume or cross-sectional areas as the blast wave progressed through the passageways.

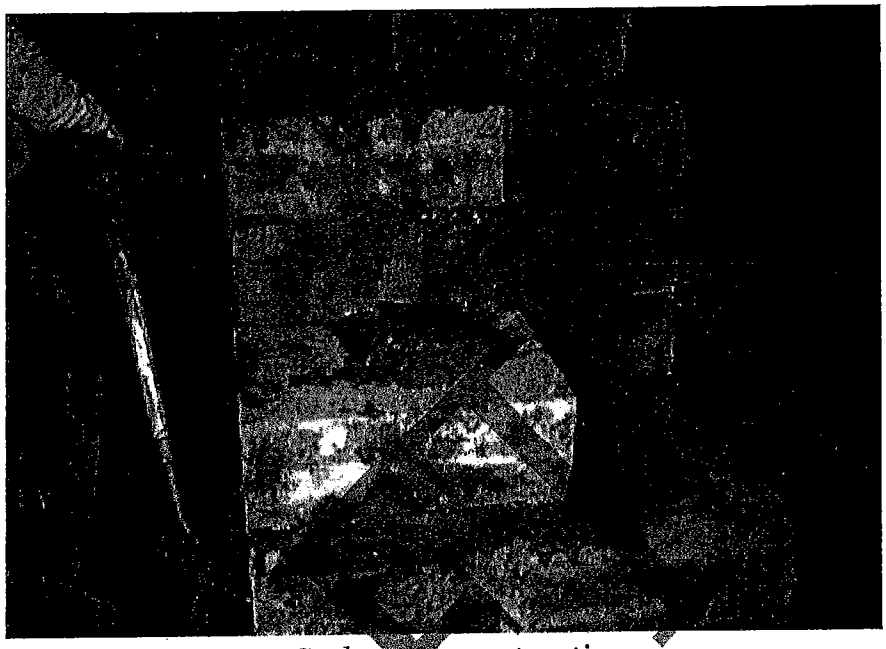

a. Omega Seal under construction

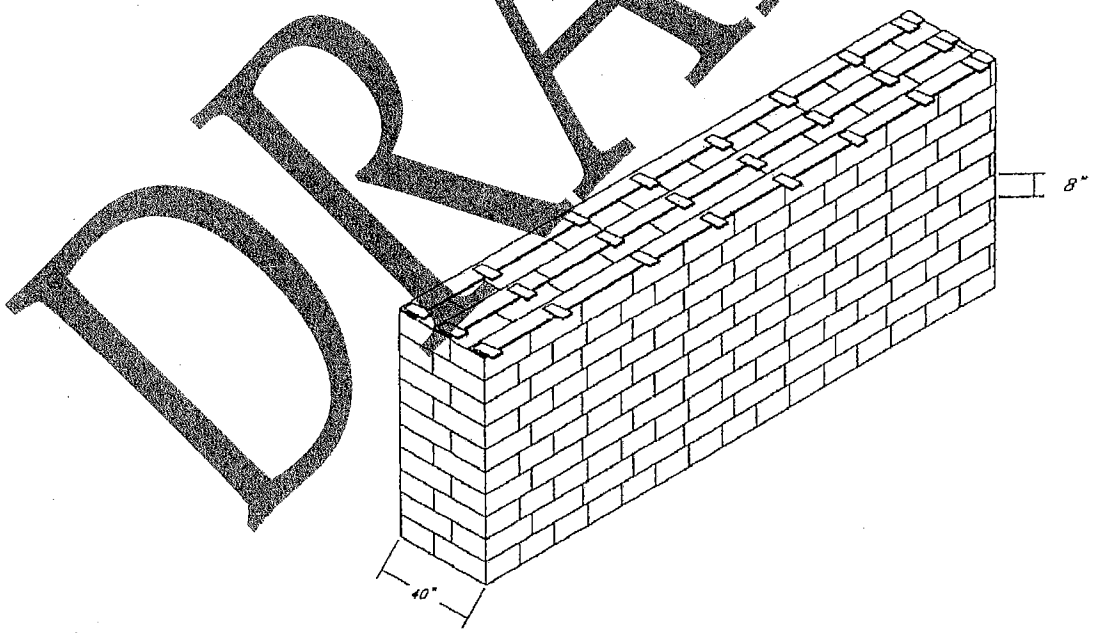

b. Staggered block courses in a wall, with planks and wedges on top.

Figure 4. Construction method for 40-inch thick Omega block seals in the Sago Mine, with the blocks laid in staggered courses and mortared.

Study Rationale, Assumptions, and Procedure

The study rationale approached the problem from two different directions: first, to define the blast environment in the Sago Mine from the postulated explosion; and second, to determine the blast forces that would be required to produce the structural damage observed from the incident. The physics and phenomenology involved in these two approaches are quite different, so different computational methods were used in order to take advantage of each method's unique attributes and capabilities.

Defining the blast environment.

A computational fluid dynamics (CFD) code named SACE was used to calculate the blast environment produced in the sealed area by a methane gas explosion, the blast loads that would be applied against the seals at their locations in the mine, and the blast environment beyond the seals after their failure (Chapter 4). The blast environment at any location is defined by a peak pressure, a total impulse, and a dynamic pressure. The peak incident pressure and impulse are normally described in the form of a pressure-time plot, such as that shown in Figure 5. The dynamic pressure is essentially the pressure exerted by the gas flowing behind the blast front, as it is driven by the expanding explosion products. When this incident wave reaches a seal in the path of the wave propagation, the incident wave is reflected up, resulting in a much higher pressure loading on the seal. The magnitude of the reflection compared to the incident wave is a function of the incident pressure magnitude and the angle of incidence between the wall and the incident wave, and the material properties of the wall and gas. Empirical formula for shock reflection factors for explosions in air can be found in (Reference 11). Given an air shock reflecting against a rigid surface at 90 degrees (normal reflection), the reflection factor ranges from 3 at 20 psi (60 psi reflected) to 6.4 at 250 psi (1600 psi reflected).

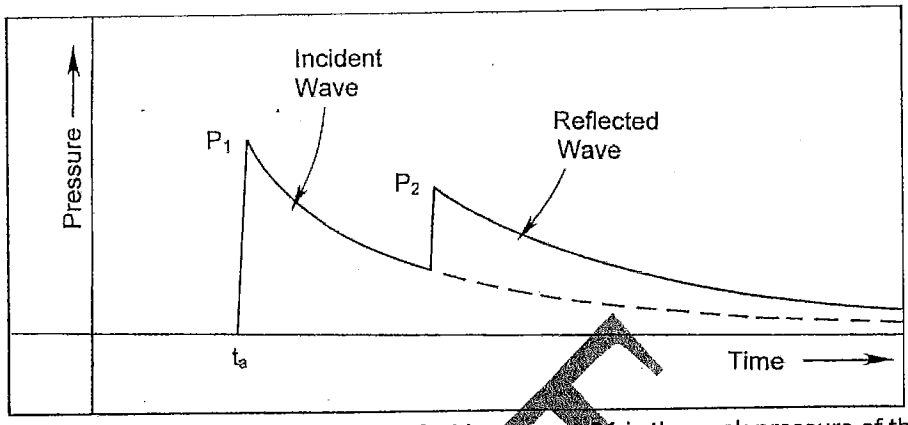

Figure 5. Characteristic pressure-time history of a blast wave. P1 is the peak pressure of the incident blast wave, whose arrival time after the explosion is ta, and whose decay is shown by the dashed curve. In some situations, a reflection of the incident wave will follow behind, giving a total pressure of P2 at its arrival time.

In a typical mine, the non-uniformity of the tunnel profiles, the roughness of the tunnel walls, the presence of debris on the tunnel floor, and other factors tend to create turbulence in the blast wave, along with multiple reflections behind the blast front as it travels from the explosion initiation point to other locations in the mine. In addition, the array of tunnels and crosscuts means that multiple wave fronts can arrive from different directions at a point of interest. Consequently, the pressure-time histories produced in an environment such as the Sago Mine will be much more complex than the idealized form shown in Figure 5. The purpose of the CFD calculation was to determine the actual level of blast loading on the seals, in a manner that accounts for the complexities of the Sago Mine environment.

The January 2006 accident occurred 22 days after the Second Left Mains area was sealed. Samples were taken quarterly of the methane liberation rate in the mine over the previous year, and during the recovery operation after the accident, and at intervals following the accident. The amount of methane remaining in the sealed area after the accident was measured during the re-ventilation.

Using this information, MSHA's Sago Accident Investigation Team determined that, for this analysis, it should be assumed that there were two volumes of methane with different concentration levels in the sealed area at the time of the explosion. Above an elevation of 1,408 feet was roughly 1,750,000 cubic feet of methane at a concentration level of 8.1%, and below that elevation was roughly 1,188,000 cubic feet of methane at a concentration of 17.3% (Reference 12).

The ignition point for the Sage calculations of the methane consumed in the event was supplied by MSHA from an analysis of the flames and forces observed in the mine. This point was determined to be near Spad 4010.

In order to have confidence in the results of a complex computer calculation, it is necessary to validate, in some way, the model's ability to calculate the phenomena of interest. This was done by using the SAGE code to calculate the pressure-time histories at various locations from methane gas explosion tests conducted at NIOSH's LLEM facility in Pennsylvania. The experiments involved the explosion of 9,0% and 9.5 % of a methane/air mixture in a 7 -foot high, 20-foot wide tunnel, with adjacent tunnels connected by crosscuts. The accuracy of the SAGE calculation results was indicated by comparing them with the pressures recorded in the tests.

Relating Blast Forces to Structural Damage

Damage to Steel Support Items. Investigations conducted after the explosion revealed that many of the belt hangers, spider plates, and pie pans in the sealed area were damaged by the blast. The hangers were bent to varying degrees, and the spider plates and pie pans had corners or sides folded back – in some cases, on more than one side (Figure 6). If the blast force required to cause a given level of damage to these items could be determined, then the damage level observed at any location could be used to indicate the blast force at that point. This value could then be compared with the SAGE calculations to further verify the accuracy of the computer model results. Chapter 5 describes a second set of calculations using two Finite Element codes, LSDYNA and DYSMAS, to calculate the damage to the spider plates, pie pans, and belt hangers that would be expected from different levels of blast loadings. If the blast levels required to produce the damage matched the blast levels predicted for those locations by any of the three SAGE calculations, then the volume and methane/air mixture assumed for that calculation must be correct. If the calculated blast levels were higher or lower, then the assumed methane blast source must have been too great or too small.

In addition, a Single Degree of Freedom (SDOF) analysis was performed for belt hangers representative of those in the Second Left Mains. As with the finite element analysis, the purpose was to establish a rough correlation between a level of loading and the degree of bending that would it would produce. Although not as accurate, the SDOF technique provides a relatively quick and easy way to estimate blast levels as a function of the bending damage to the belt hangers that was observed in the Second Left Mains.

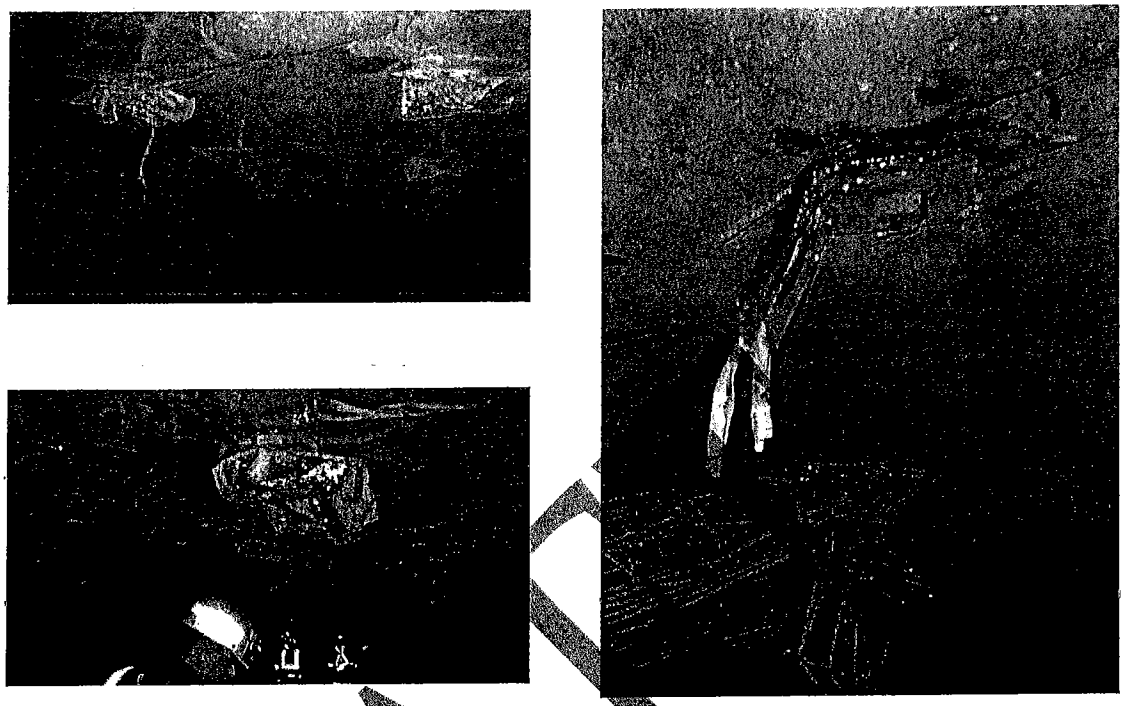

Figure 6. **Damage to spider plates, pie pans, and belt hangers in the 2nd Left Mains.**

Analysis of Seal Failures. A finite element (FE) analysis was performed on the Sago Mine seal designs to gain an understanding of how they failed, and the levels of loading that would produce different degrees of failure in that seal design. An FE analysis uses detailed information on the loading history and distribution over the structure, and on the physical properties of the structure materials and design to describe how a structure responds to a complex loading. It is particularly useful (although much more difficult) for analyzing a dynamic response to a blast load. The ultimate application of such a technique, once it is validated, is to enable evaluations of new designs for mine seals. With such a method, the degree to which modifications in an initial design will improve or degrade the performance of a structure can be quantified in order to produce the best compromise between strength and affordability.

While FE techniques provide accurate and detailed information on a structures response to dynamic loads, they require a great deal of time and effort to set up and run. A much easier and quicker method to determine the general performance level of a simple structure is to conduct an SDOF analysis. If an SDOF analysis indicates that a design is close to the performance level desired, then a more rigorous finite element analysis can be performed to refine the response assessment. An SDOF analysis was made of the Sago seal designs to demonstrate the potential usefulness of this technique.

The following chapters provide details on the procedures and results of the CFD and the Finite Element model calculations.

4 Computational Fluid Dynamics Study

SAGE Code Description

The calculations of this study were performed with the SAGE (SAIC Adaptive Gridding Eulerian) hydrocode (Reference 13) on Cray XT3 Computers. SAGE is a multi-material Eulerian finite difference code with strength and special boundary condition treatments for concrete/air and other solid/fluid interfaces. The code has a wide selection of equations of state that may be used to model many diverse materials. The Nobel version of SAGE has the capability to model chemical explosions and use time-dependent detonation and burn models. SAGE applies second order, directional-splitting, Godunov-Riemann solver (shock following) techniques (Reference 14, 15). The code has automatic mesh refinement (AMR), and runs on massively parallel computers. Calculations have been shown to scale well for thousands of central processing units (CPUs).

There are available several time-dependant burn models --Arrhenius, Ignition and Growth (Reference 16), and Forest Fire (Reference 17). The code has been optimized for the strong shock environment and large material deformations. SAGE has a number of other capabilities that were not used in this study, such as heat transfer, radiation transport, and combustion (or afterburn) of explosion products as they mix with air.

One key capability of SAGE that was essential in this study is the ability to read a 3-D geometry from a single or multiple stereolithograph (STL) files that were generated from AutoCAD files. The calculations could not have been done without this type of capability and a very robust code for generating the calculational grid.

SAGE has been well validated for a wide range of applications, including the following:

(1) Explosions in and around multi-room buildings, in or near tunnels, underwater with/without concrete dams

(2) Explosions from unusual explosive compositions

(3) Noise around shoulder-fired weapons

(4) Shaped charges

(5) Armor penetration

(6) Asteroid impact in the Gulf of Mexico

(7) Supernova

(8) Tsunami motion

(9) Fluid instability problems

(10) Fuel/air military explosions and methane-air explosions in mines

SAGE has been developed by SAIC and Los Alamos National Laboratory under the Crestone Project. Early development was performed for the Defense Nuclear Agency for modeling underwater nuclear explosions, including shock reflections from the ocean bottom.

Cheetah Code Description

Cheetah is an equilibrium thermodynamics code developed by the Energetic Materials Center at Lawrence Livermore National Laboratory (References 18 and 19). The code is a descendant of Tiger (Reference 20). Cheetah has a wide variety of capabilities used by the energetic materials community, and a large library of reactants, including methane. Calculations may be obtained for arbitrary mixtures of these reactants, such as 8% methane in air.

In this study, the code was used to calculate the explosive detonation point from Chapman-Jouget (C-J) detonation theory and the adiabatic expansion (the Rankine-Hugoniot adiabat). From these calculations were obtained the C-J pressure, particle velocity, shock propagation velocity, temperature, density, sound speed, and chemical components. Also obtained were pressure-density pairs for a number of pressures, from the C-J level down to atmospheric pressure along the adiabat (constant energy) that were used to develop equations of state (EOS) for burned methane-air mixtures.

Cheetah was also used to compute the static pressure and temperature for a "constant volume explosion"; that is, the chemical and thermodynamic state obtained when a material is burned or exploded in a confined volume. This is the condition that develops in late time when there is no heat loss and no venting.

NIST REFPROP Code

The code REFPROP (REFerence fluid PROPerties) Version 7.0 (Reference 21) was developed by the National Institute of Standards and Technology (NIST). It provides tables and plots of the thermodynamic and transport properties of many fluids and their mixtures, including hydrocarbons. According to the on-line information (Reference 21), "REFPROP is based on the most accurate pure fluid and mixture models currently available. It implements three models for the thermodynamic properties of pure fluids: equations of state explicit in Helmholtz energy, the modified Benedict-Webb-Rubin equation of state, and an extended corresponding states (ECS) model. Mixture calculations employ a model which applies mixing rules to the Helmholtz energy of the mixture components; it uses a departure function to account for the departure from ideal mixing. Viscosity and thermal conductivity are modeled with either fluid-specific correlations or an ECS method." REFPROP, along with Cheetah, was used in developing equations of state for methane/air mixtures.

Equation of State for Methane/Air Mixtures

Variations of Grüneisen equations of state (EOS) were used for both burned and unburned methane/air mixtures. See equation 6 below. The EOS of the burned methane/air mixtures were curve fit to calculations from Version 4.0 of the Cheetah code of the Chapman-Jouget (C-J) state and the adiabatic expansion. The EOS exactly match the C-J pressure and density. The shock velocity is matched to better than 0.5%. Table 2 contains the values of the C-J and constant volume state parameters computed by Cheetah. Note that methane/air mixtures of 8.0 % and 9.5% by volume are about 5.04% and 6% by mass, respectively. Figures 7a and 7b compare the EOS curve fits with the Cheetah values. The EOS for unburned methane were curve fit to calculations from the NIST REFPROP 7.0 code. The fit parameters for the Grüneisen equations of state for the methane/air mixtures are provided in Table 3.

Table 2. Parameters at the Chapman-Jouget and constant volume states.

C-J Parameter	8.0 % Methane/Air	9.5% Methane/Air
Overpressure, MPa	1.610	1.695
Overpressure, psi	233.5	245.8
Shock Velocity, m/s	1783	1830.1
Particle Velocity, m/s	789.8	814.9
Sound Velocity, m/s	993.4	1015.1
Temperature, Deg K	2745	2808
Density, kg/m^3	2.0521	2.0488
Energy Release, J/kg	1.6795 x 10^6	1.8505 x 10^6
Constant Volume Explosion State, MPa	0.7750	0.8437
Constant Volume Explosion State, psi	112.4	122.4

The Cheetah calculations are performed for a temperature of 25 deg C. The ambient temperature in the mine is closer to 15 deg C (59 deg F). The EOS for burned methane/air mixtures were revised to 15 Deg C using NIST REFPROP calculations.

There are several formulae called "Grüneisen" equations of state. The simplest form that is suitable for some applications with gases is

$$P = (\gamma-1)\,\rho\, I \tag{1}$$

Where

P = absolute pressure

ρ = density

I = specific internal energy

$\gamma = C_p / C_v$ (ratio of specific heats)

The expression γ-1 is often called the Grüneisen ratio.

Harlow and Amsden (1971) (Reference 16) use a more general form

$$P = P_H + (\gamma-1)\,\rho\,(I - I_H) \tag{2}$$

where

$$P_H = c^2 (V_o - V) / [V_o - s (V_o - V)]^2 \tag{3}$$

$$I_H = 0.5 [c (V_o - V) / (V_o - s (V_o - V)]^2 \tag{4}$$

ρ_o = density at ambient pressure and temperature

$V = 1/\rho + (\gamma-1)\,\rho\, I$

c = speed of sound

and

s = a parameter related to the shock velocity and particle velocity on the Rankine-Hugoniot adiabat.

The coefficients s, c and γ may be considered "fit parameters" that may be varied to optimize the equation of state for a particular application. For example, c and γ may not always be chosen to be the values at ambient conditions.

After dividing numerator and denominator of Equation 2 by V^2 and defining μ as

$$\mu = \rho/\rho_o - 1$$

Equation 2 may be expressed as follows

$$P = \rho c^2 \mu [1 - 0.5 (\gamma-1) \mu] / [1 + \mu (1-s)]^2 + (\gamma-1) \rho I \quad (5)$$

SAGE uses the following variation of this equation:

$$P = \rho_o c^2 \mu [1 - 0.5 (\gamma-1) \mu + \mu] / [1 + \mu (1-s)]^2 + (\gamma-1) \rho I \quad (6)$$

The significant differences are the ρ_o out front in Equation 6 rather than ρ in Equation 5 and the extra μ in Equation 6. Because of these changes, Equation 6 provides a more accurate fit to the Rankine-Hugoniot adiabat than does Equation 5, especially at the higher pressures. Equation 6 was used in all of the SAGE calculations described in this report. SAGE also allows the use of higher powers of μ in both the numerator and denominator of the first term, along with additional fit coefficients.

Selection of Burn Model

The initial SAGE calculations used a first-cut ignition and growth explosive burn model (Reference 16). These calculations were compared with measurements of pressure in a 520-mm diameter pipe, performed by M. Kuznetsov, et al.(Reference 23). The SAGE results were in fair agreement with the Kuznetsov data, but improvements in the burn model were needed. This model can reproduce detonation conditions, but because the burn rate is a function only of pressure and density (and not temperature) ignition and growth models are not appropriate for deflagration and the transition to detonation. Subsequent calculations used the Arrhenius burn model described below, that more accurately models the deflagration and run-up to detonation.

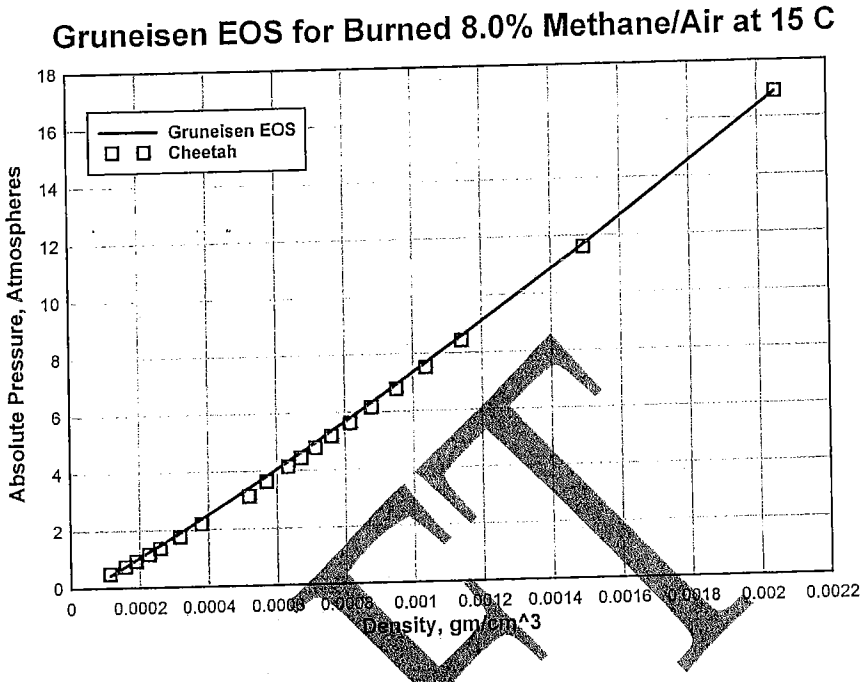

a. Comparison for 8.0% methane/air.

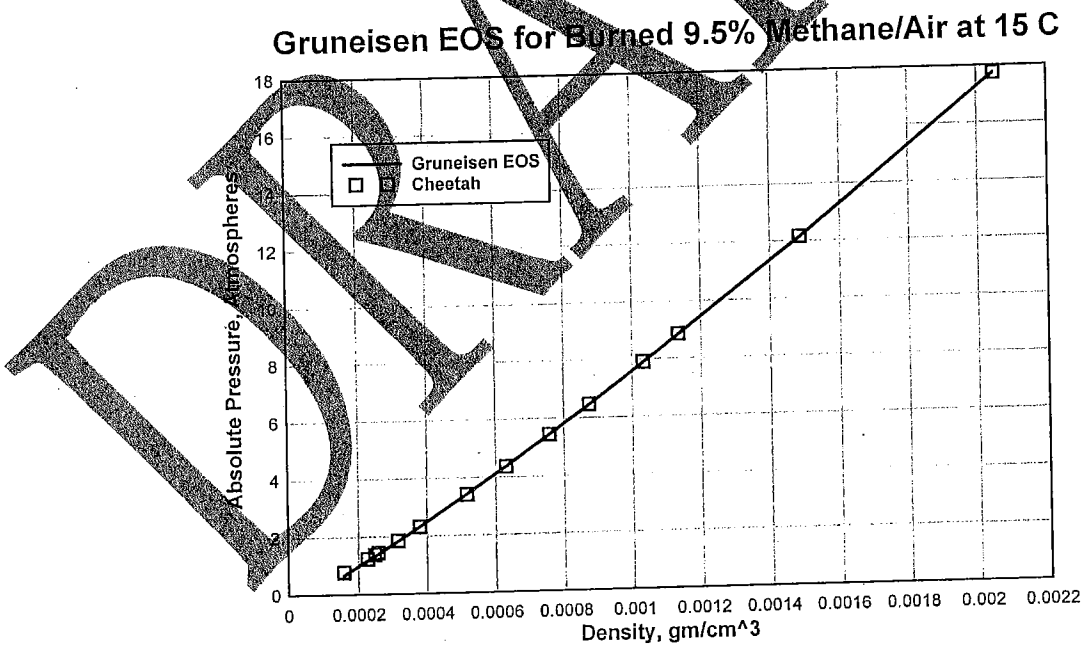

b. Comparison for 9.5% methane/air

Figure 7. Gruneisen Equation of State compared to the Cheetah values for 8.0% (a) and 9.5% (b) methane/air mixtures.

Table 3. Coefficients of the Grüneisen equations of state for methane/air mixtures

Material	Density ρ_o	$\gamma = C_p / C_V$	Sound Speed	S
	kg/m³		m/s	
8.0% Methane/Air Unburned	1.1775	0.3919	346.00	0.9
8.0% Methane/Air Burned	1.1775	0.3919	346.00	0.885
9.5% Methane/Air Unburned	1.1689	0.3901	347.06	0.9
9.5% Methane/Air burned	1.1689	0.3901	386.50	0.877
17% Methane/Air Unburned	1.1248	0.3812	352.64	0.9

Arrhenius Burn Model

In the Arrhenius burn model (Refernces 17 and 24), the burn fraction F in a computational cell is a function of the local temperature T, as follows:

$$F\, dF/dt = -Z\, e^{-E^*/T} \qquad (7)$$

where $F = M_u / (M_r + M_u)$

M_u = mass unreacted

M_r = mass reacted

Z and E^* are coefficients that determine the burn rate.

Burn occurs only when T is greater than an activation temperature T_a of 0.07 ev (812.31 deg K or about 1000 deg F).

The coefficients Z and E* were chosen to match the burn rates reported by M. Sapko, et al., Reference 25, (about 14 m/s at distance 0 – 4 m and 100 m/s for 4 –

26 m) for Tests 347 and 506 in the LLEM. The flame propagation speed was found to be approximately linearly proportional to the minimum computational cell size of the calculation. Hence, when the minimum cell size was changed, the coefficient Z was varied accordingly. Calculations in the Sago mine and in Test 506 in the LLEM used a minimum cell size of 25 cm after the initial spherical or hemispherical initiation. In this case, the value of Z was 0.000336/sec and E* was 1614 ev (1.8730 x 107 deg K).

Validation of the SAGE Code for Methane/Air Explosions

Comparison with Russian Pipe Tests

Experiments performed by Kuznetsov, et al. (Reference 23) investigated the deflagration-to-detonation transition in methane/air mixtures in pipes with diameters of 174 mm and 520 mm. The pipes had orifice plates spaced at one tube diameter. Tests were conducted with blockage ratios of 0.3 and 0.6 (the ration of baffle area in the pipe to the pipe cross-section). In the larger pipe with 0.3 blockage, the authors observed what they called "quasi-detonation" for methane concentrations from 8.5 to 12%. The burn accelerated to a steady-state speed just below the CJ detonation velocity by about 15 m from the ignition end. Mixture concentrations of 7, 8, and 13.5% developed flame speeds close to the speed of sound, which is about half the CJ detonation velocity.

We used the experimental data from the 520 mm tube with 0.3 blockage and 9.5% methane concentration for our initial investigation of the burn models used in SAGE. The first calculations used Lee-Tarver Ignition and Growth (IG) reactive burn models that are commonly used for high explosives such as TNT. In these calculations, the methane/air burn quickly transitioned to detonation in both the pipe tests and in Lake Lynn Experimental Mine (LLEM) Test 347 (Reference 25). Calculated pressure levels of waveforms in the detonation region of the pipe tests were close to the measurements. The calculated peak pressures for Test 347 in the LLEM were slightly higher than those reported by Sapko, et al. In both cases, arrival times were much too early and there were no precursors in the LLEM pressure pulses. While it was clear that the IG model was not ideal for use in methane/air mixtures, these calculations gave confidence that SAGE, using our EOS for the burned gas would properly reproduce the CJ conditions.

We next turned to an Arrhenius burn model, in which the burn rate is a function of temperature, rather than density and pressure as in the IG model. Coefficients Z and E^* (Equation 1) were chosen to match the burn rates reported by M. Sapko, et al. (about 14 m/s at distance 0 to 4 m and 100 m/s for 4 to 26 m) for Test 347 in the LLEM.

A SAGE calculation was performed for the test of M. Kuznetsov, et al. in a 520-mm diameter pipe with 9.5% methane and an obstruction ratio of 0.3. The Arrhenius coefficients were set as above for the 0 to 4 m range. The turbulence caused by the orifice plates generated a transition to detonation and a flame speed acceleration very close to the measurements, as shown in Figure 8.

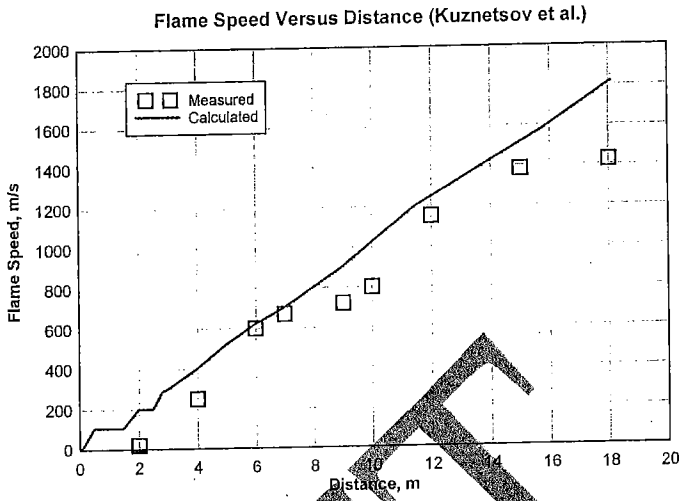

Figure 8. Flame speed versus distance in a 520-mm diameter pipe (Kuznetsov et al.).

SAGE Validation against LLEM Experiments

In order to verify the accuracy and reliability of SAGE calculations of explosions in methane/air mixtures, the code was run to calculate the results of two of the NIOSH experiments conducted in C-Drift of the LLEM: Test 347 (Reference 25) and Test 506, conducted in 2006. Figure 9 is a drawing of the testing area of the LLEM. The first experiment contained a 190-m^3 (6710 ft^3) zone of 9% methane/air that extended 47 ft from the inby end of C-Drift. The second experiment used 1,265 ft^3 of 9.5% methane/air in a zone that extended 71 ft from the end. This test was designed to produce approximately 90 psi pressure on a 40-in thick Omega Block seal positioned across C-Drift 320 ft from the end. Pressure sensors were located 84, 134, 184, 234, 304, 403, 501, 598, and 767 ft from the end of the drift.

We continued to refine the Arrhenius burn model that had been first tested against the pipe tests described above, and in Test 347 in LLEM. After our initial efforts with Test 347, we concentrated our final modeling on Test 506 that used the 9.5% methane concentration of our Sago Runs 1 and 2, and had a larger methane zone and higher pressure levels. Various zoning schemes (minimum cell dimensions) in SAGE were investigated and Arrhenius coefficients Z and E* were optimized (see table 3) to match the burn rates and pressure waveforms of Test 506. These calculations also modeled the Omega Block seal, two cribs inby and two outby the seal, and a CMU ventilation stopping wall (at location 384 ft). Also treated were open crosscuts 4-7 that connected C-Drift and D-Drift. crosscuts 1-3 and E-Drift were closed off from C-Drift. The initial burn to 316 msec was performed as a 1-D spherical event, using an initial burned energy of 2500 J (in a hemisphere) to

represent an electric match. This calculation was performed with a fine grid zoning in the region of the electric match. Three hemispherical regions (2.3 m diameter) were then overlaid onto the full 3-D grid. The grid along the length of the C and D-Drifts extended 525 m (1722 ft) from the end of ignition (y = 0). A uniform ceiling height of 2.1 m was used, and the slope of the floor up to the blast door was modeled. The water-filled barrels used as turbulence generators in the test were also modeled. The roughness of the floor, ceiling and side walls was ignored. Because the SAGE calculations for the Sago mine used a 25 cm minimum cell size, a similar size (26.25 cm) was selected for the final LBEM calculations. The largest cell size used by SAGE was 52.5 cm (1/4 of the ceiling height).

Figure 10 shows an inby view of the seal, cribs, and pressure sensors used in test 506. Figure 11 shows three views of the SAGE model for Test 506. On the left is a close-up of the model, from ignition end at the bottom to the stopping shown in red at the top. The five dots near the bottom are the barrels. The region containing the methane/air mixture extended out past the first crosscut. In the center is a view of the complete model, showing the open crosscuts between C and D-Drifts. On the right is a close-up view of the seal, cribs, and stopping.

Figures 12-14 compare results of the SAGE calculations with measurements at three gage locations: C5 at 234 ft, C6 at 304 ft, and C7 at 403 ft. Gages C5 and C5 are inby the seal and Gage C7 is outby the CMU stopping wall. In the Gage C5 measurement, the initial pulse is the side-on (or incident) wave propagating from the explosion toward the seal. The pulse at 644 ms is the reflection from the seal and the pulse at 800 ms reflected first from the seal, and then from the ignition end of C-Drift. In the Gage C6 measurement, the reflection from the seal arrives about 24 ms after the initial pulse. The reflection, first from the seal and then the end of C-Drift, arrives at 854 ms. The pressure behind the CMU wall was reduced to about 5 psi, which was much lower than the pressure at Gage C6. Since there is an open cross-cut between the seal and the stopping, the blast obviously propagated around the wall, before it failed, as well as later going through the destroyed wall.

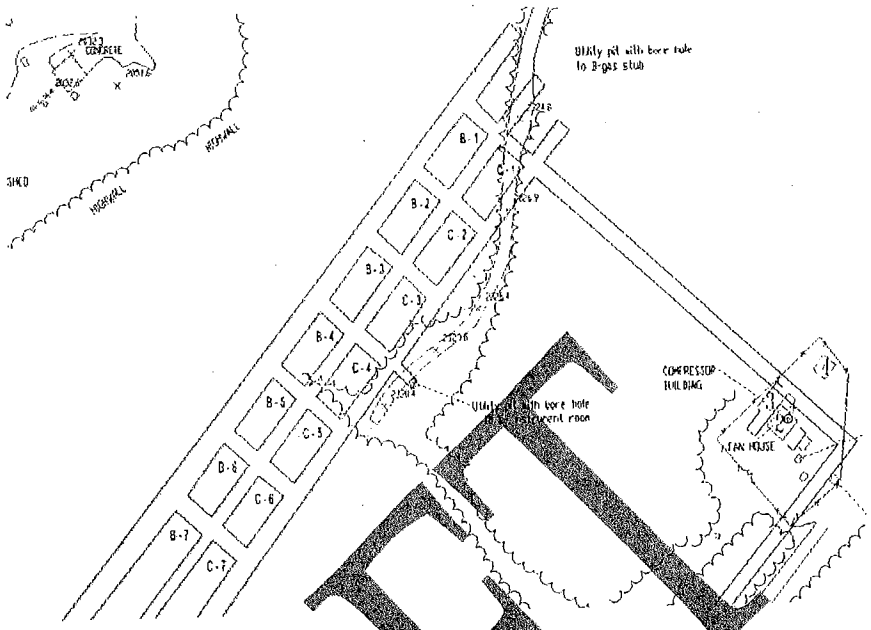

Figure 9. Drawing of seal test area of LLEM.

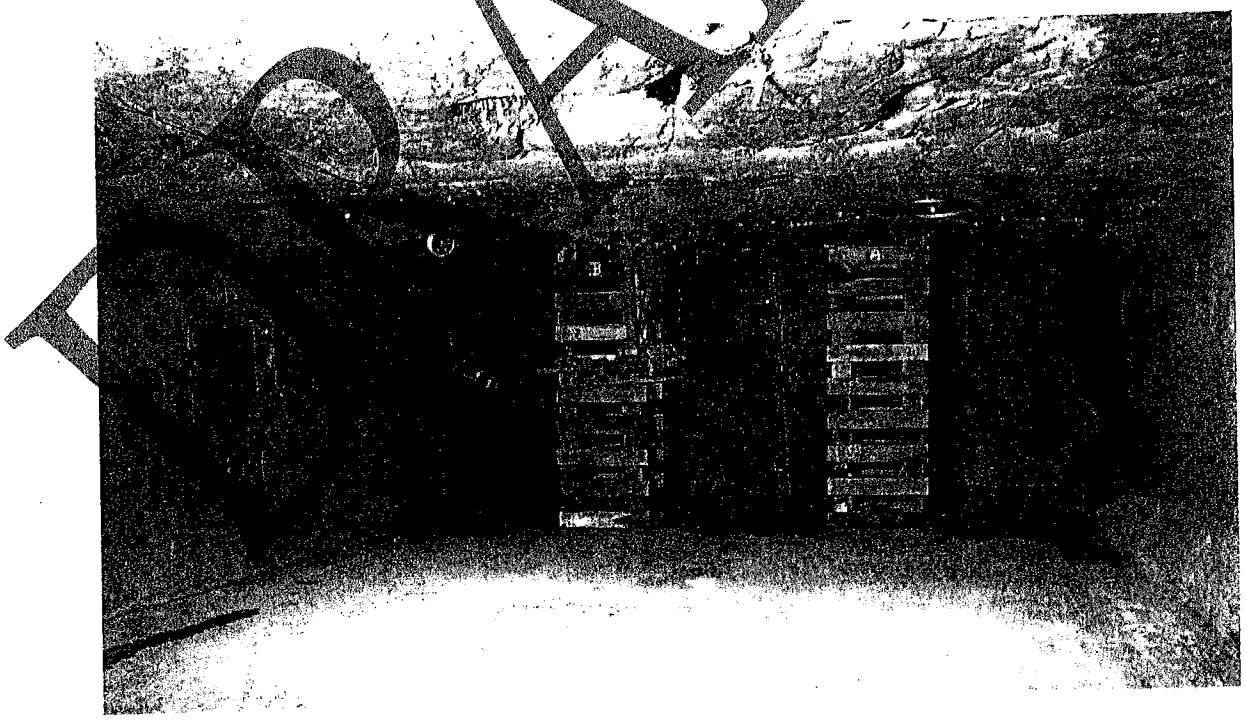

Figure 10. Inby view of Test 506 seal and cribs.

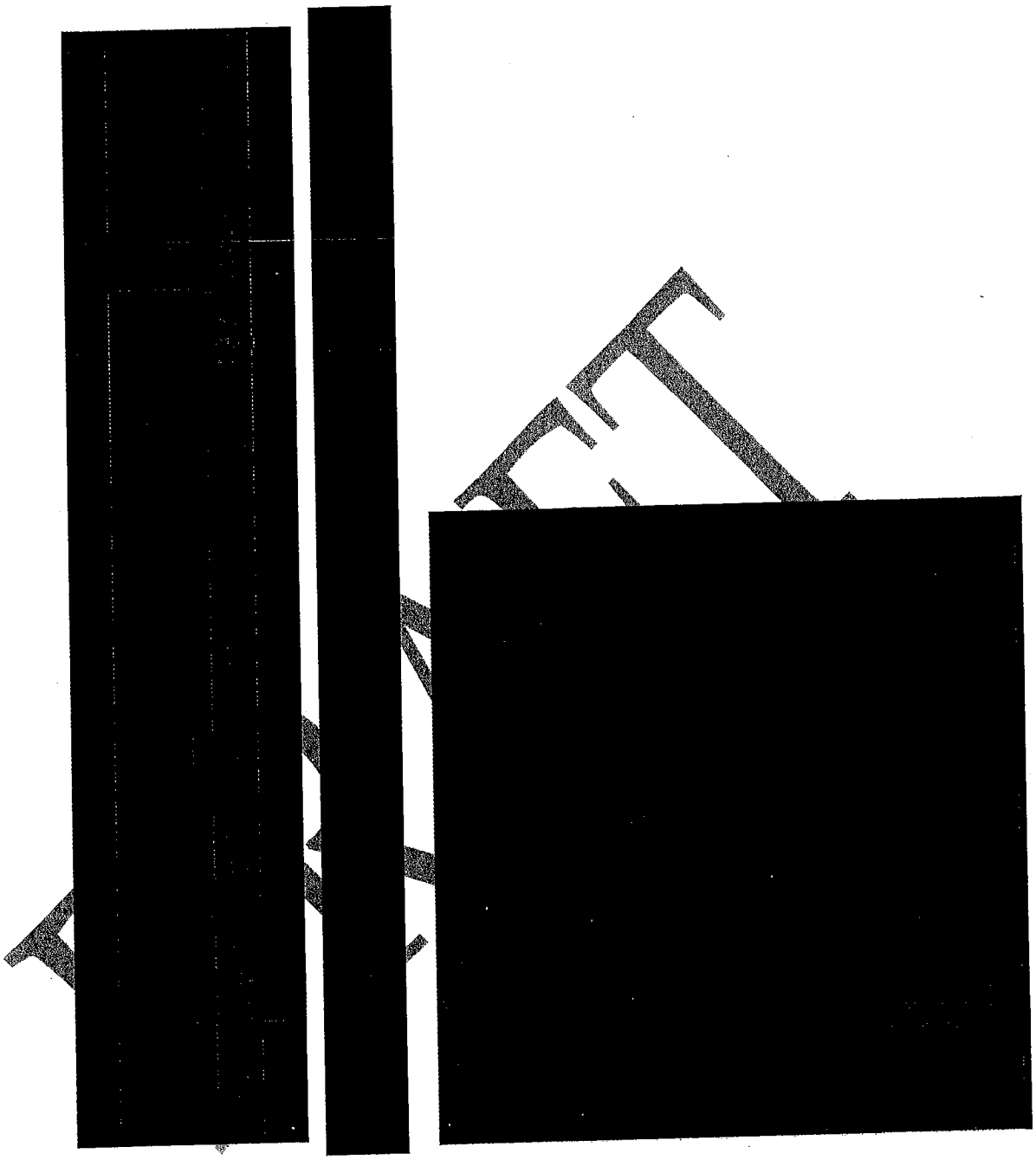

Figure 11. Three views of SAGE model of Test 506: ignition end to stopping, full view, and a close-up of the seal, the cribs, and the stopping (at the top).

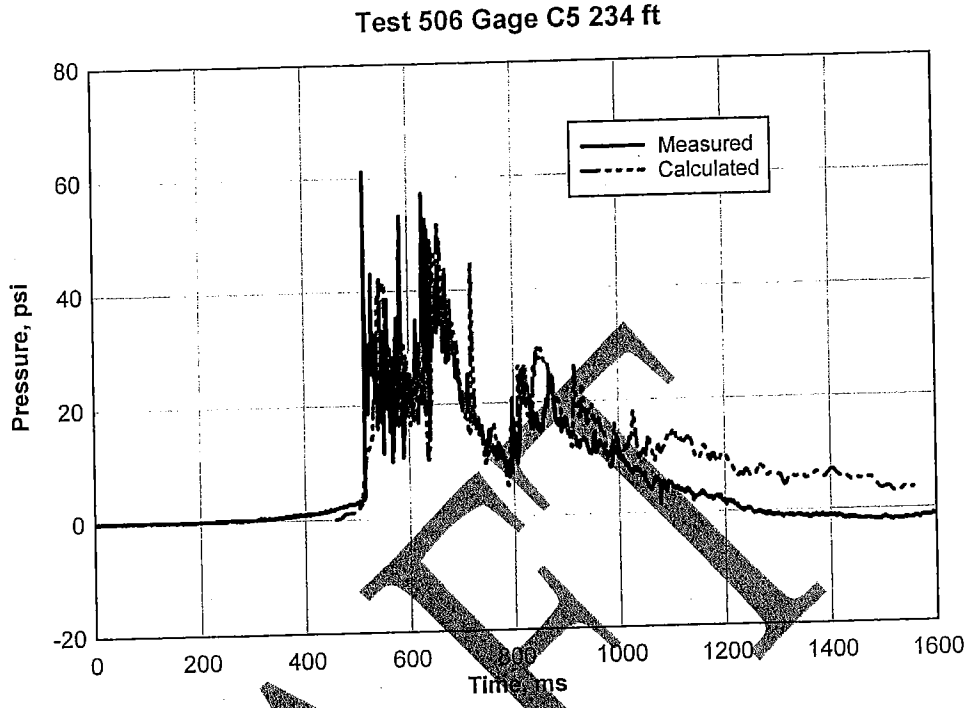

Figure 12. Pressure at Gage C5 LLEM Test 506.

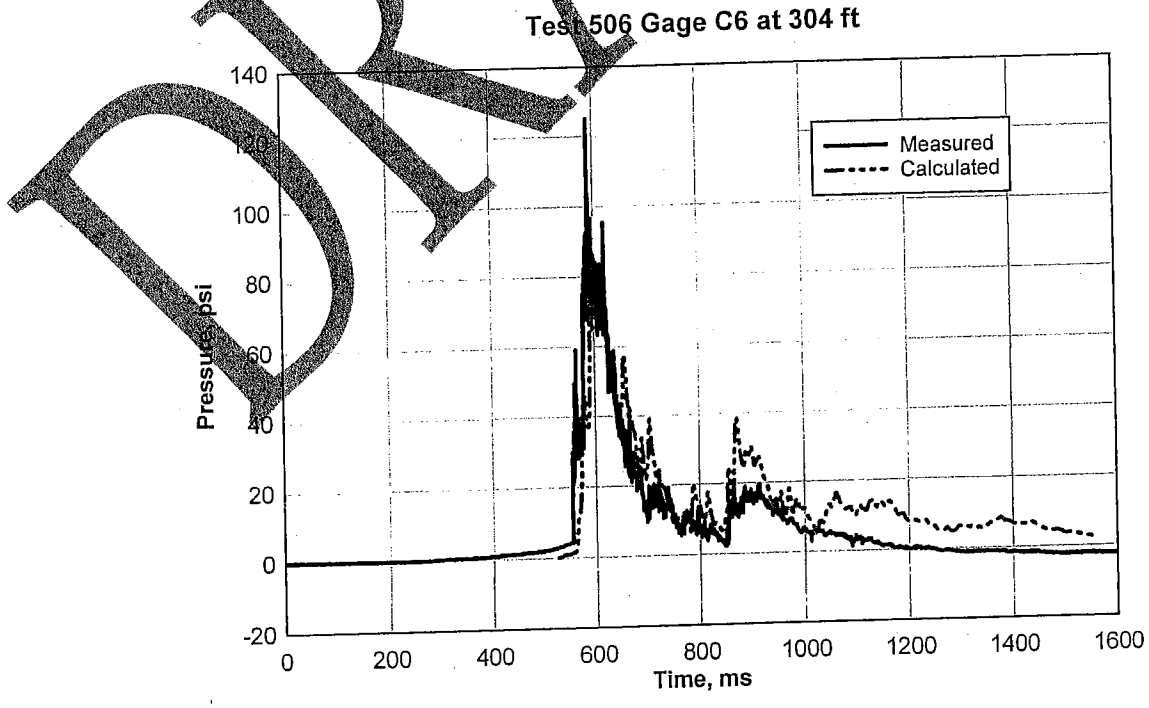

Figure 13. Pressure at Gage C6 in LLEM Test 506.

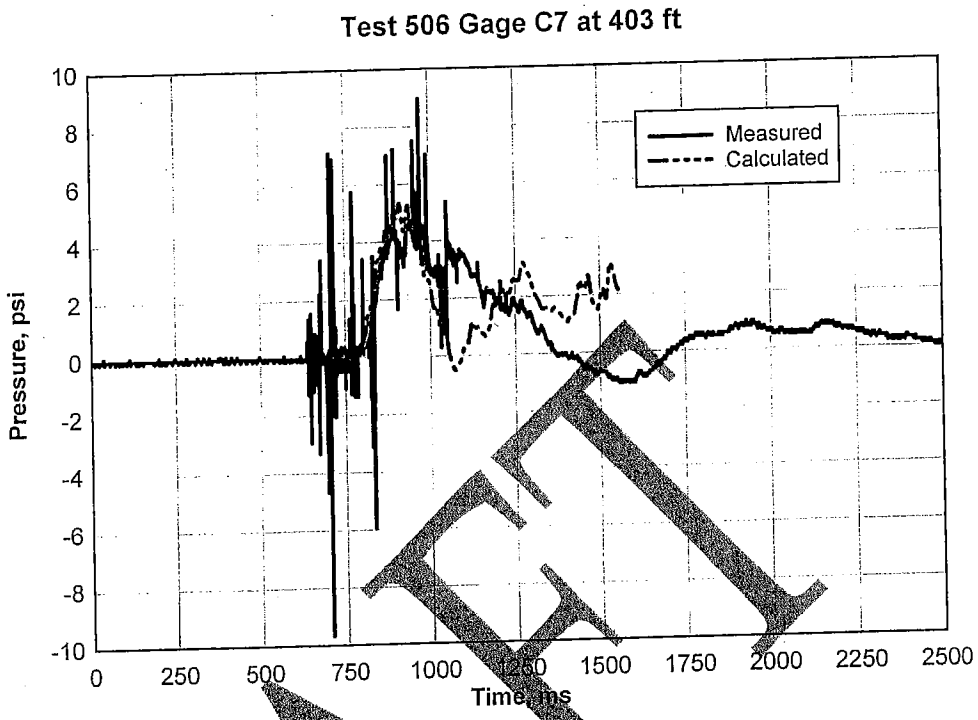

Figure 14. Pressure at Gage C7 in LLEM Test 506.

Problem Set-up

Basic assumptions of SAGE calculations

In all of the SAGE calculations of methane/air explosions, the walls, floors and ceilings of the mines were treated as non-conforming (rigid walls) and heat conduction was ignored. Water that existed in some of the lower elevations of the Sago mine was not explicitly modeled other than affecting the floor-to-ceiling height. Steam produced by the heat of the burned methane was ignored. In Run 3, the 17% methane/air mixture was treated as inert and was not allowed to mix with air to produce a less concentrated mixture that would burn.

A two-part Arrhenius burn model was used: (1) a slow initial burn of about 1 m/sec until the combustion interacts with the mine walls, floor or ceiling and (2) a faster burn that matched the burn rate in Tests 347 and 506 in the Lake Lynn Experimental Mine using 9.5% methane/air mixtures. The same burn model was used for 8.0% methane/air. The initial burn was calculated as spherical 1-D and overlaid into the 3-D grid to start 3-D calculations.

The equations of state for the burned methane/air mixtures were generated by the Cheetah code that uses ideal equilibrium thermodynamics. In a mine such as Sago, however, the burn conditions may be less than ideal.

A dry air equation of state (from the SESAME tables of Sandia National Laboratories) at 59 deg F (15 deg C) was used. Cheetah calculations with air at 100% relative humidity (about 1.3% water at 15 deg C) showed that the CJ pressures and velocities were changed from the dry air values by less than 0.6%. The greatest changes were decreases in temperature of 0.68% and 1.86% for 9.5% and 8% methane/air, respectively. Dust entrainment was not treated in these calculations. Large amounts of dust can lower the temperature and pressure and could quench the burn in extreme situations.

Because of the minimum cell dimension of 25 cm (9.84") used in the Sago calculations, the CMU walls were modeled as only one cell width thick. In calculations of wall response, several cells across the thickness are desired.

The cribs are constructed out of 6"x6" hardwood timbers 30" long. Since 6" (15.24 cm) is somewhat less than the minimum cell size, it was not practical to model the detailed shape of a crib. All of the wood in a crib was lumped into a single column that was connected to the floor and the ceiling. Because of the high strength of the wood, the columns did not break and move with the gas flow. In a future calculation it would be desirable to use a smaller cell size and a more realistic

model of the cribs, with blocks that can separate and move with the flow. In the present calculations, movement of the cribs and other debris by the high velocity gas flows was not considered.

For the Second Left Mains(SLM), MSHA provided floor and ceiling elevation contours at 1-ft increments. This roughness is modeled in the calculations as closely as can be realized with the 25-cm minimum cell dimensions. There was no information provided on side wall roughness; consequently, these walls were modeled as smooth. The floor and ceiling roughness generates turbulence and accelerates the combustion and transition to detonation. On the other hand, the roughness generates local reflections that cause some obstruction to the blast propagation through the mine.

Computer resources used in SAGE calculations

All calculations were performed on Cray XT3 computers at either ERDC MSRC or AHPCRC. A total of 25 fully 3-D calculations were performed to model methane/air explosions in the Lake Lynn Experimental Mine with various mine configurations, burn model coefficients, and input for Omega Block walls, CMU ventilation stoppings and cribs. Various selections of minimum computational cell size were used to determine the effect of this parameter. Calculation 25 (Test 506), which was carried to 4 sec with a 25-cm minimum cell size and modeled 420 m (1378 ft) of B and C drifts with crosscuts, required 3,260 cpu-hrs using up to 128 cpus. Axi-symmetric calculations of the pipe tests of Kuznetsov, et al were performed in 2-D, and required less than 100 hrs, even with very fine zoning.

The calculations in the Sago mine were all 3-D and consumed much greater resources. A preliminary calculation, Run 1a, of the sealed SLM filled with 9.5% methane/air and using 12.5-cm minimum cells required 23,700 cpu hrs to obtain 383 msec of simulation time. The calculation used 512 cpus and from 49 to 59 million cells. The final Run 1 with 25-cm minimum cells required 12,000 cpu hrs to obtain 1,395 ms of simulation time using from 12 to 14 million cells. Time steps varied from 0.02 msec when high-pressure shock waves were active to 0.094 msec near the end of the calculation.

Runs 2 and 3 modeled a much larger portion of the mine and also treated the solid materials of the Omega Block seals, CMU ventilation stoppings, and cribs, and required much larger resources. Run 2 was carried to 1,539 msec of simulation time and required 137,700 cpu hrs. From 31 to 40 million cells were used on 512 cpus. Time steps varied from 0.02 msec to 0.03 msec for most of the calculation but increased to 0.048 msec in the last 500 msec of the simulation.

Run 3 was carried to 2,233 msec of simulation time and required 330,000 cpu hrs using from 512 to 1024 cpus. The number of cells ranged from 30 to 34 M. The time steps varied from 0.02 to 0.048 msec in the first 800 msec of the simulation, and then decreased to 0.025 msec around 1000 msec of the simulation. From that time on, the time step continued to decrease (rather than increase as in Run 2) and was 0.018 msec at the end of the calculation.

Sago mine model

The geometry of the portion of the Sago mine used in the SAGE hydrocode calculations was developed from 2-D AutoCAD drawings provided by MSHA. The drawings for the sealed SLM contained elevation contours at one foot increments from the engineering surveys. Using the computer code SolidWorks, each of the contours from the AutoCAD file were imported and converted to a fully 3-D model. The file was then exported as a stereolithograph (STL) file that could be read into SAGE. The AutoCAD drawing provided for the region of the mine outside the sealed area did not contain detailed elevation information. In this case, a constant ceiling height of 2 m (6.56 ft) was used. SolidWorks was again used to import the 2-D files and produce a 3-D model. The drawings inside and outside the SLM did not perfectly match, and work was required to merge the 3-D models near the seals.

The portion of the Sago mine modeled in our calculations is shown in Figure 15. Three files, one for each of the colored regions, were produced and merged as needed for the various calculations. The sealed SLM is shown as the turquoise-colored region. A large volume of air was connected at the upper left of the rose-colored region to serve as a vent sink simulating the remainder of the mine. The purple line goes through the region of the seals. In Run 3 the SLM was split into two regions (and two files) at the Elevation 1408 ft, which is 30.5 ft above the lowest point of SLM. In SAGE this height was rounded off to 930 cm (30.512 ft).

The final SAGE calculations, designated Run 1, Run 2, and Run 3, used a minimum computation cell that was a cube 25 cm (0.8202 ft) on each side. Thus, the resolution of any dimension was to the nearest multiple of 25 cm. In Runs 2 and 3 the model of the mine outside the seals contained 16,100,000 ft^3 of air. In Runs 1 and 2 the methane/air volumes from SAGE were 3,320,000 and 3,280,000 ft^3, respectively. In Run 3 the volume of gas in the SLM obtained by SAGE was 3,300,000 ft^3, which is 12.4% higher than the value of 2,938,157 ft^3 obtained from the survey by Alpha Engineering. In a preliminary calculation of a sealed SLM (Run 1a) using a smaller cell dimension of 12.5 cm, the volume computed by SAGE was 3,147,000 ft^3 (7.09% higher than the measured value), indicating that as the

cell size is decreased, the SAGE volume approaches the measured value. In Run 3 the realized distribution of 8% methane/air and 17% methane/air was 62.5% and 37.5%, respectively.

Figure 16 shows a horizontal cut through a portion of SLM near Spad 4010, where initiation of the explosion was assumed to occur. The drawing shows an example of the floor contours as modeled in the SAGE calculation. The blue hemisphere represents an initiation region. As shown here, the region intersects the floor. Subsequently, the region was reduced to 1 m diameter and positioned so that it did not intersect the floor, ceiling or side walls. In the calculations for the Sago mine, the explosion was started from a 2.5 Joule spark in a sphere of the methane-air mixture. An Arrhenius burn model with an average burn rate of 1 m/sec was used for this initial burn. At the time the burn reached a radius of 0.5 m, the 1-D spherical calculation was stopped and was used to initiate the 3-D calculations.

Figures 17-19 show the locations of stations (in red) in the SAGE calculations at which waveforms of pressure, density, particle velocity, and temperature were output and the corresponding spad numbers. Stations 1-134 were used in Run 1, Stations 1-188 were used in Run 2, and all 191 stations were used in Run 3. The initiation point near Spad 4010 is in the center of the intersection between stations 122-125. Seals are shown as triple blue lines and named S1 through S10. The ventilation stoppings and overcasts are shown as double green lines. The stoppings are named A through NN, and the overcasts are named OO-VV. Figure 20 shows the placement of seals and cribs, the meshing of the SLM with the outby entries, and floor contours in SLM.

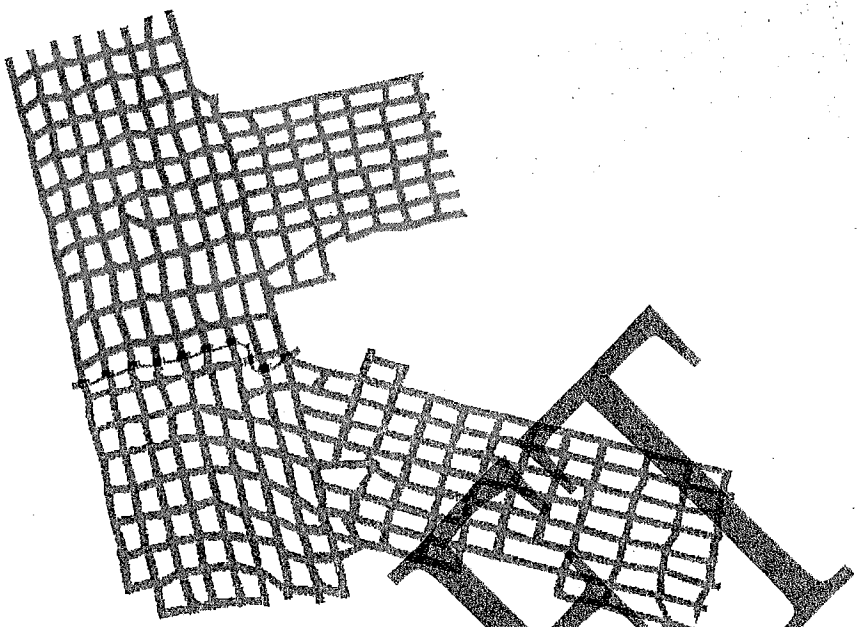

Figure 15. Area of Sago Mine modeled in the SAGE Calculations; blue sealed area; red, portion of Second North Mains and part of Second Left Mains; yellow, remainder of Second Left Mains.

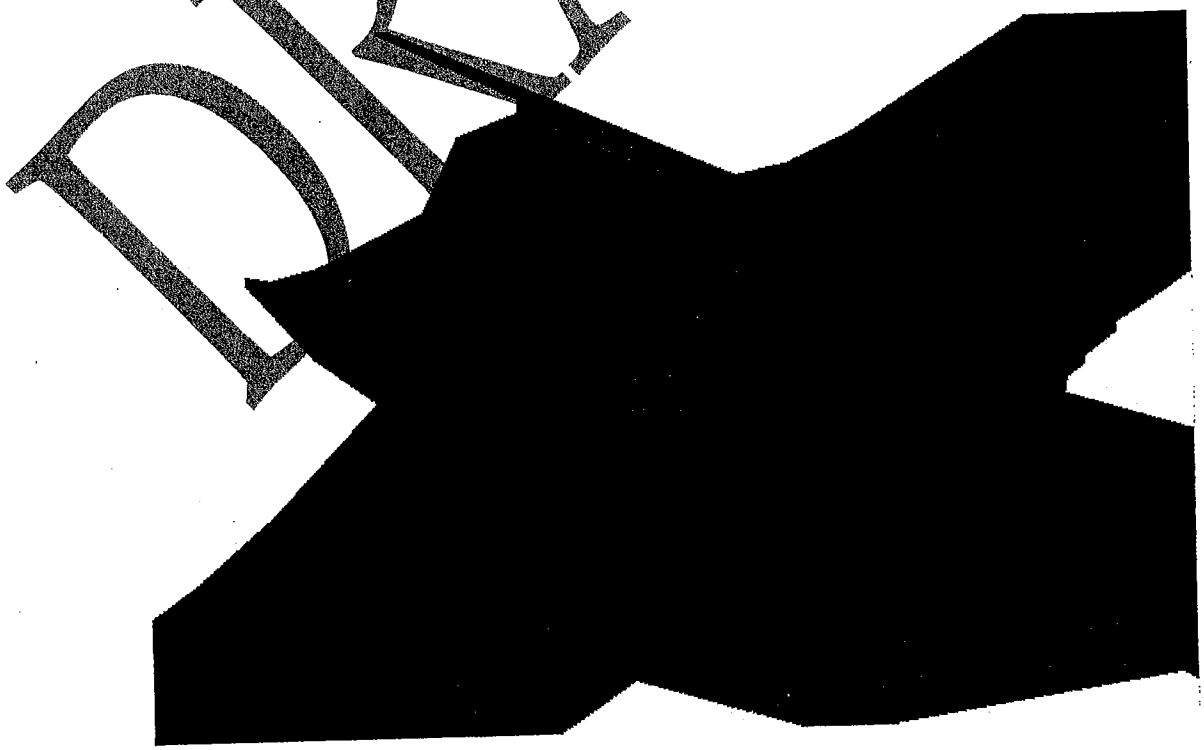

Figure 16. Horizontal cut of the Second Left Mains region where initiation occurred.

Figure 17. Output stations in inby portion of Second Left Mains (a) and corresponding spad numbers (b)

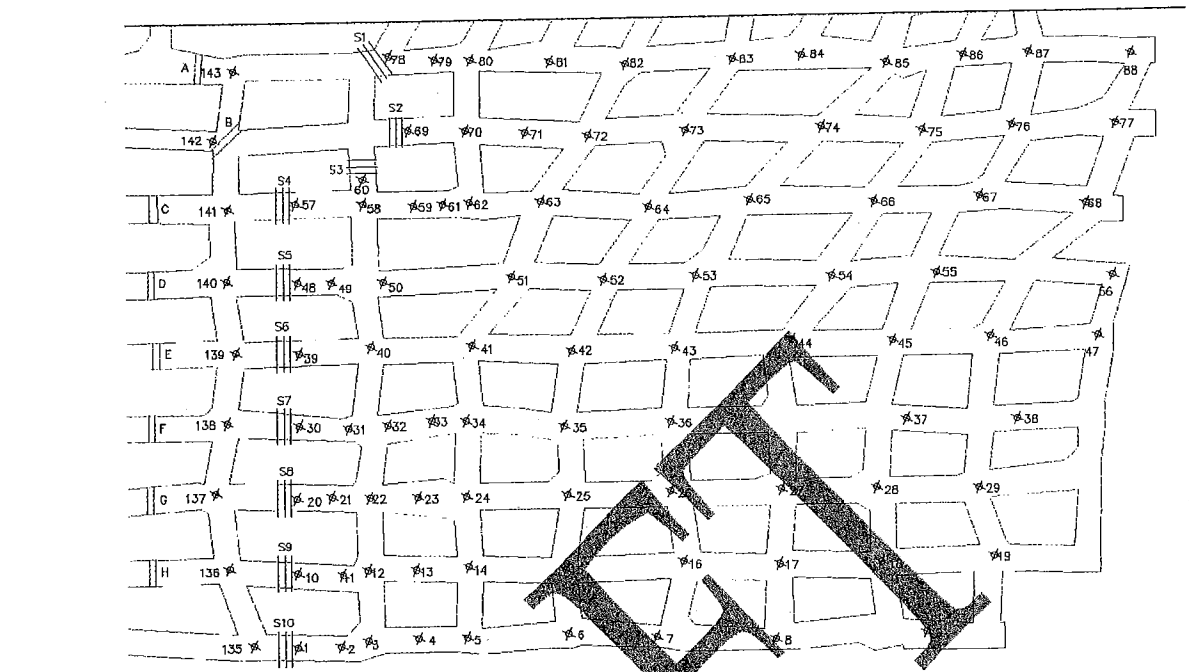

(a)

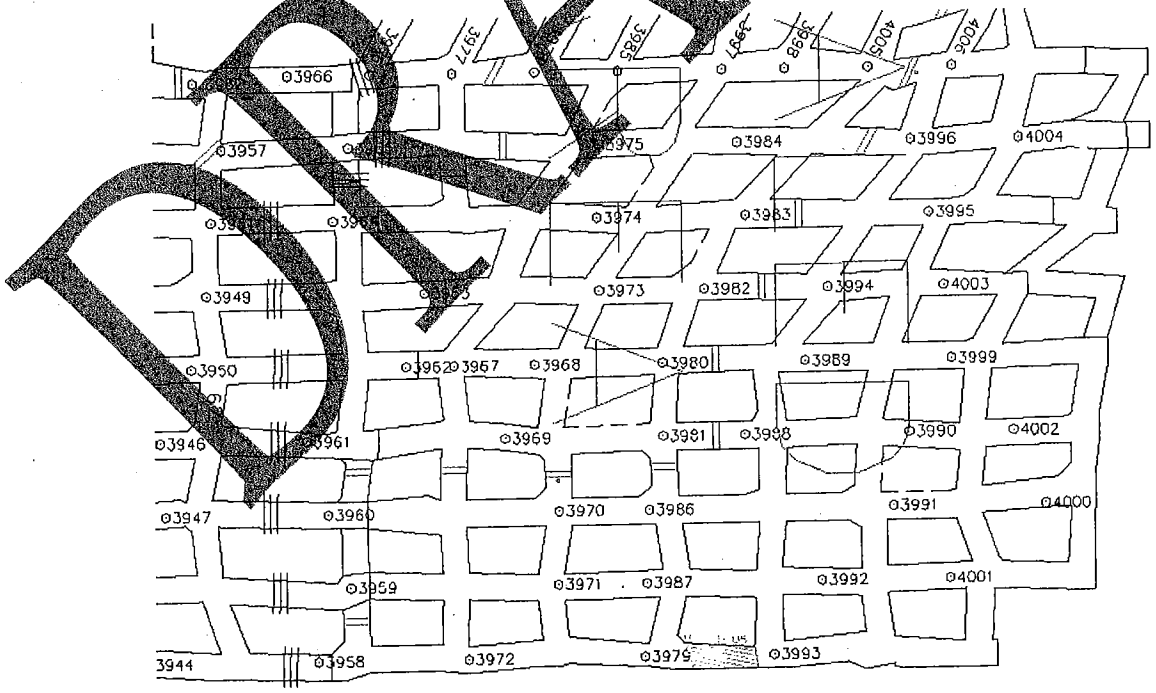

(b)

Figure 18. Output stations inby of seals (a) and corresponding spad numbers (b)

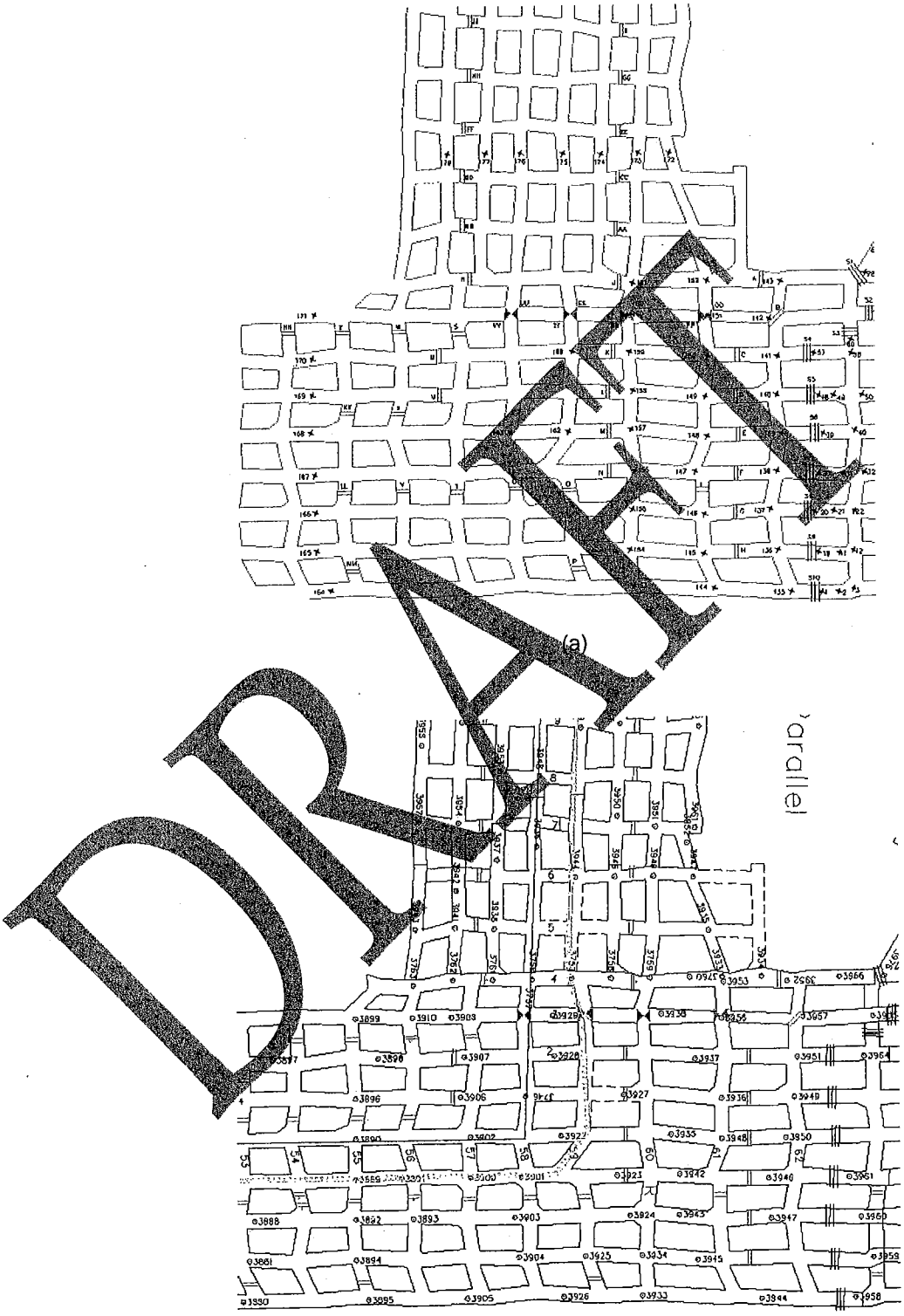

Figure 19. Output stations in Second Left Parallel and Second Mains, including stoppings and overcasts (a) and the corresponding Spad numbers.

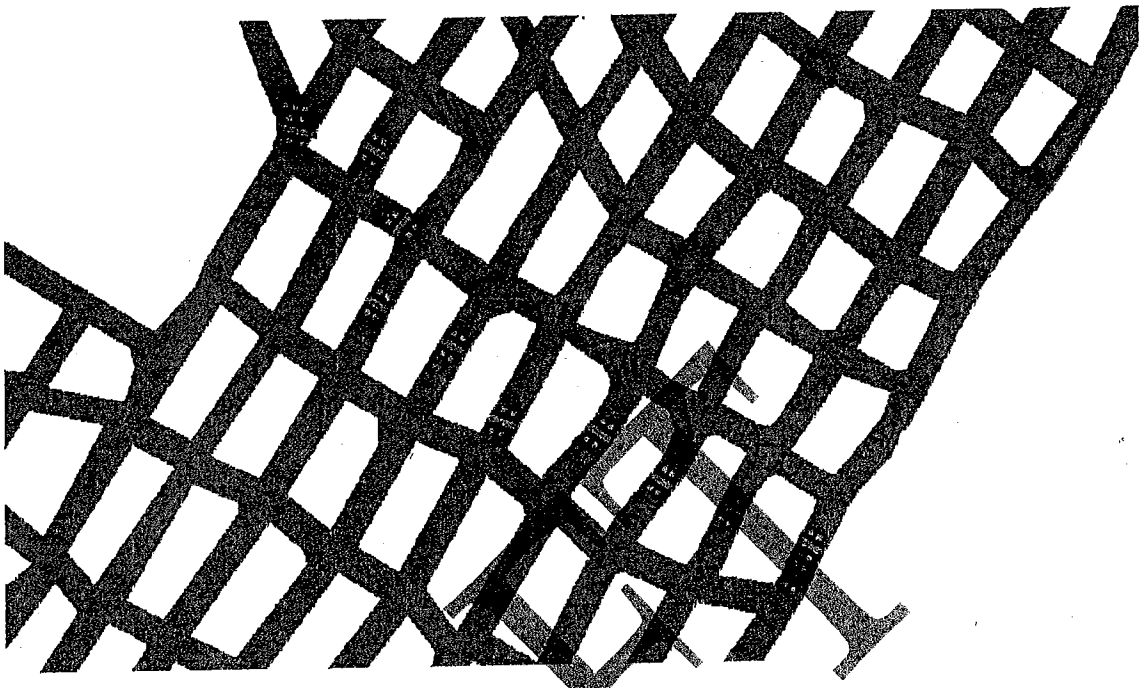

Figure 20. View of the placement of seals and cribs, with floor contours.

Results of Calculations or the Sago Mine

Runs 1 and 2: Second Left Mains with 9.5% methane/air

Runs 1 and 2 were intended to investigate what could be considered the "worst case" pressure loads that could be generated from a methane explosion in the mine. The volume of the Second Left Mains (SLM) was filled with 9.5% methane/air mixture (by volume) that is near the ideal mixture for combustion and detonation. In Run 1, rigid walls were placed at the locations of the seals and only the SLM was modeled, so there was no venting to the mine outby the seals. In Run 2, Omega Block seals, cribs, ventilation stoppings, and overcasts outby the seals were added. Venting to the mine outby the seals became important.

The calculations were started (as was Run 3) with a 1-m diameter sphere (centered at Elevation 650 cm, or 21.33 ft) of burned gas from a 1-D calculation started with a 2.5 J spark and representing he first 107.6 msec of the simulation. At this time there was little overpressure (less than 1 psi) and velocity (about 10 ft/sec Initially, the burn spreads slowly reaching station 124 (44 ft away) at 261 msec. The acoustic out-running motion arrived earlier at 150 msec. Outby (toward the seals) transition to detonation occurs at Stations 80, 52, and 53 that are distances 306, 312, and 270 ft respectively, from the ignition point. The first evidence of detonation inby is at station 108 located 310 ft from the ignition point. At all of the seals, the pressure and temperature levels indicate that a detonation had occurred. Figure 21 shows a sequence of pressure snapshots as the burn propagates out from the ignition point. Detonation occurs only when the pressure exceeds 200 psi, as indicated by the red areas.

Figure 22 compares pressure waveforms at Station 82, Spad 3985 for preliminary Run 1a, using a 12.5-cm minimum cell size, with results from Run 1, using 25-cm minimum cells. The smaller cells are desirable but would require about 16 times as much computer resources. From this and other comparisons we concluded that 25 cm cells were adequate, and were the smallest that were practical for Runs 2 and 3, using larger portions of the Sago mine. The arrival times of Runs 1a, 1, and 2 differ slightly because the output stations are not at identical locations, and because SAGE gridded the two problems differently. Also, the presence of the solids (Omega Blocks, CMU, and wood) in Run 2 caused finer time stepping at some times. In all direct comparisons, the arrival times of Run 1 have been shifted to align with the curves from Run 1a and 2.

Figures 23-24 compare pressure and particle velocity at Station 1, Seal 10 for Runs 1 and 2. Late time quasi-static pressure is much higher in Run 1 because the hot gases cannot vent out through the seals. In Run 1, the "seal" wall is rigid and the

reflected pressure (592 psi) is about 2.1 times the pressure (280 psi) incident to the wall. Consequently, the total pressure (incident plus reflected) is 872 psi, or about 3.1 times the incident. In contrast, the Omega Block seal of Run 2 is light weight with a low acoustic impedance (density x sound speed), and the reflection is much lower than in Run 1. The total pressure on the seal is about 445 psi. Further, cribs (modeled in Run 2 but not in Run 1) attenuated the blast impacting the seal, to some degree.

When a shock waves impacts the deformable Omega material, stress waves are transmitted into the material as well as reflected. Particle motions are generated inside the Omega material from the front face toward the back. At the same time, a reflected wave in the gas causes particle motions away from the seal. In the case of the rigid wall, there is zero velocity on the wall. The incident and reflected velocity must add to zero. The reflected velocity causes an abrupt change in direction since the Station 1 location is slightly inby of the wall. For the Omega seal, the velocity amplitude decreases because of the reflection but the velocity never fully changes direction because the Omega wall is moving. The wall near Station 1 displaces about 3 ft in 5 msec.

Figures 25-42 compare results from Runs 1 and 2 for a sequence of stations (78-84 and 124) just behind the seals, from Seal 1 back toward the ignition point. This sequence of stations shows how the pressure waveform develops with increasing distance from the ignition. The burn starts slowly and picks up speed as the floor and ceiling roughness, reflections from walls, and collision of converging waves increase the burn rate. The burn transitions to a detonation near Station 81. Figures 43 and 44 show waveforms at other locations in the SLM.

Figure 45 illustrates the pressure attenuation in Entry 5 outby Seal 6. There are significant pressure drops as the pulses destroy Seal 6 and ventilation Stoppings E and M. The pressure, temperature, and particle velocity at Station 162 are shown in Figures 46. The high temperature gas from the burned methane passes this location at about 1 sec. Velocities exceed 1000 ft/s and the pressure is over 50 psi. Figures 47 and 48 show that the pressures at Stations 169 and 171 are still in the 20-25 psi range, but the temperatures are much lower than at Station 162.

Figures 49 and 50 summarize the pressure and temperature at stations in the Second Left Parallel. Burned gas at at temperature over 2000 deg F pass Station 172 at about 1100 msec and Station 173 at about 1460 msec. By the end of the calculation, the peak pressure had exceeded 20 psi at all the stations.

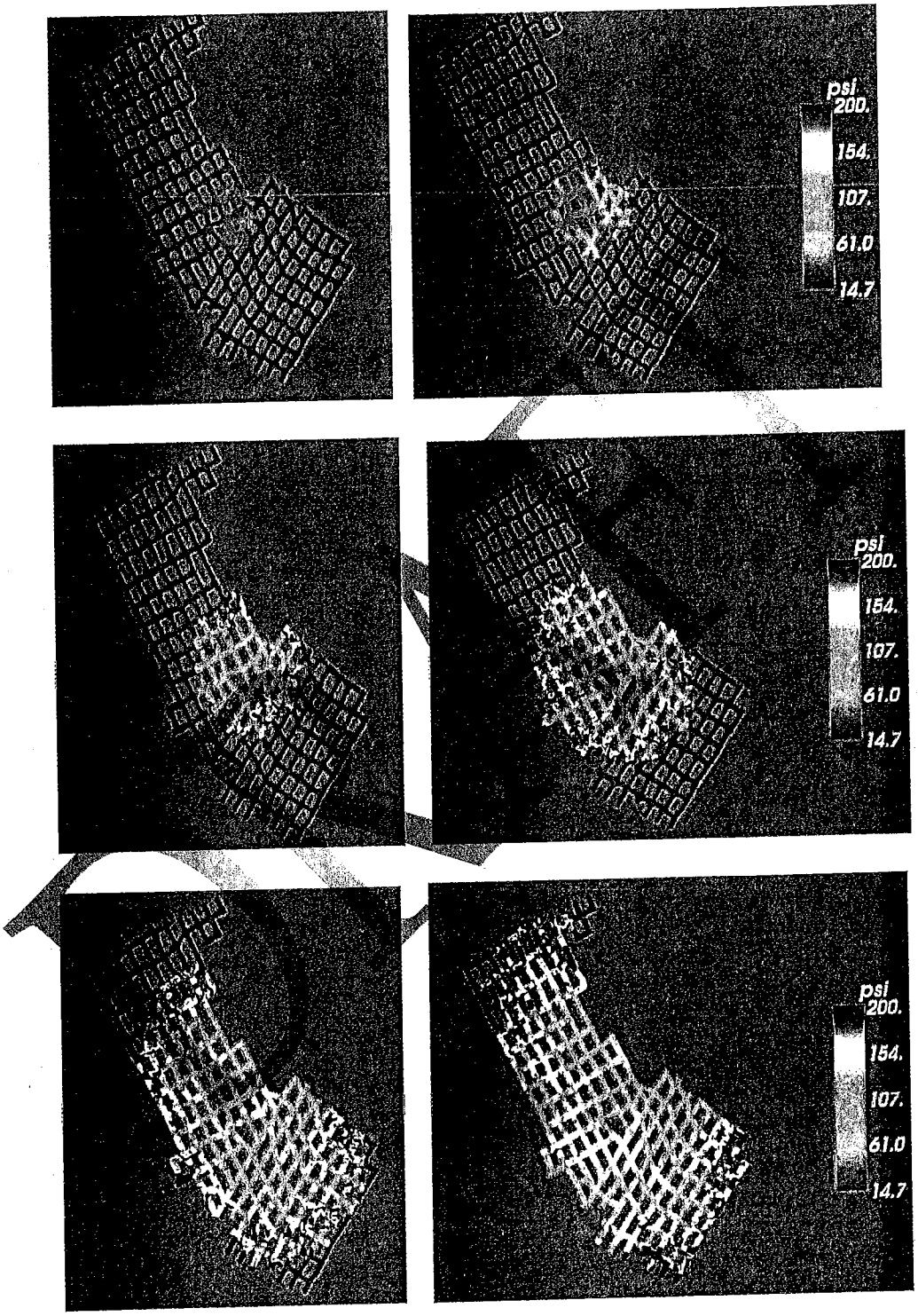

Figure 21. SAGE calculation of the expansion of the methane burn and explosion through the Second Left Mains.

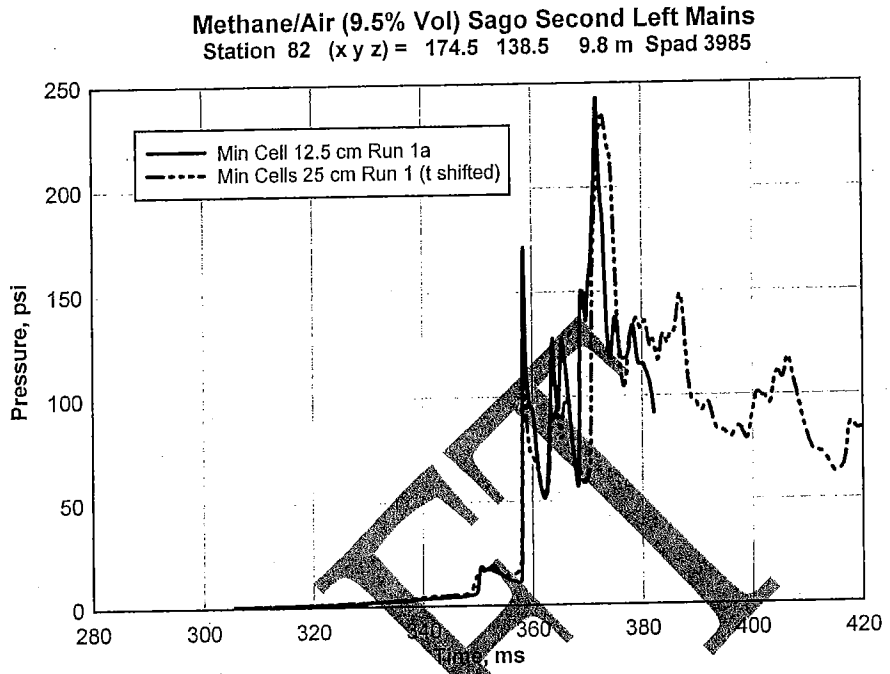

Figure 22. Pressure at Station 82 Runs 1a and 1, with 12.5 and 25-cm cells.

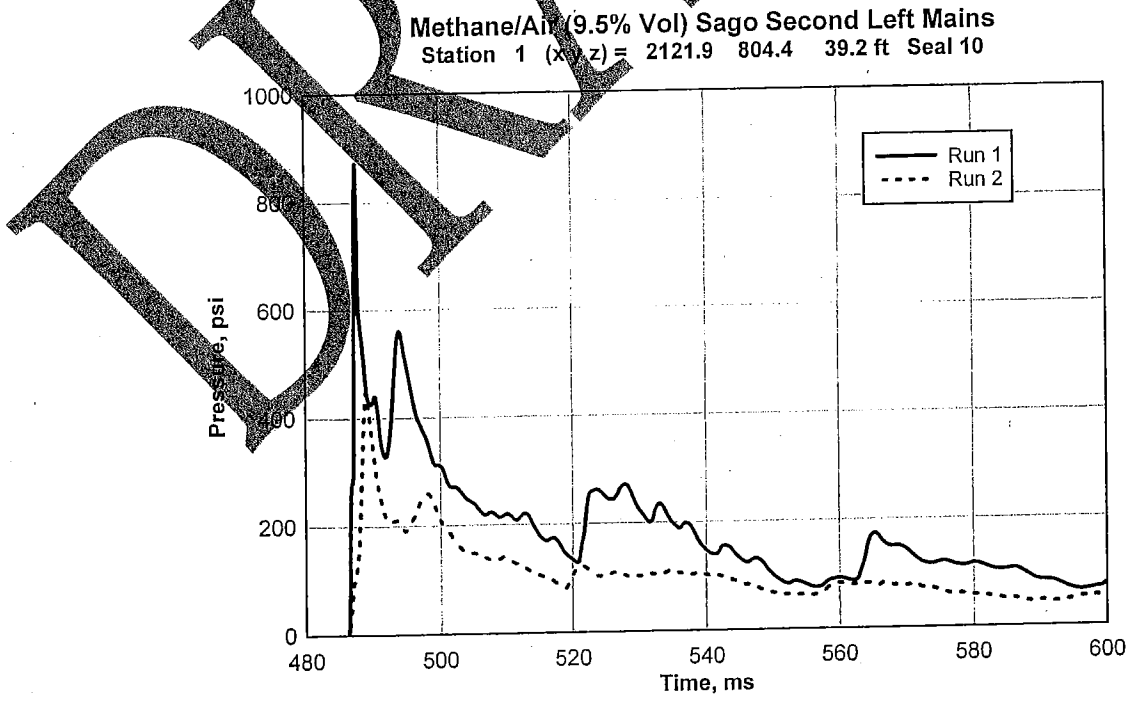

Figure 23. Early time pressure for Runs 1 and 2 at Station 1, Seal 10.

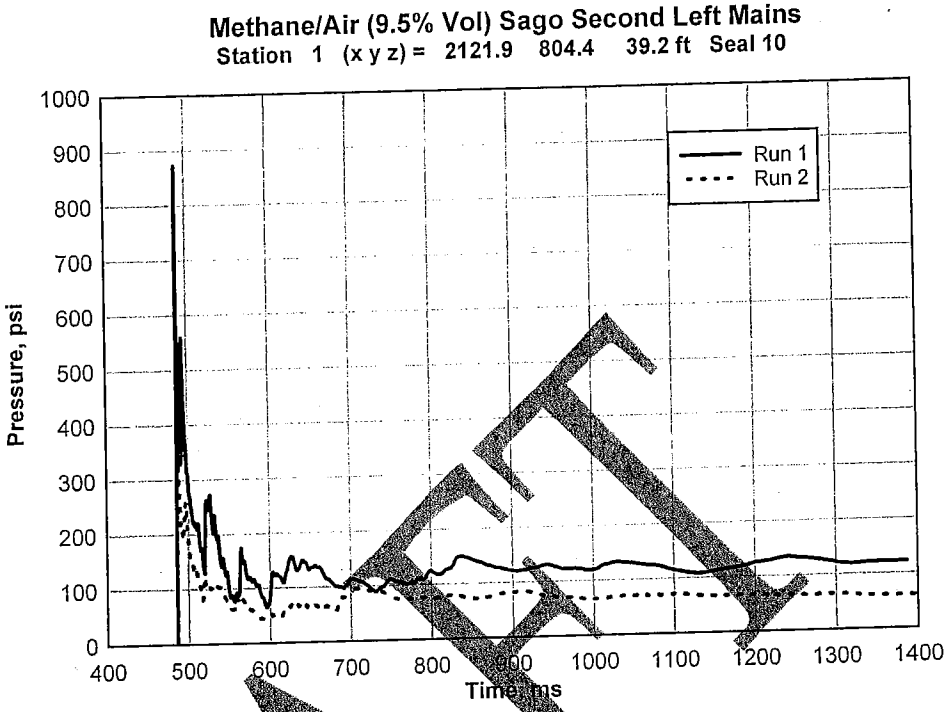

Figure 24. Long duration pressure for Runs 1 and 2 at Station 1, Seal 10.

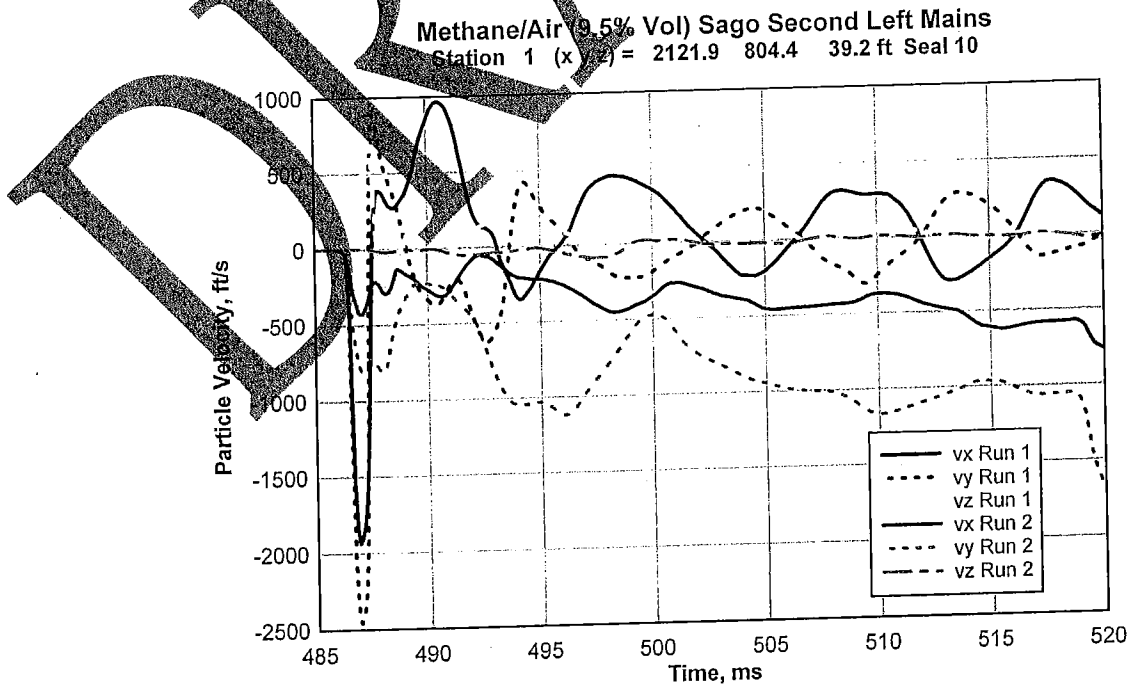

Figure 25. Early time particle velocity Seal 10, Runs 1 and 2.

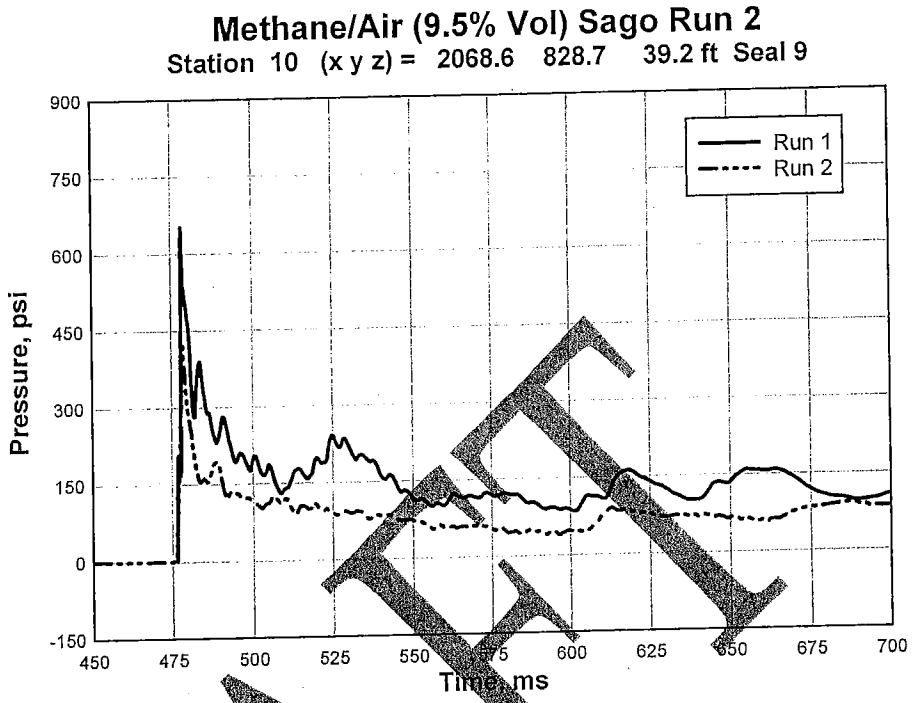

Figure 26. Pressure at Station 10, Seal 9 for Runs 1 and 2.

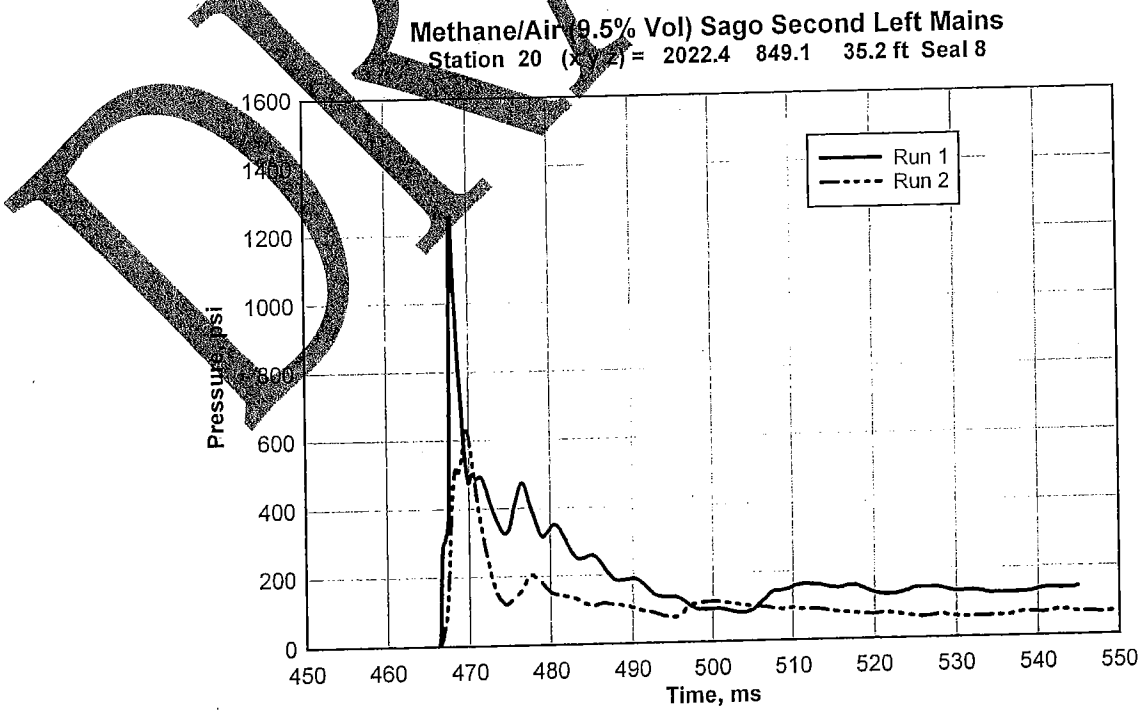

Figure 27. Pressure at Station 20, Seal 8 for Runs 1 and 2.

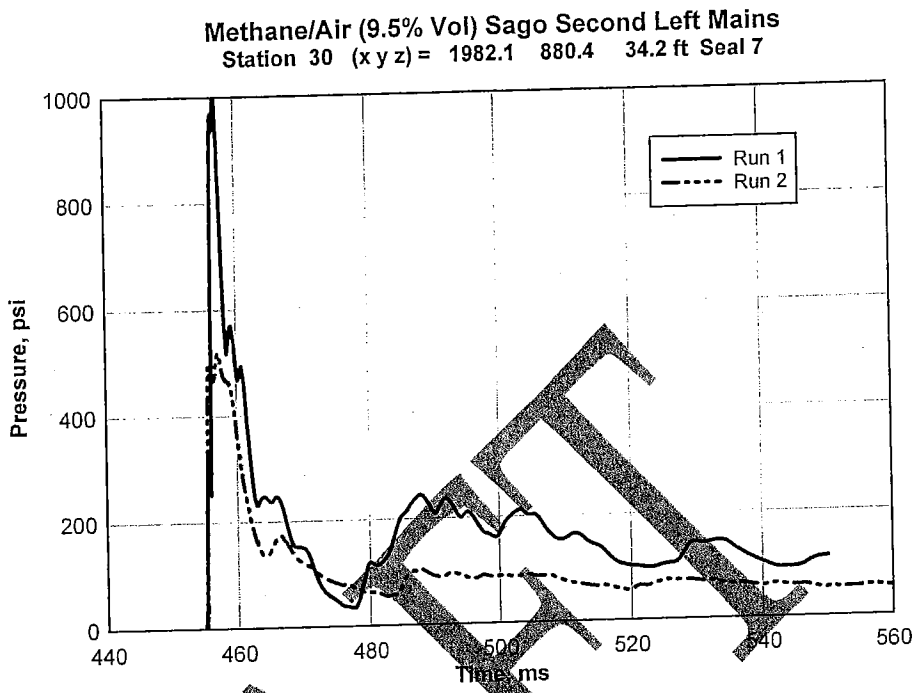

Figure 28. Pressure at Station 30, Seal 7 from Runs 1 and 2.

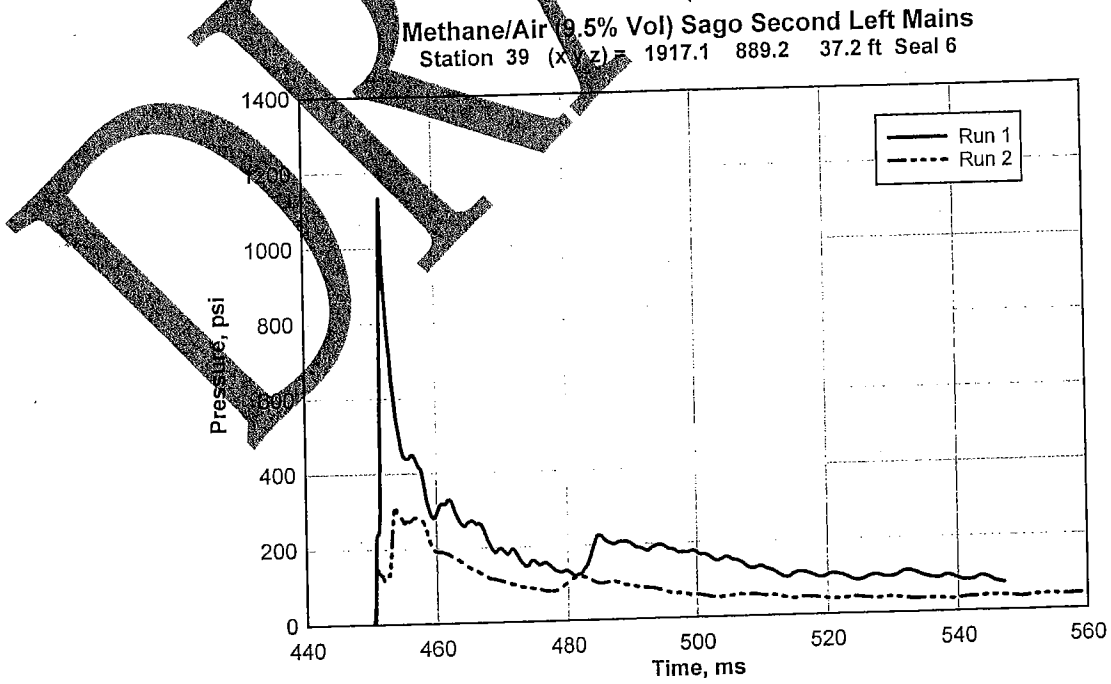

Figure 29. Pressure at Station 39, Seal 6 from Runs 1 and 2.

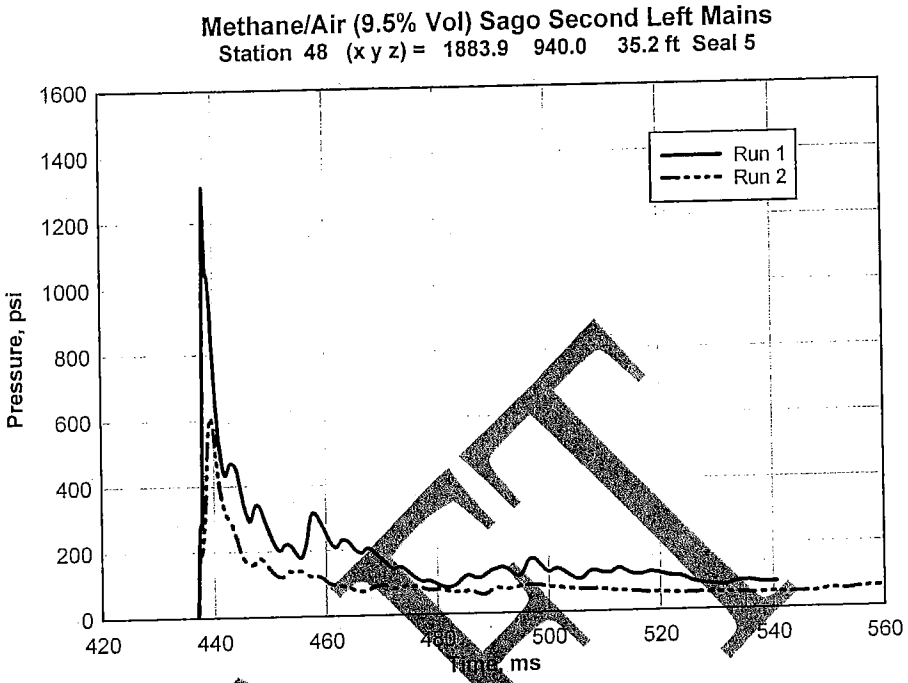

Figure 30. Pressure at Station 48, Seal 5 from Runs 1 and 2.

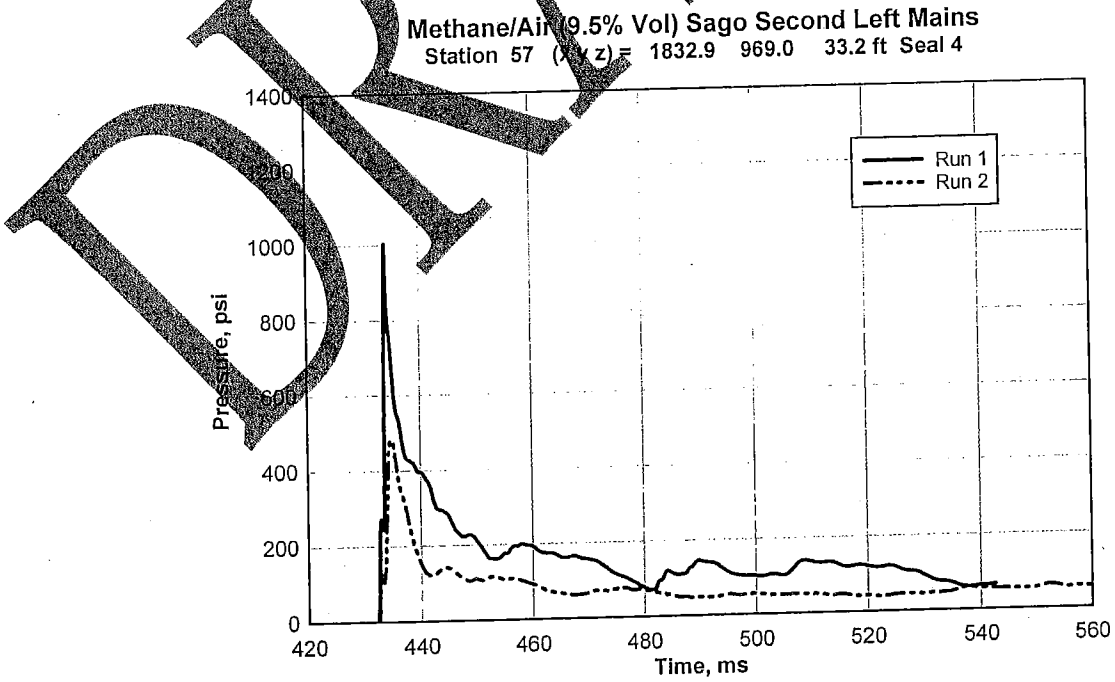

Figure 31. Pressure at Station 57, Seal, from 4 Runs 1 and 2.

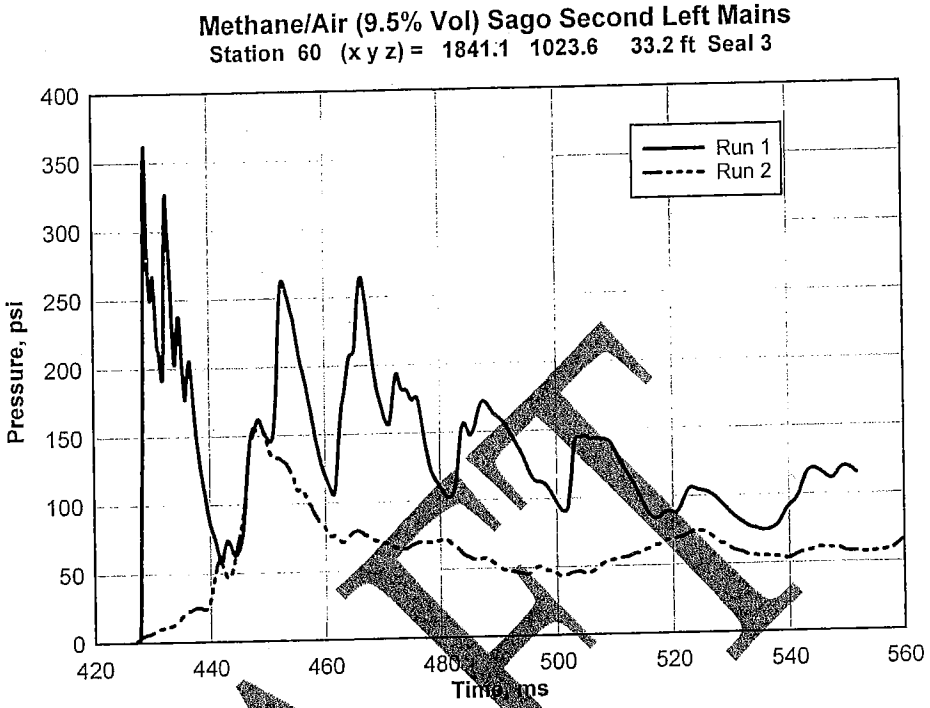

Figure 32. Pressure at Station 60, Seal, from 3 Runs 1 and 2.

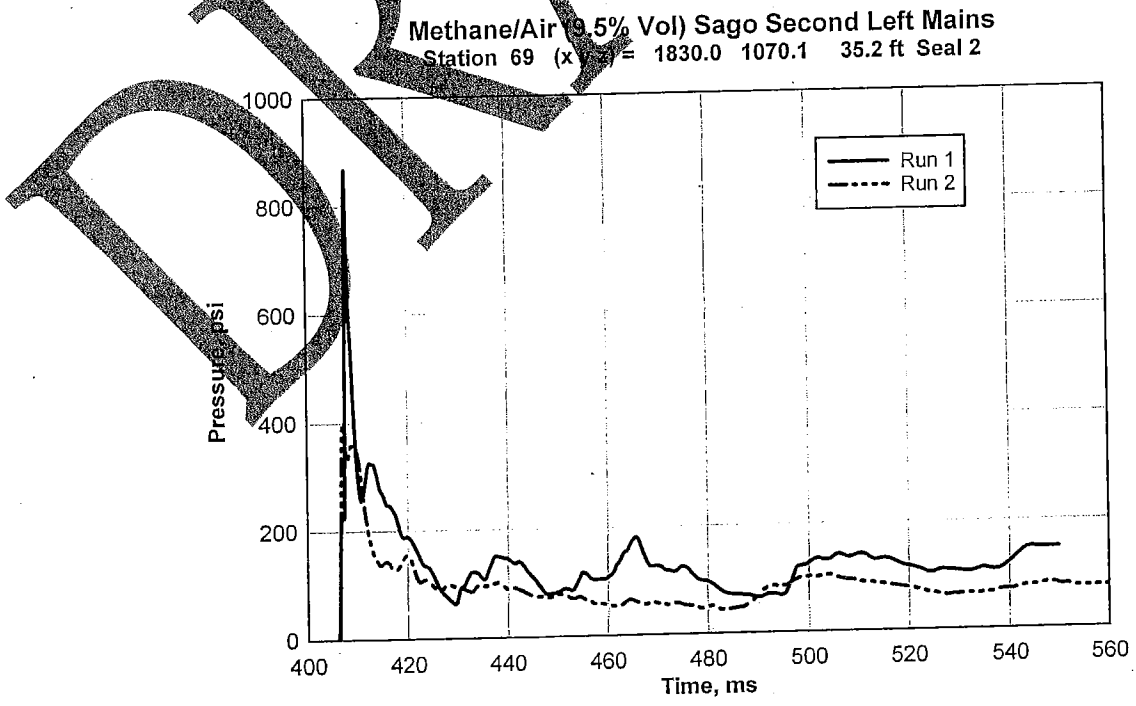

Figure 33. Pressure at Station 69, Seal, from 2 Runs 1 and 2.

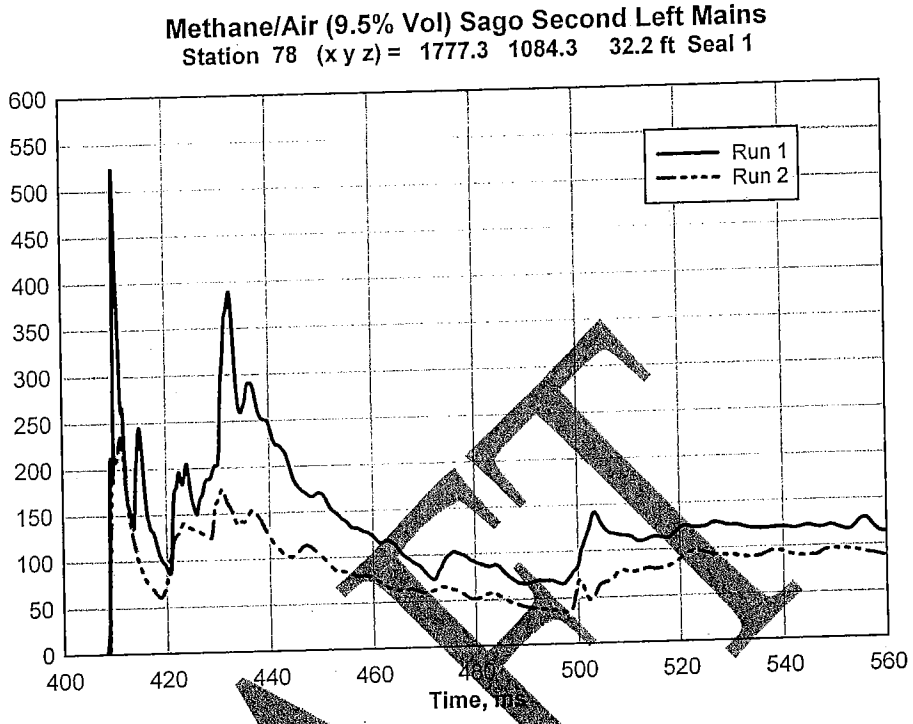

Figure 34. Pressure at Station 78, Seal, from 1 Runs 1 and 2.

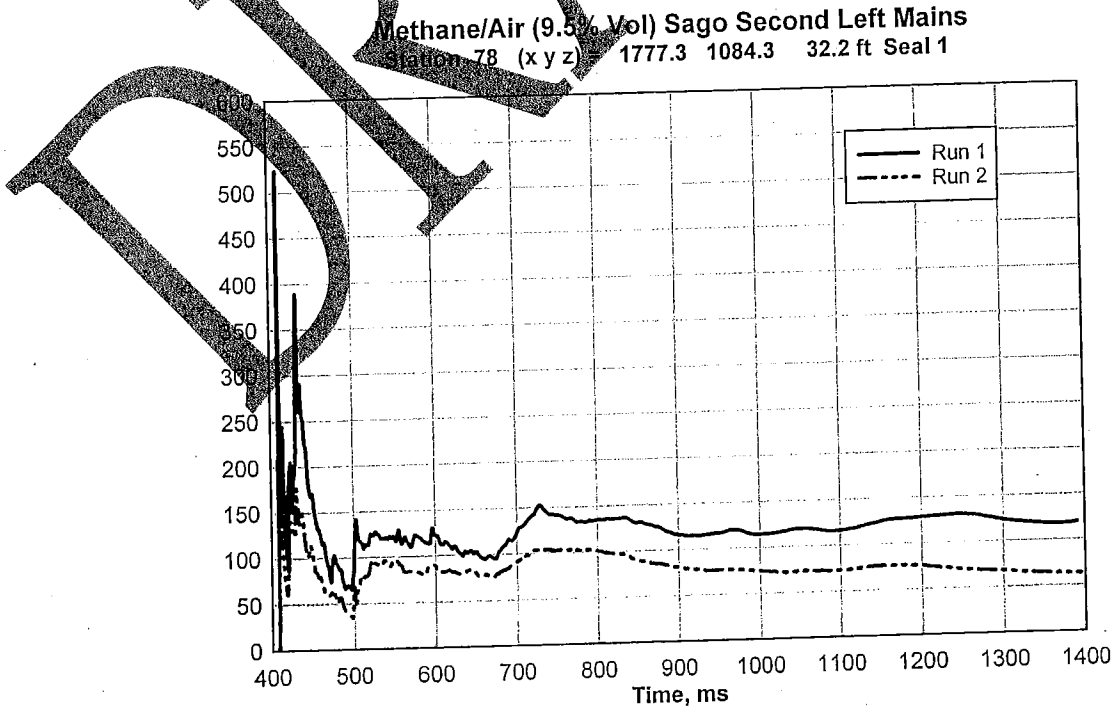

Figure 35. Long duration pressure at station 78, seal 1 Runs 1 and 2.

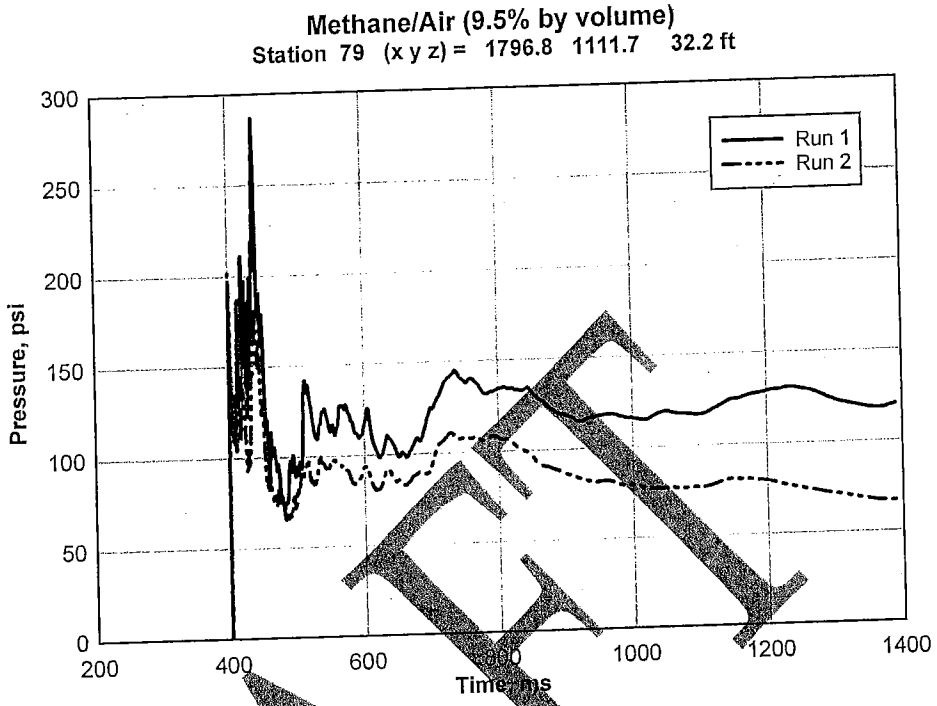

Figure 36. Pressure at station 79, Runs 1 and 2.

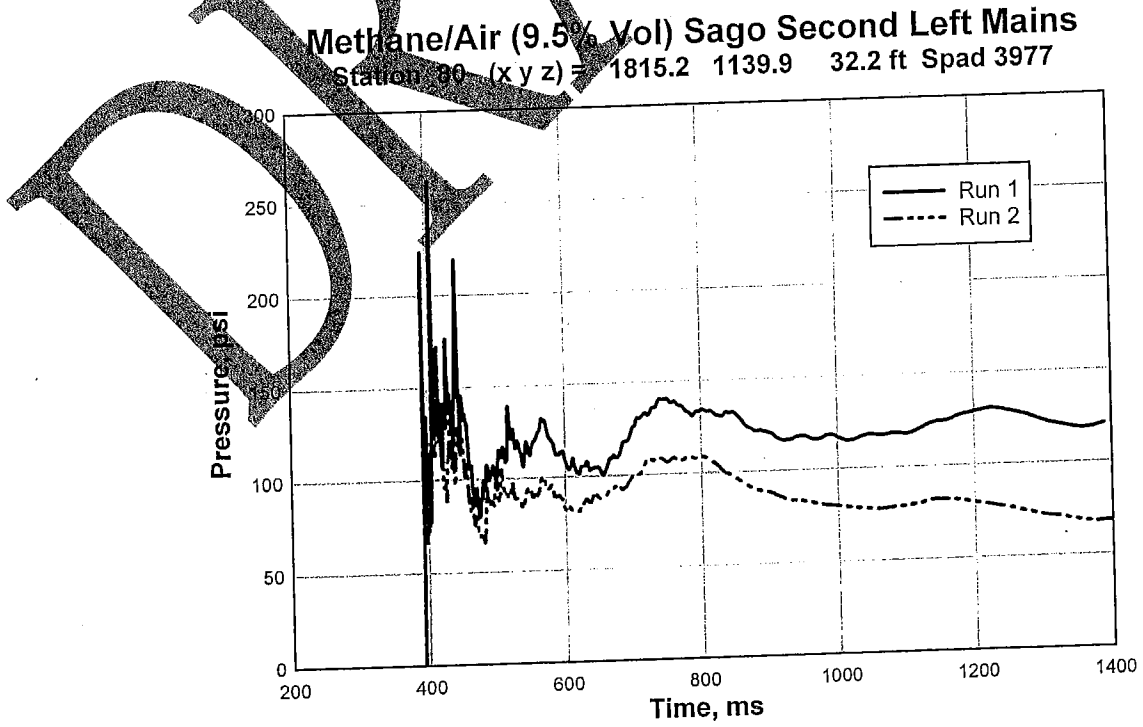

Figure 37. Pressure at station 80, Runs 1 and 2.

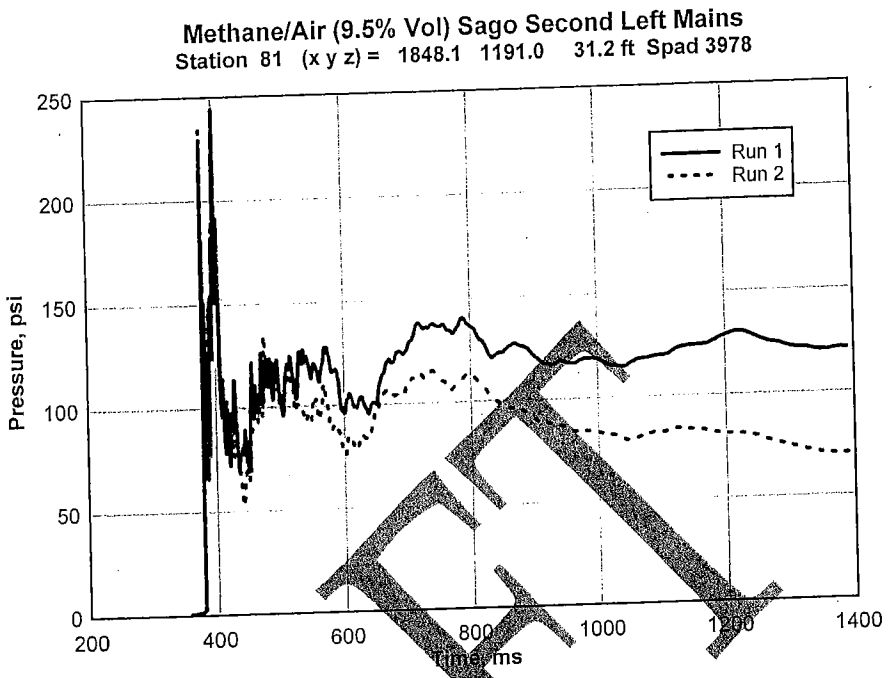

Figure 38. Pressure at station 81, Runs 1 and 2.

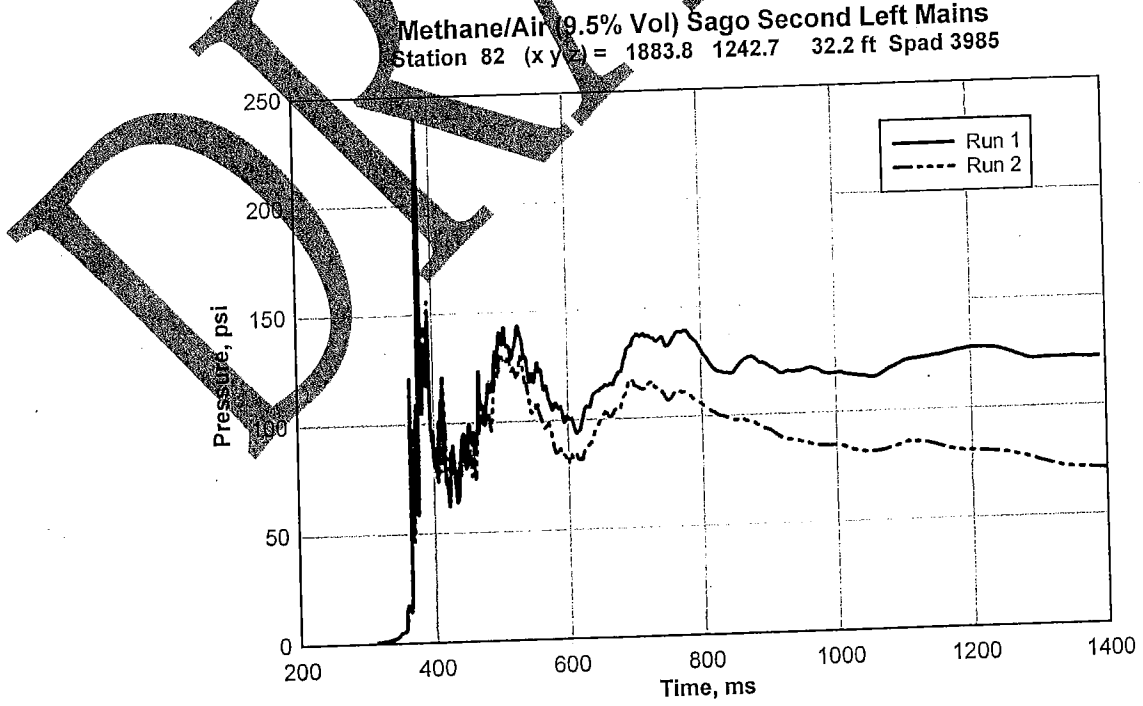

Figure 39. Pressure at station 82, Runs 1 and 2.

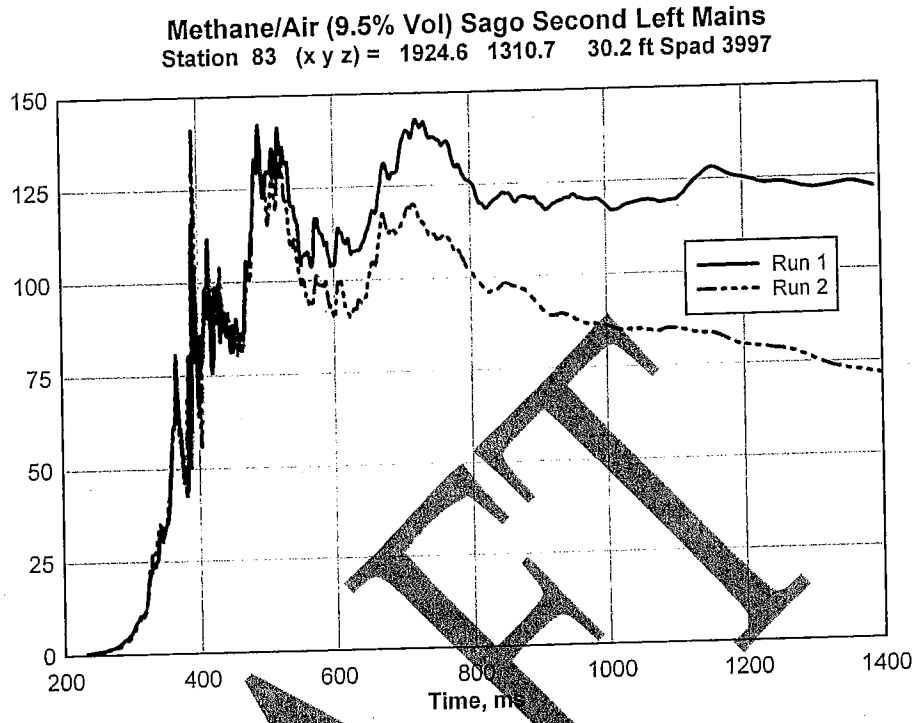

Figure 40. Pressure at station 83, Runs 1 and 2.

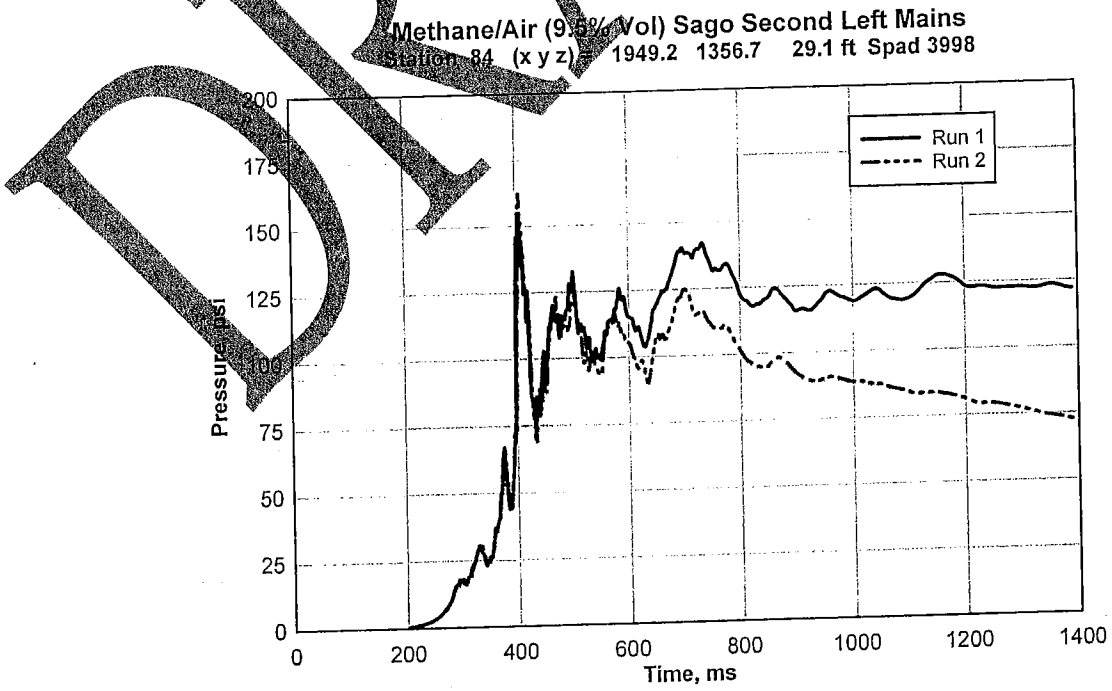

Figure 41. Pressure at station 84, Runs 1 and 2.

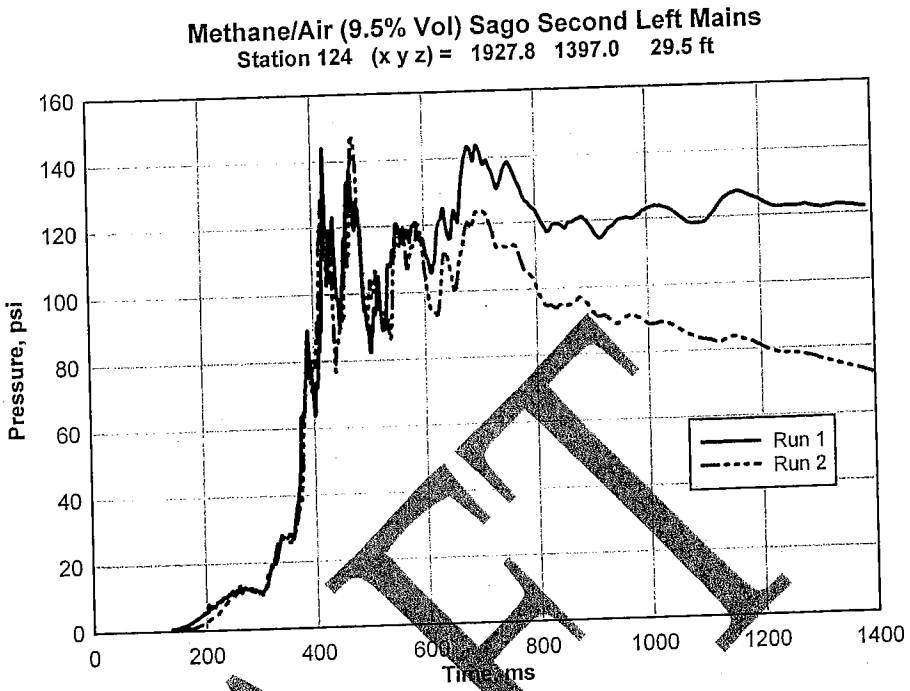

Figure 42. Pressure at station 124, Runs 1 and 2.

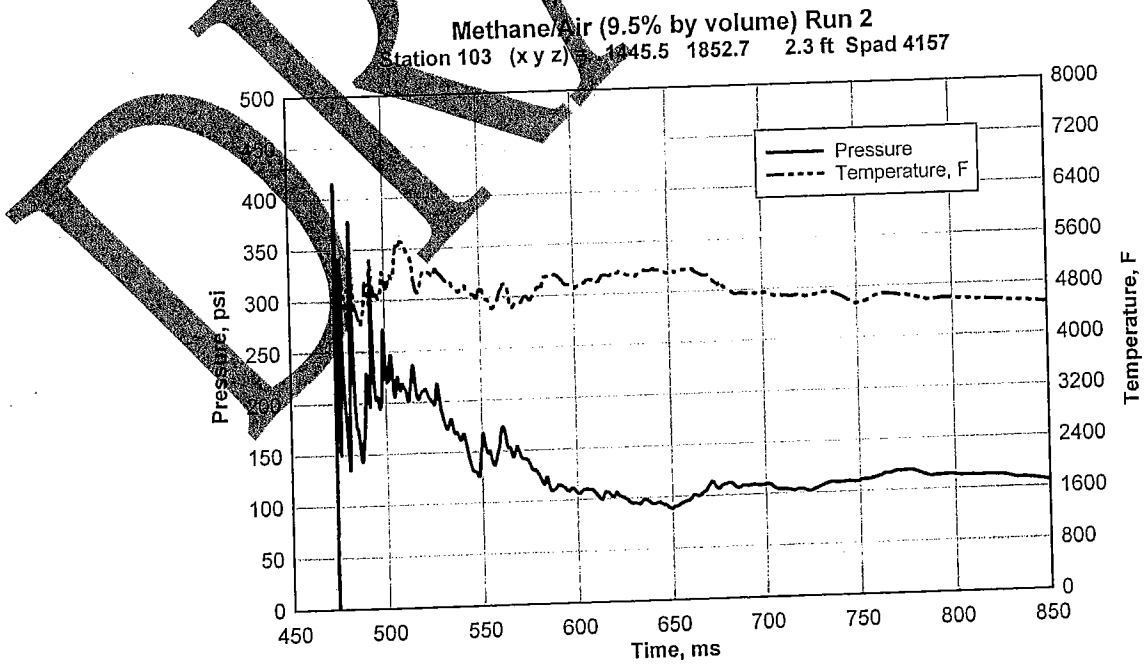

Figure 43. Pressure and temperature at station 103, Run 2.

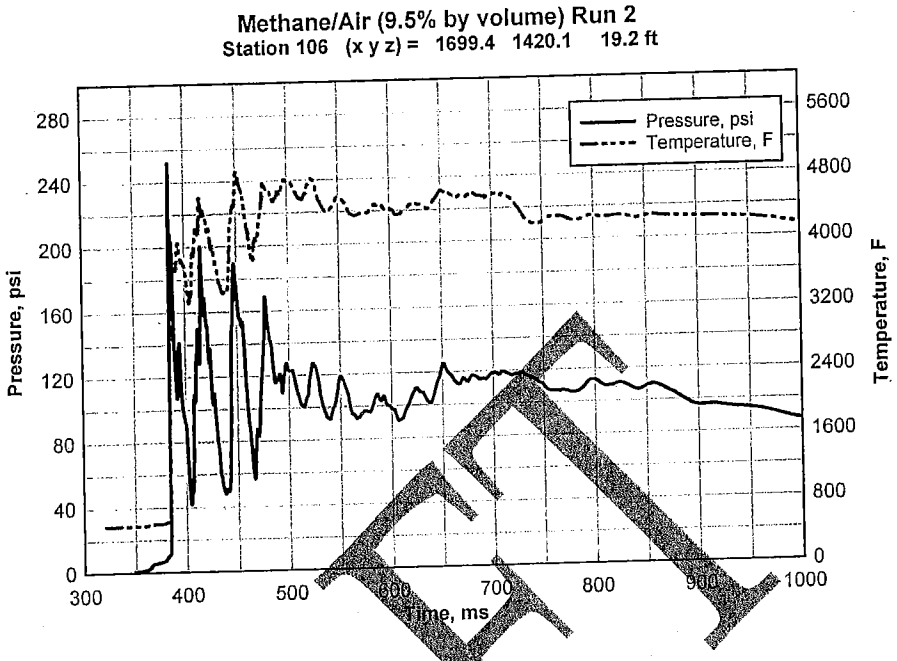

Figure 44. Pressure and temperature at station 106, Run 2.

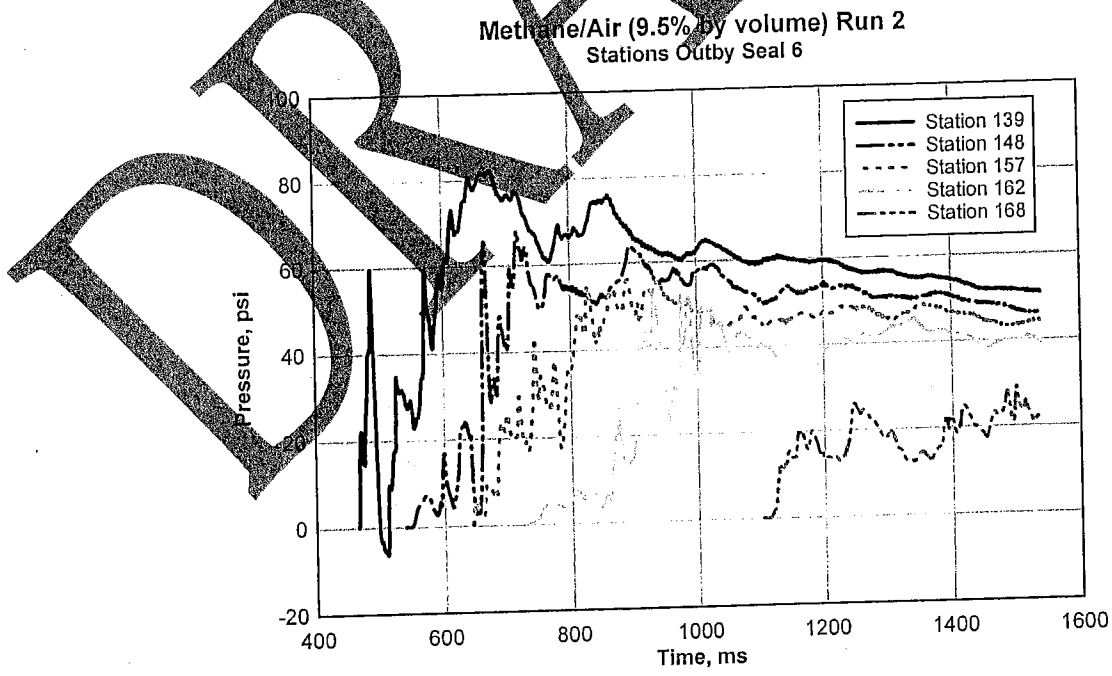

Figure 45. Pressure at stations on entry 5, Run 2.

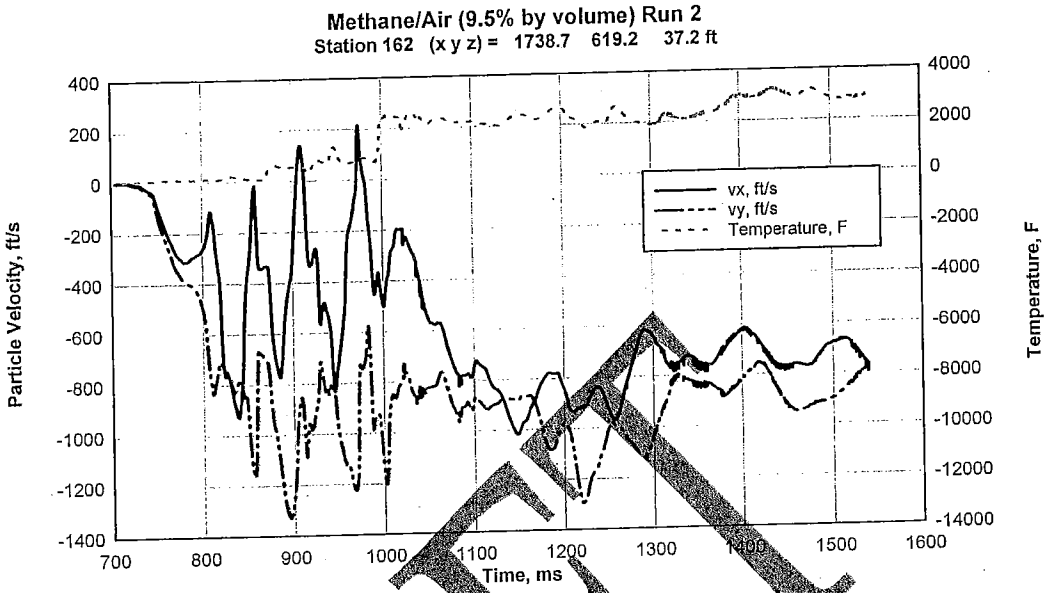

Figure 46. Particle Velocity and Temperature at station 162, Run 2.

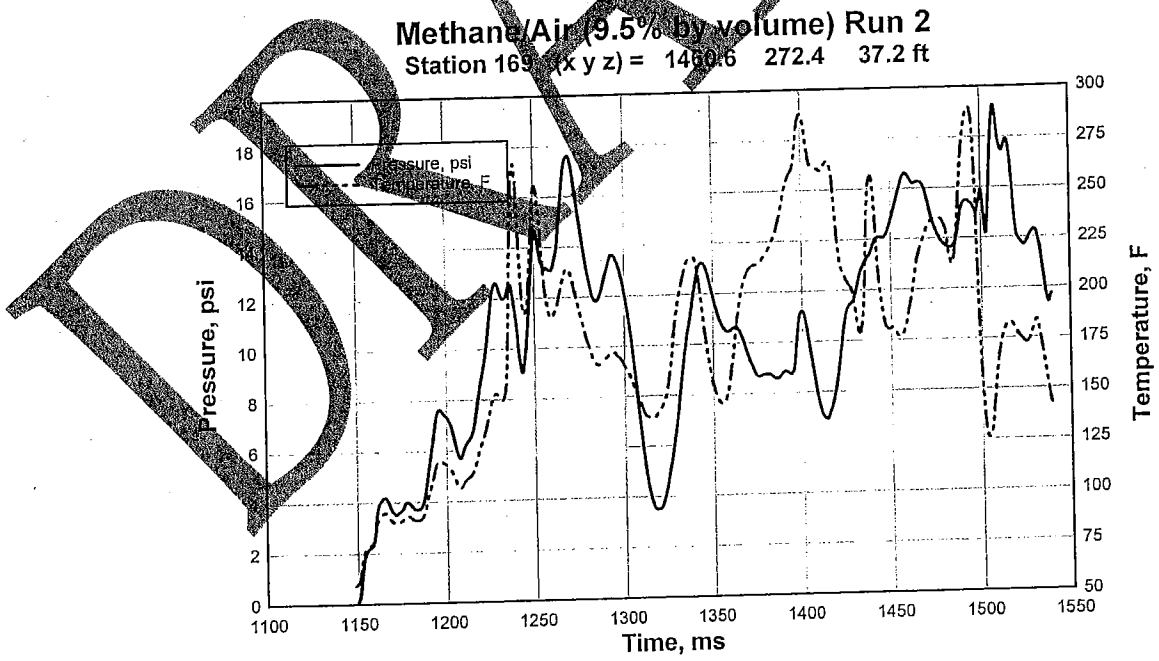

Figure 47. Pressure and temperature at station 169, Run 2.

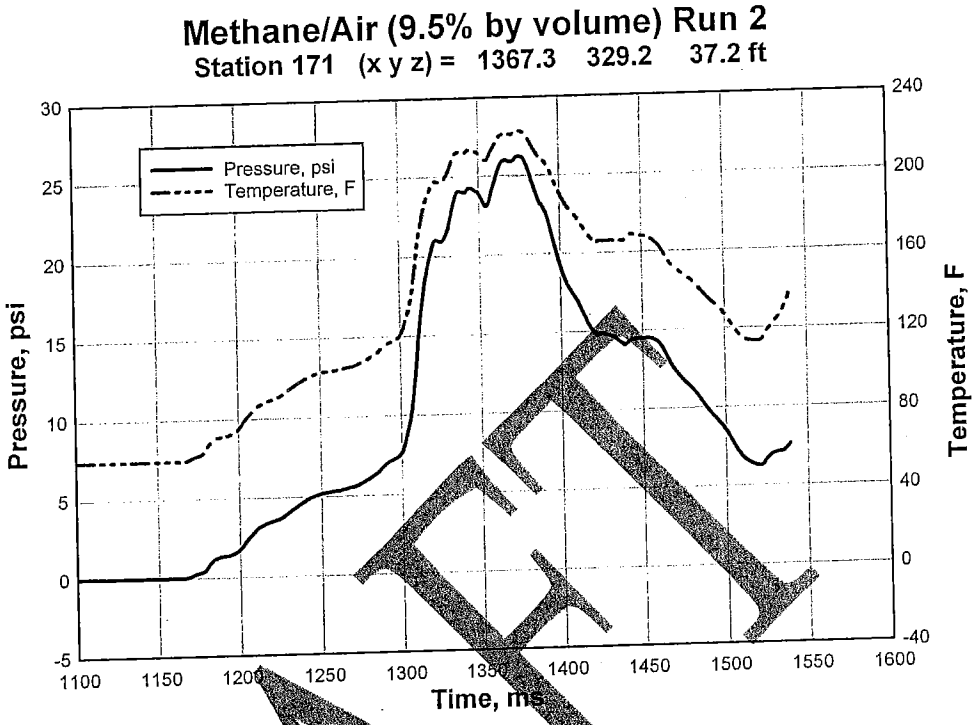

Figure 48. Pressure and temperature at station 171, Run 2.

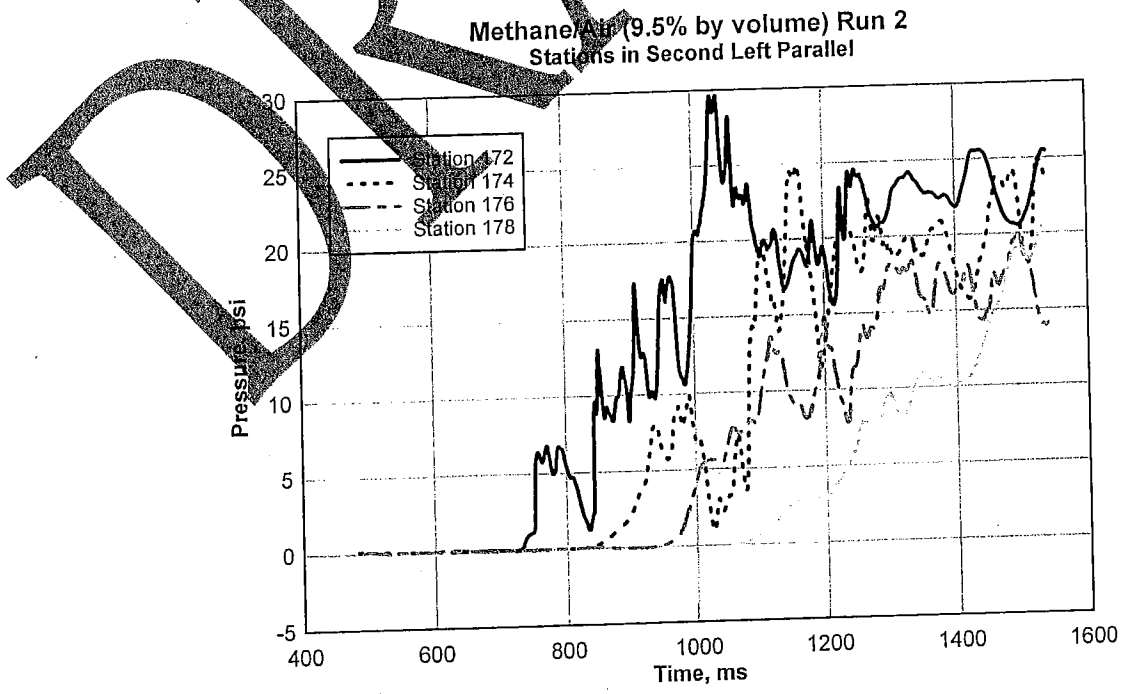

Figure 49. Pressure in Second Left Parallel, Run 2.

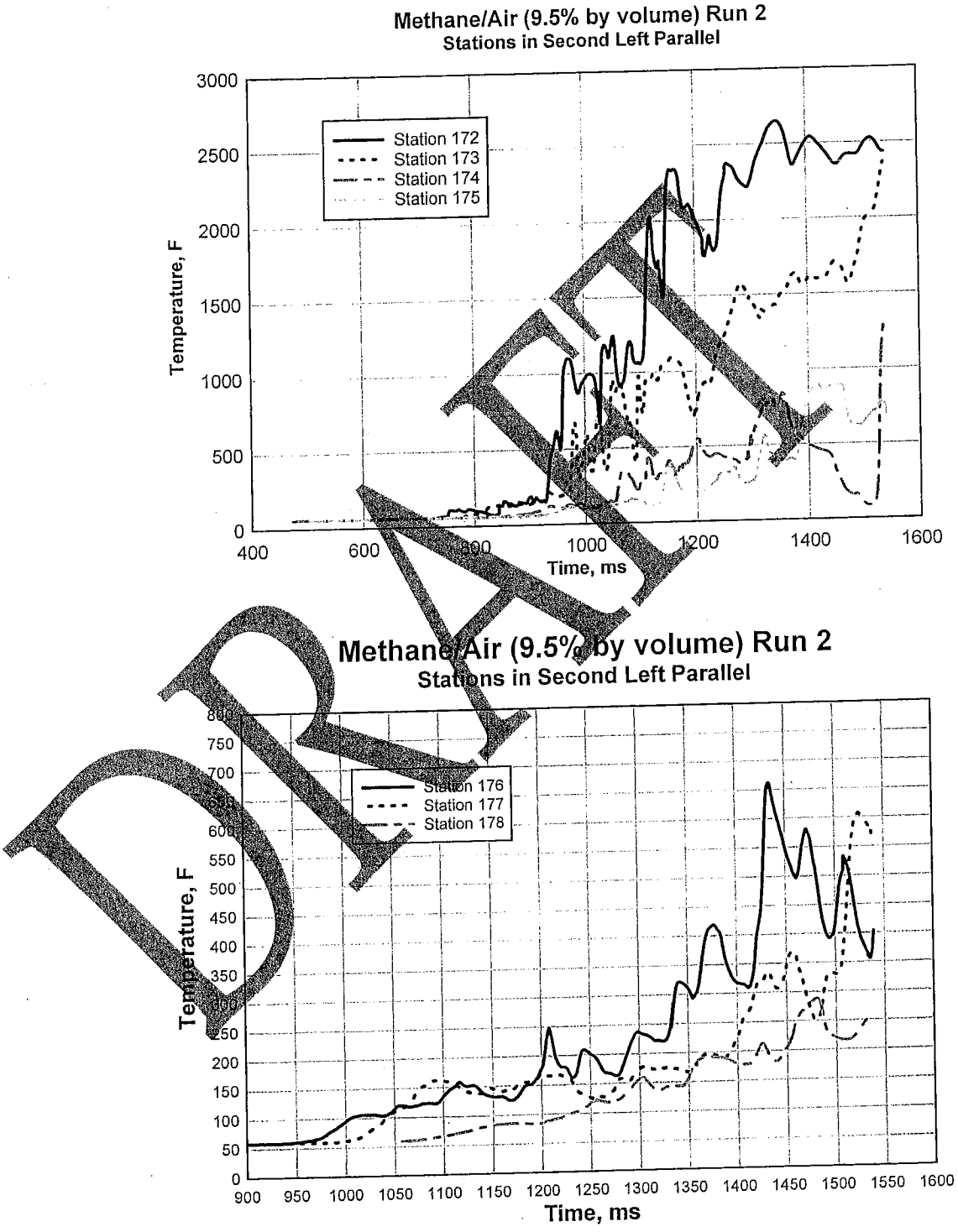

Figure 50. Temperature in Second Left Parallel.

Run 3: Sago Mine with 8% and 17% methane/air

Run 3 assumed that the Second Left Mains (SLM) sealed area was filled with 8% methane/air up to Elevation 1408 (from the bottom of SLM up 30.5 ft) and 17% methane/air above this level. Figure 3 shows the extent of each mixture. There is 8% gas near the floor at Seals 1, 3, and 4. Only Seal 1 has any significant amount of this gas – from 2 to 3 ft out of a ceiling height of 7 to 8 ft. Seals 3 and 4 had 1 ft of 8% gas. The floor level of Seals 2, 5, and 7 was 30.5 ft. The regions of SLM around the ignition point (Spad 4010) and inby (toward top of the figure) were all filled floor-to-ceiling with 8% gas. Because the SLM contained less mass of methane burned and a lower percentage methane in the mixture than in Runs 1 and 2, there was a lower energy release, much lower shock front pressures, and about 40% lower quasi-static pressure.

The calculation was started (as were Runs 1 and 2) with a 1-m diameter sphere (with center at Elevation 650 cm or 21.33 ft) of burned gas from a 1-D calculation started with a 2.5 J spark and represented the first 107. 6 msec of the simulation. At this time there was little overpressure (less than 1 psi) and velocity (about 10 ft/sec). The burn spreads slowly, reaching station 124 (44 ft away) at 273 msec. The acoustic out-running motion arrived earlier at 150 msec.

Figures 52-56 are absolute pressure snapshots at times between 446 and 610 msec. At 446 msec pressure waves are approaching seal 1 from two directions but have not yet reached the seal. At 456 msec both Seals 1 and 2 are experiencing strong pressure loads. By 546 msec loads have reached Seal 6 and ventilation stopping A outby Seal 1. At 561 msec a second larger pulse has loaded Seal 6 and there are loads on stopping B coming from both Seals 1 and 2. By 610 msec blast has reached Seal 9 but not Seal 10. At 720 msec (Figure 57) Seal 10 experiences a strong load and the blast has penetrated the seal and loaded a crib outby. The blast has broken through ventilation stoppings A-E and is approaching stopping F. By 1139 msec (Figure 58) the blast has reached stations 162, 163 and 188 in the Second Left Mains and stations 172-174 in the Second Left Parallel.

Figures 59-62 show the development of the pressure waveforms from the ignition point to Stations 124, 84, 83, 82, 81, 80, 79, and 78 at Seal 1. The high pressures (such as at Station 81) are not detonations, but are produced by colliding shock pulses whose arrivals nearly coincide. For example, a pulse going from Station 111 to 81 will reflect from the side wall near 81. Station 79 is not in an intersection and does not have high pressure spikes. Figure 63 illustrates how pressure pulses coming from two directions (79 and 89) combine to produce the load on Seal 1

Station 78. Neither pulse is normal to the seal, so reflections are less than for normal incidence.

Compare the load at Seal 1 with the pressure at Seal 2 in Figure 64, where the wave propagation is normal to the seal and coming down one drift. Note, however, that because the Omega Block seals are so light weight and have such a low acoustic impedance (density x sound speed), the reflections in both cases are small. Note the more gradual rise of the initial pulse at the seals where the shock pulse has passed through the inby cribs. Figure 65 compares the early time pressure at Seal 2 for all three calculations. The reflected pressure from Run 2 (with Omega seals) is much lower that in Run 1, where the seals were represented as rigid walls. In Runs 1 and 2 the incident pressure pulse was a sharp shock detonation wave, while the pulse in Run 3 has a much more gradual rise and much lower peak pressure. Figure 65 compares the same waveforms on a longer scale to show the late-time quasi-static pressure. In Run 1 the gases are confined to the SEM, while they vent out in the other two runs after the seals are destroyed. The effect of less mass of methane burned and a lower percentage methane in the mixture was a lower energy release and about 40% lower quasi-static pressure in Run 3 than in Run 2. Figure 66 compares particle velocities for the three runs. In Run 1, the rigid wall stops the particle velocity at the seal location and the reflection reverses the velocity at Station 69, just inby the seal. In Runs 2 and 3 the seal begins moving almost immediately, and eventually no longer obstructs the flow. Figure 67 provides more details of the velocity for Run 3.

Figure 68 shows pressure waveforms for all ten seals. In general, the peak pressure decreases from Seal 1 to Seal 10 as the distance from the explosion ignition area increases. There are two exceptions: (1) seal 3 is side-on to the primary direction of blast propagation and has a pressure considerably lower than stations 4, 5, and 6 and (2) the pressures at Stations 9 and 10 are higher than at 7 and 8. There is no clear evidence that the bottom mining inby several seals makes significant changes in the pressure waveforms.

Figure 69 shows the sequence of pressure waveforms at stations 39-46 leading up to Seal 6 (station 39). The floor has been bottom-mined inby with floor elevations down to 24.8 ft, compared to 30.5 ft near the seal. Because of pressure waves coming to this Entry 5 through crosscuts inby toward the ignition point, it is difficult to identify effects of the changing floor elevations in the complex pressure waveforms. Figures 70 and 71 show particle velocity at Station 40. Again there is no clear evidence that the inby bottom mining increases the loads on the seal.

In a single drift of a tunnel, pressure changes proportional to $\sqrt{(A_1 / A_2)}$ when propagated from one region with cross sectional area A_1 to another region with area A_2 (Reference 26). Thus pressure drops when $A_2 > A_1$. However, when the blast wave propagates out of the larger region back into the region with smaller cross sectional area, the pressure rises by the inverse factor and there is no net effect. Near the areas of transition, the environment is much more complex, with local pressure wave reflections depending on the detailed tunnel geometry.

Extent of detonation. There was no transition to detonation outby the ignition point (toward the seals). A transition to detonation occurred at Stations 108, 109, 191, and further inby. The closest station to the ignition point with detonation, is Station 108, 310 ft from the ignition point.

Flow of unburned 17% methane/air. Unburned methane flowed past Station 164 from 1918 to 1951 msec after igniting, but only air flowed pass this location in later time. Similarly, unburned methane flowed past Station 165 from 2079 to 2094 msec. At Station 153, unburned gas began flowing at 1177 msec and continued (with a few short breaks) to the end of the calculation. Unburned methane began to flow past station 156 at 1179 msec, and at 1394 msec the temperature exceeded 1000 deg F the ignition point of methane. Both unburned methane and burned methane passed Stations 162 and 163. Within and between Entries 4 and 5, unburned methane and temperatures above 1000 deg F exist, so that there was the potential for mixing of 17% methane/air with air and producing additional combustion in this region. Figure 72 displays pressure and temperature at Stations 138 and 156 and pressure, temperature, and velocity at station 162. Figures 73 and 74 contain pressure and temperature at Stations 168 and 171. Pressures leaving the calculational region are still in the 12 to 14 psi range, but temperatures are much lower than at Stations 162 and 163.

Flow of burned methane. An examination of the materials at the output stations shows that, at the end of the calculation, burned 8% methane/air had penetrated Entries 5-9 as far as Station 163 (at 2092 msec), but not to Stations 168-171. There was no burned gas outby Seals 7-10 in Entries 1-4. There was no burned gas inby Seal 10 in Entry 1 and at stations 10-13, 20, 21, and 30. Thus no burned gas had reached Seals 7-10. In the Second Left Parallel, burned gas had reached Stations 172-174 but not 175-178. At the end of the calculation, temperatures exceeding 3000 deg F had reached only Stations 140-143, 152, and 172.

Conditions in the Second Left Parallel. Figures 75 and 76 compare pressure and temperature at Stations 172-178 in the Second Left Parallel. By 2000 msec all

locations have reached quasi- static pressures of about 12 psi. At Stations 172 and 173 there are significant pulses in early times that exceed 14 psi. These pulses are associated with a large flow that brings the hot burned gases with temperatures above 2000 deg F as shown in the temperature plot. In contrast, at Station 178 the pressure rises gradually, as would be expected from steady venting of gases, and the temperature has risen to less than 400 deg F at the end of the calculation.

Figure 51. Distribution of 8% (lower) and 17% (upper) methane/air mixtures in SLM for Run 3.

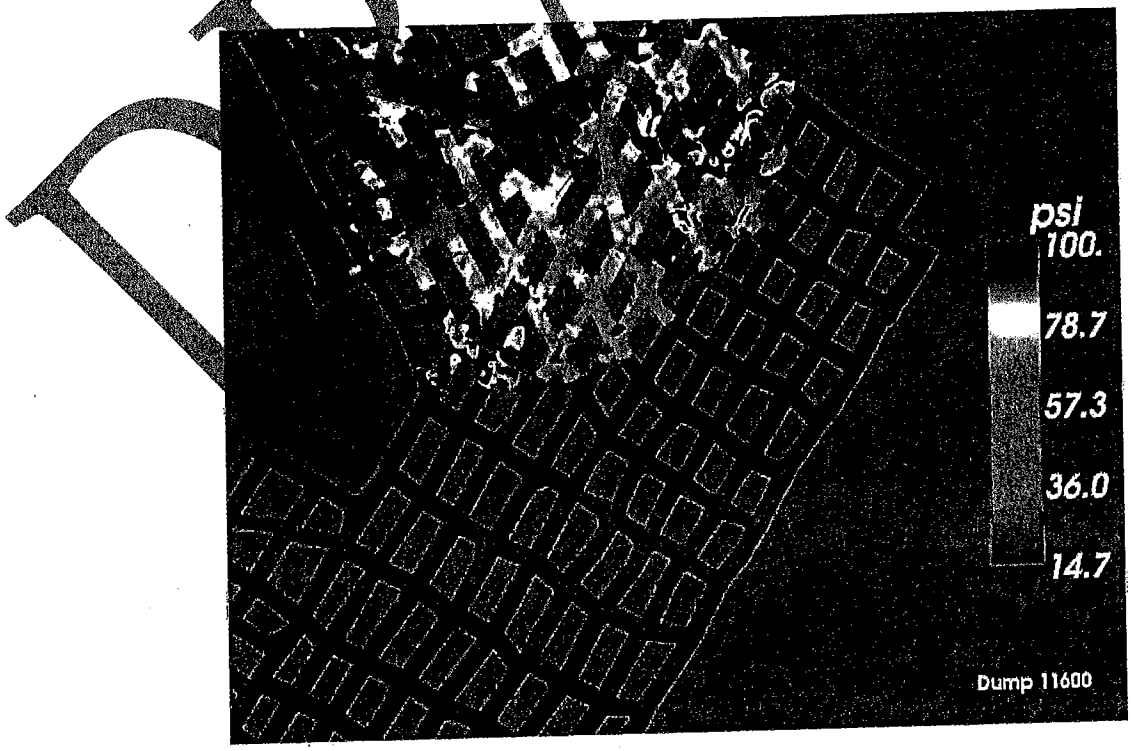

Figure 52. Absolute pressure approaching seals at 446 msec in Run 3.

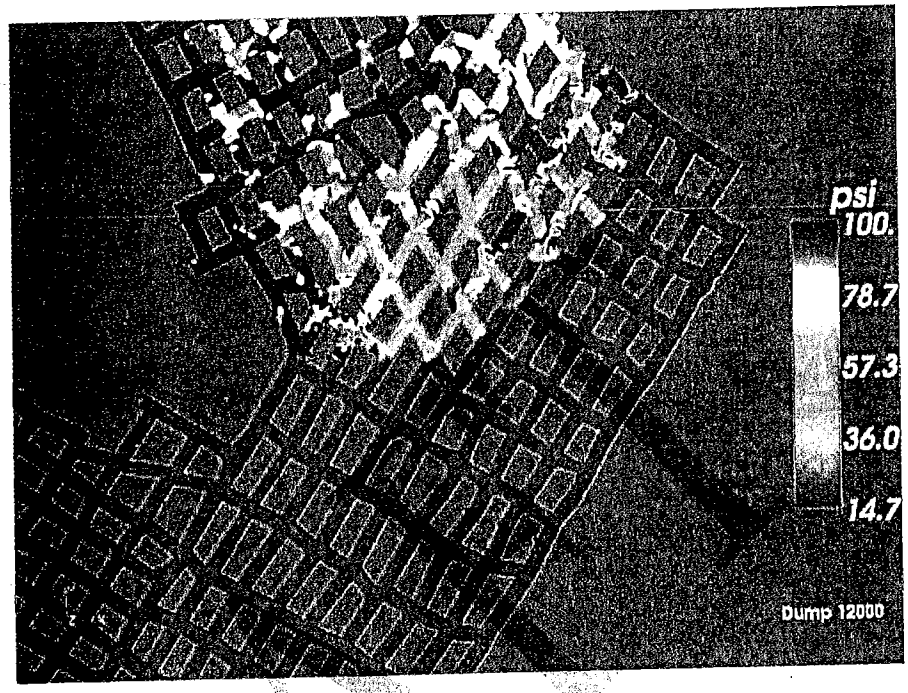

Figure 53. Absolute pressure approaching seals at 456 msec in Run 3.

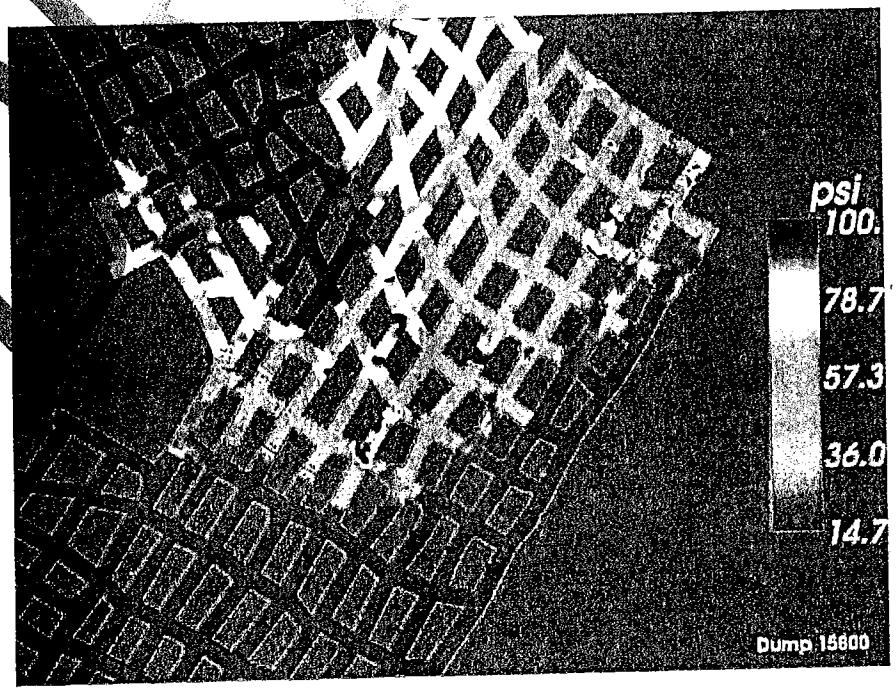

Figure 54. Absolute pressure approaching seals at 546 msec in Run 3; Seals 1-4 have been breached at this point.

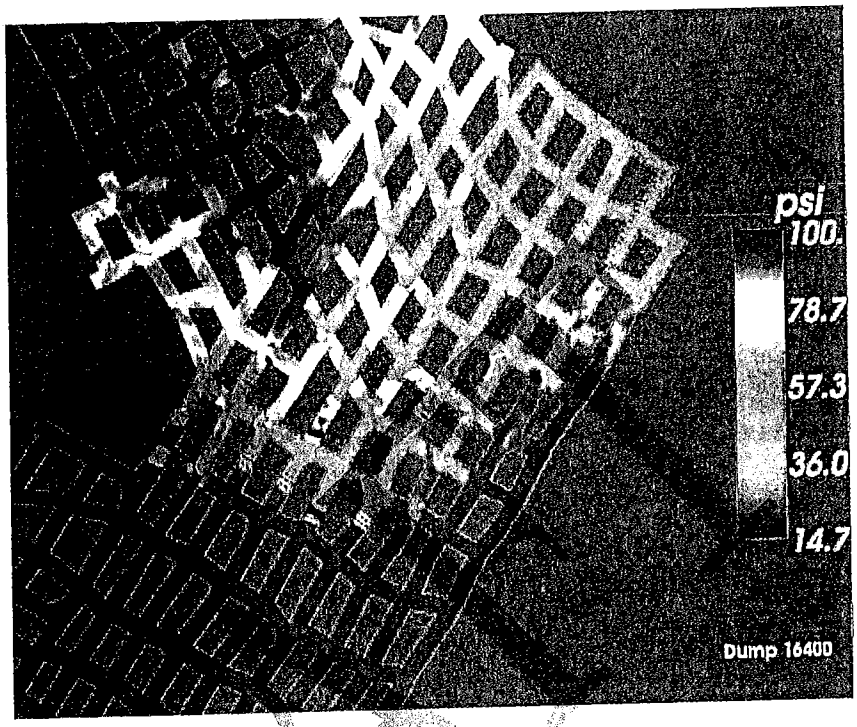

Figure 55. Absolute pressure approaching seals at 561 msec in Run 3.

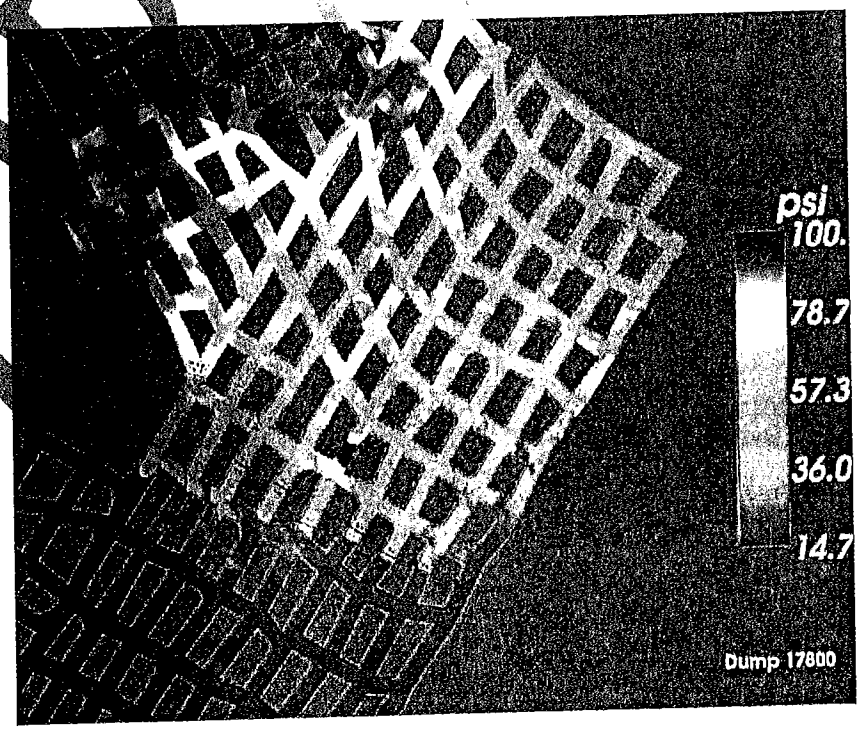

Figure 56. Absolute pressure approaching seals at 610 msec in Run 3.

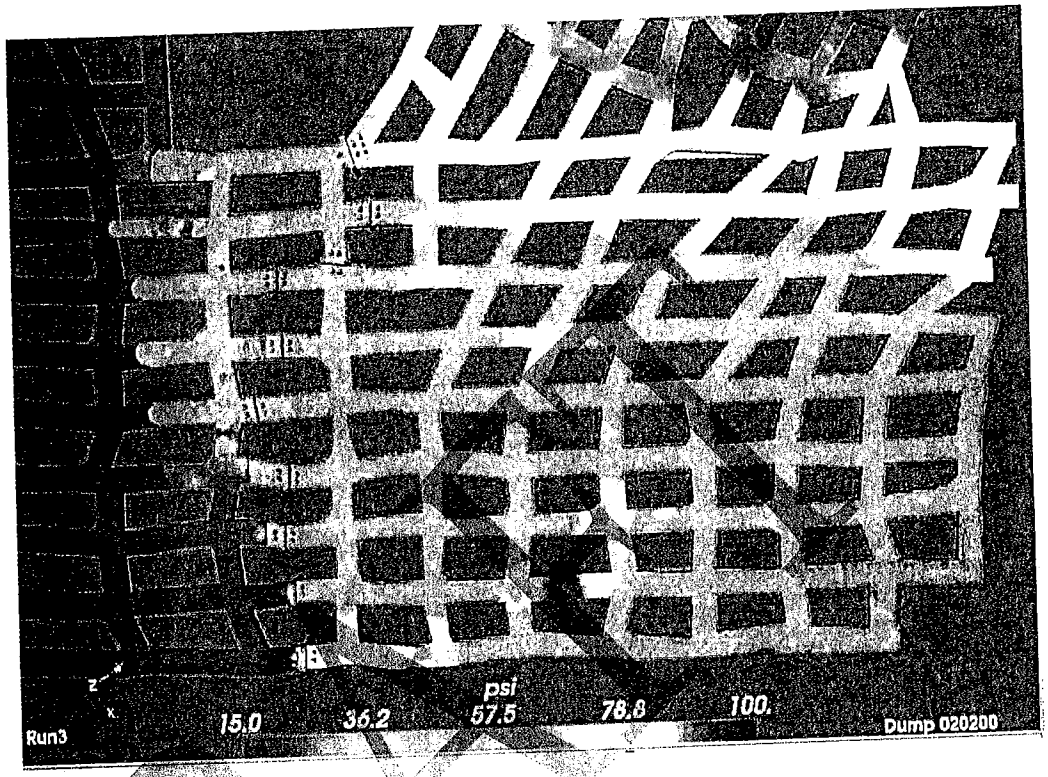

Figure 57. Absolute pressure approaching seals at 720 msec in Run 3.

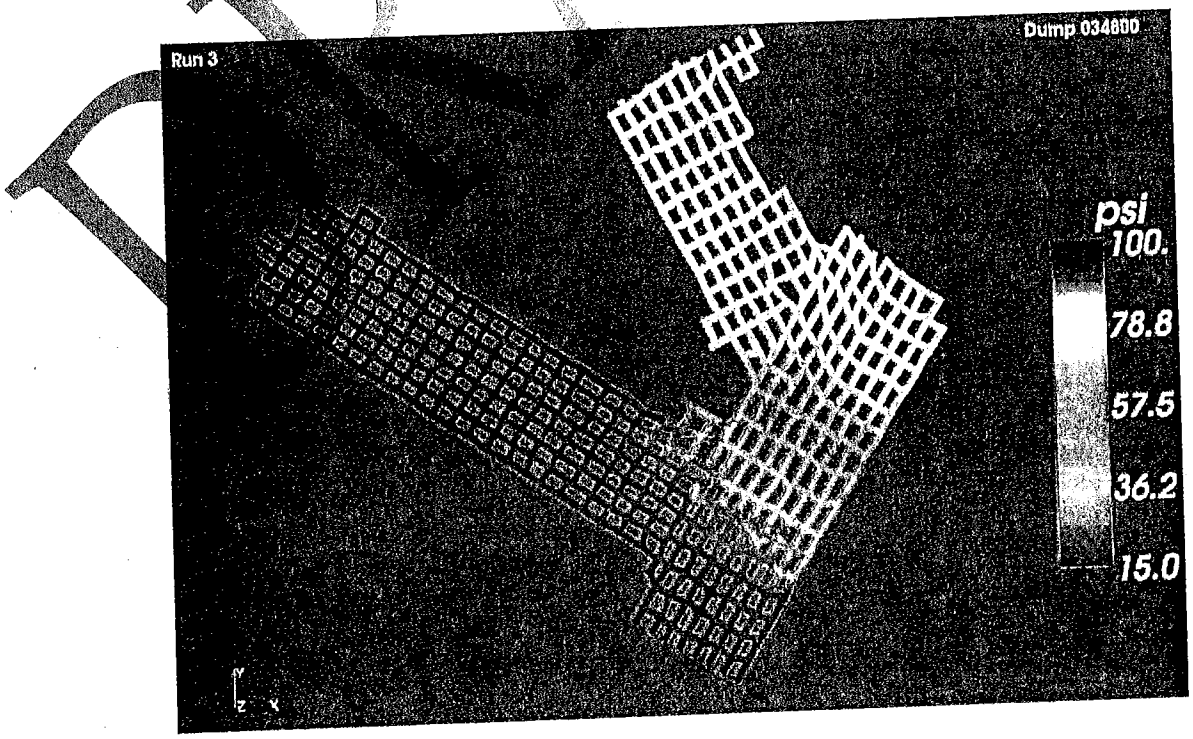

Figure 58. Absolute pressure approaching seals at 1139 msec in Run 3.

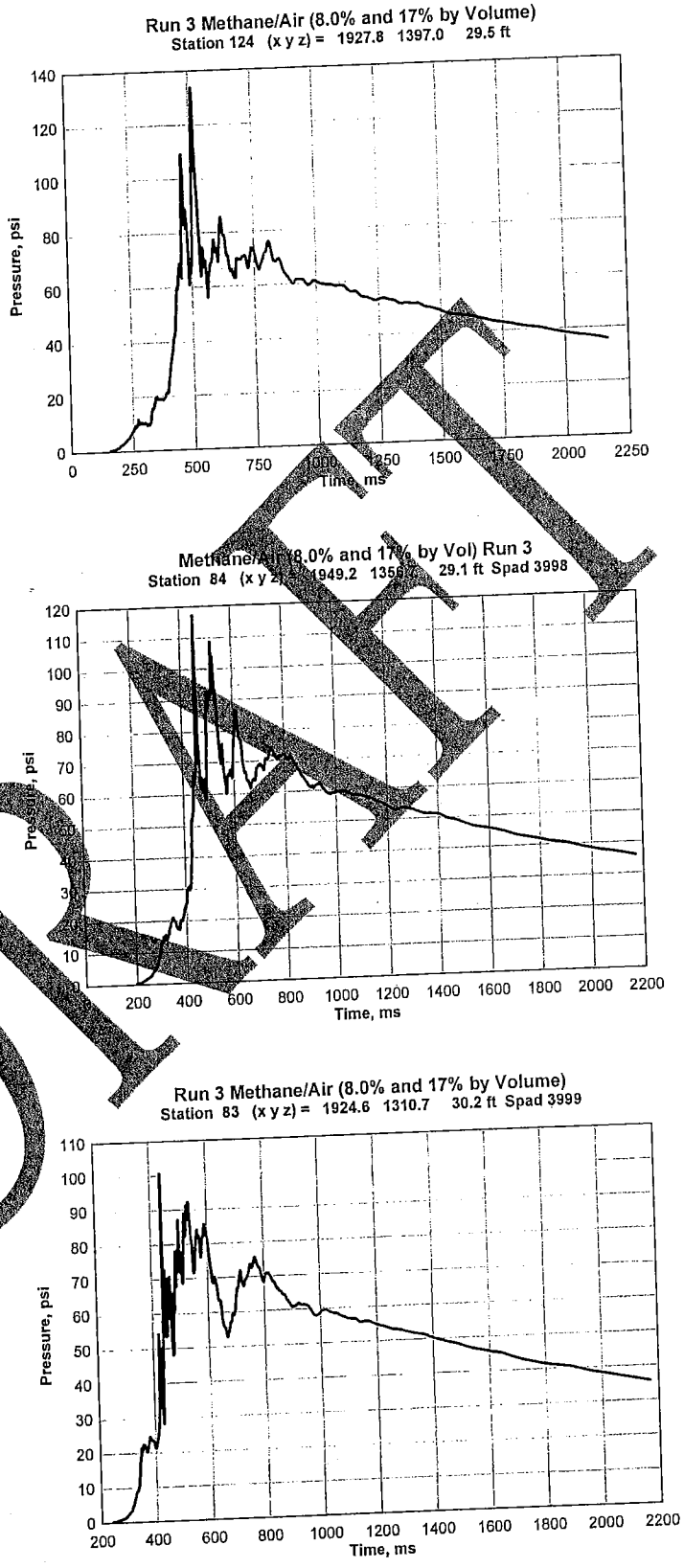

Figure 59. Pressure at Stations 124, 84, and 83.

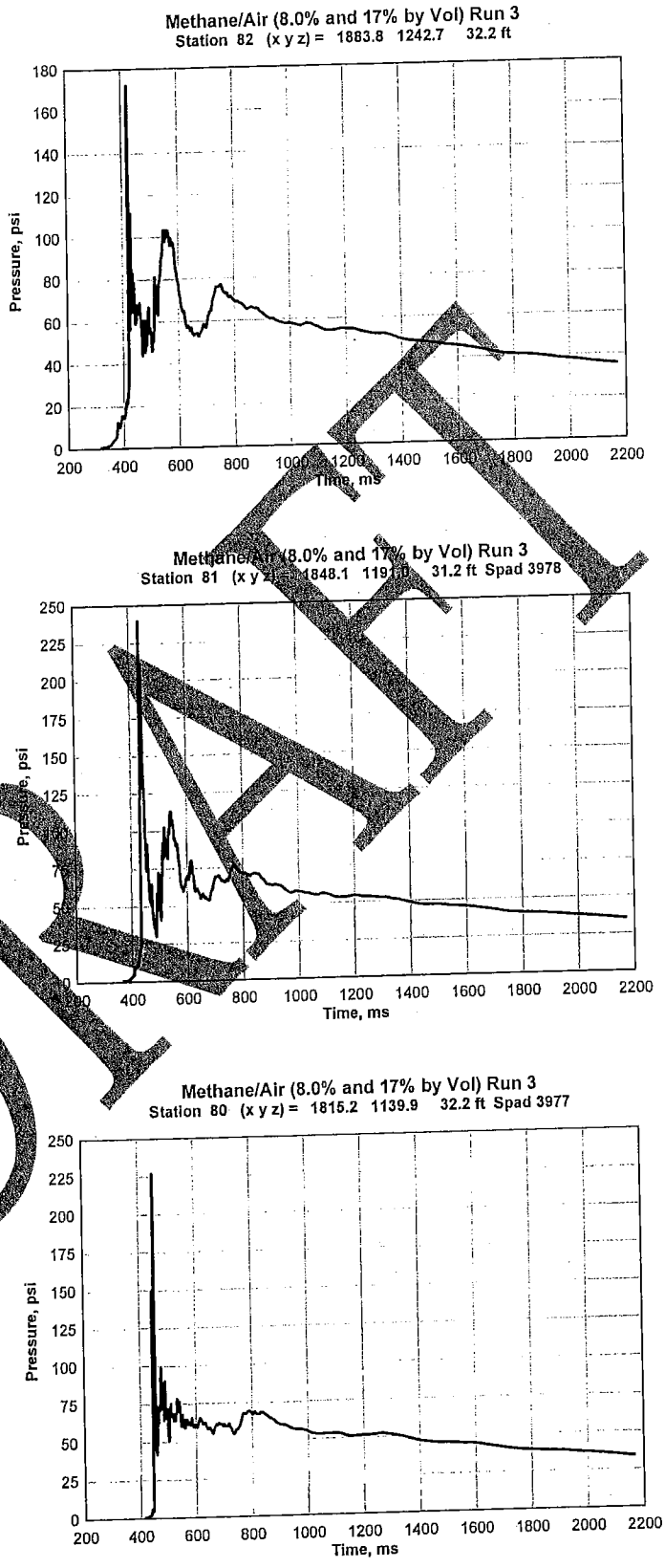

Figure 60. Pressure at Stations 80, 81, and 82.

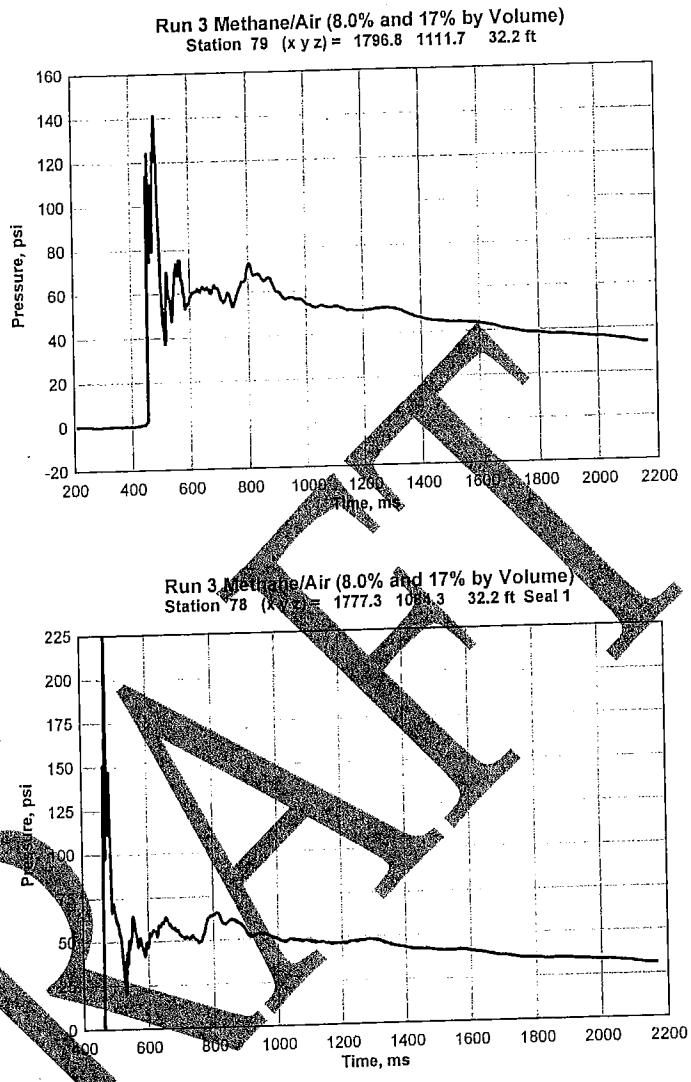

Figure 61. Pressure at Stations 78 and 79.

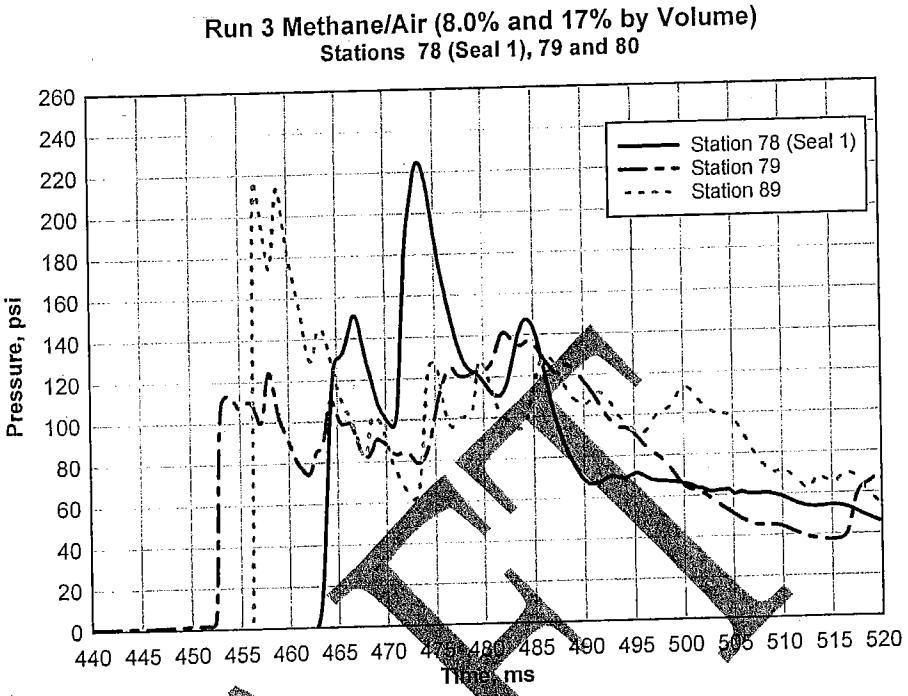

Figure 62. Pressure merging from two drifts to produce load on Seal 1.

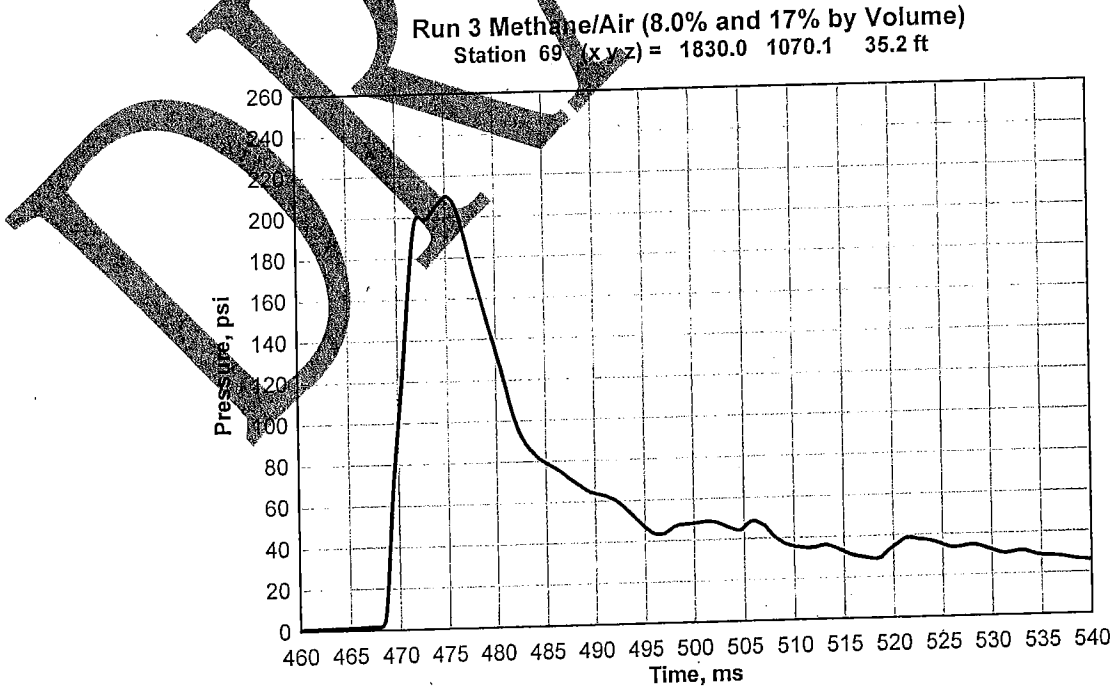

Figure 63. Pressure in one drift on Seal 2.

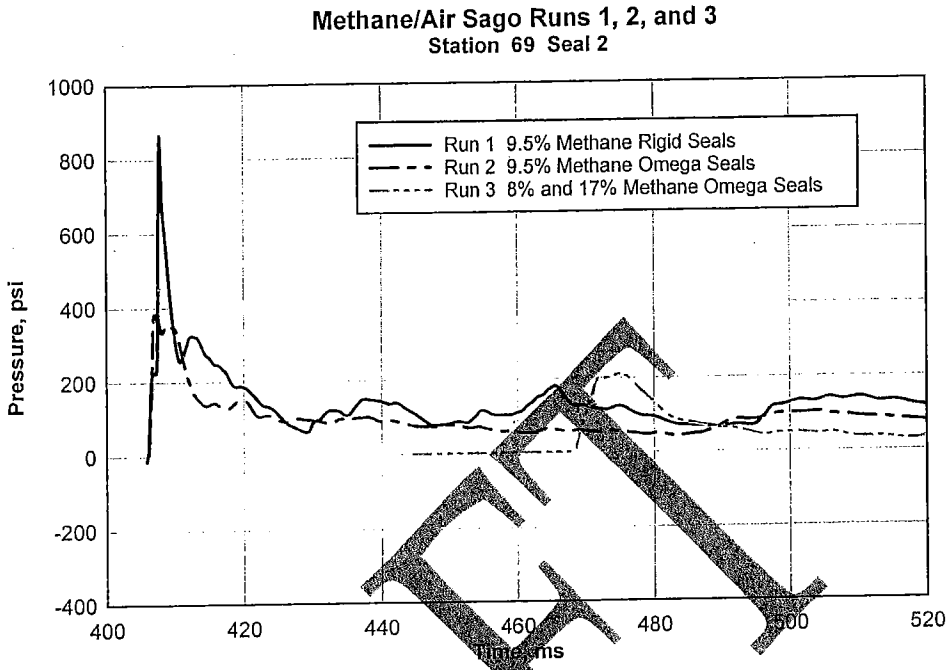

Figure 64. Early time pressure at Seal 2 for Runs 1, 2, and 3.

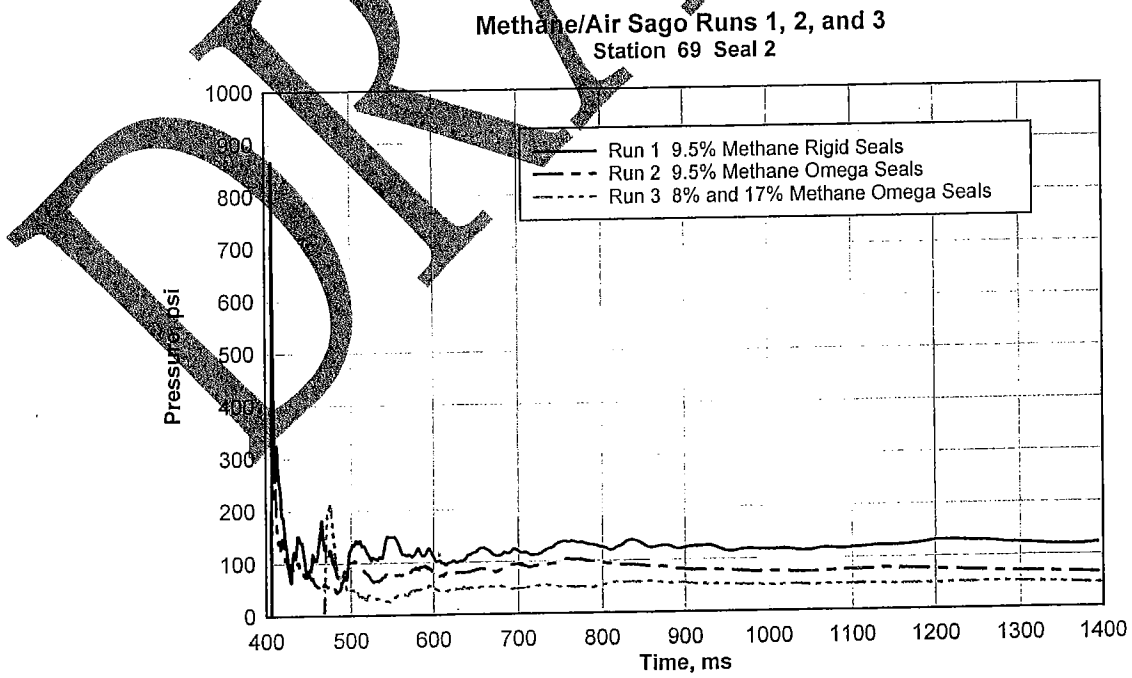

Figure 65. Long duration pressure at Seal 2 for Runs 1, 2, 3.

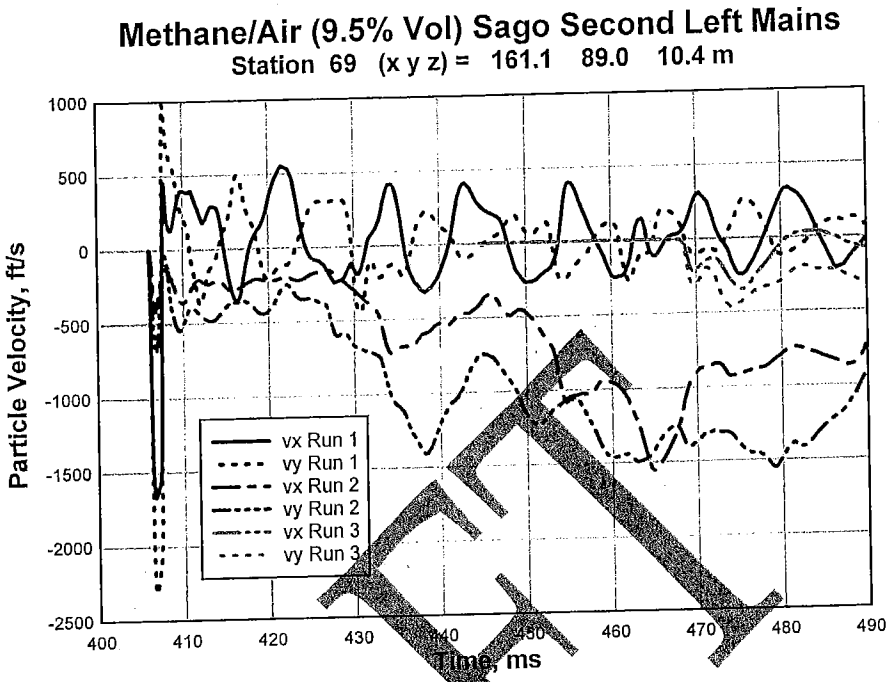

Figure 66. Early time particle velocity at Seal 2 for Runs 1, 2, and 3.

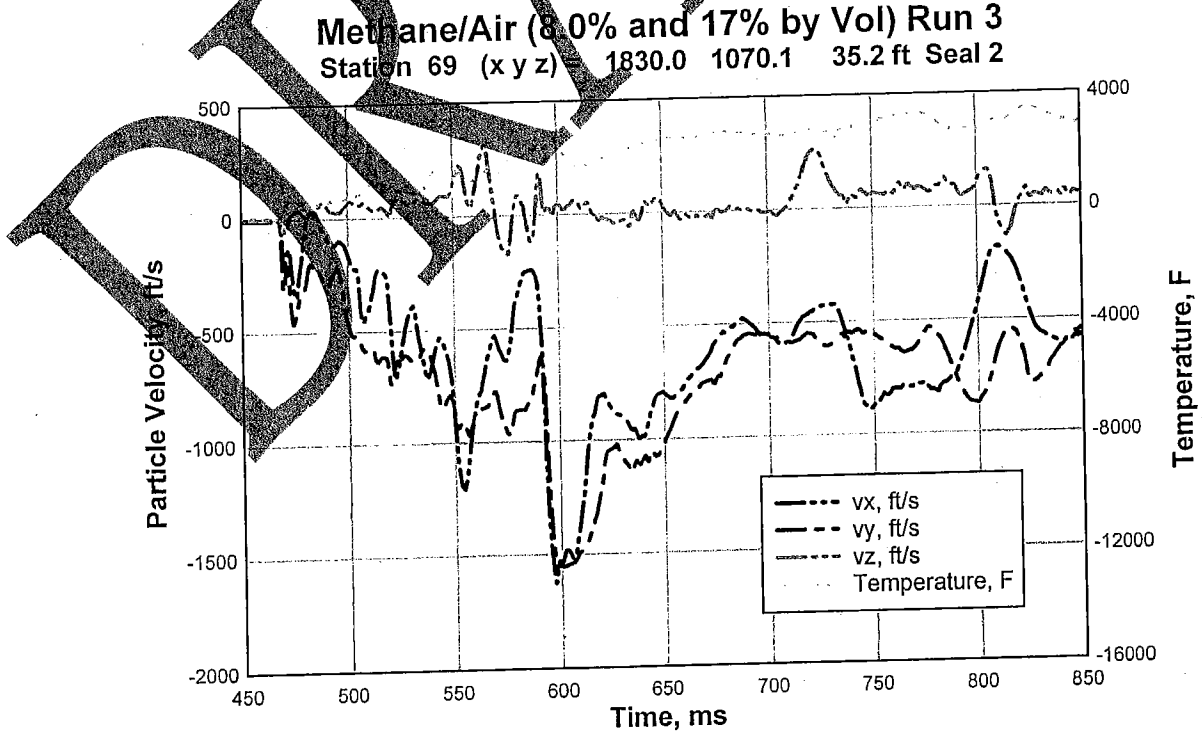

Figure 67. Detailed particle velocity and temperature at Station 69 Run 3.

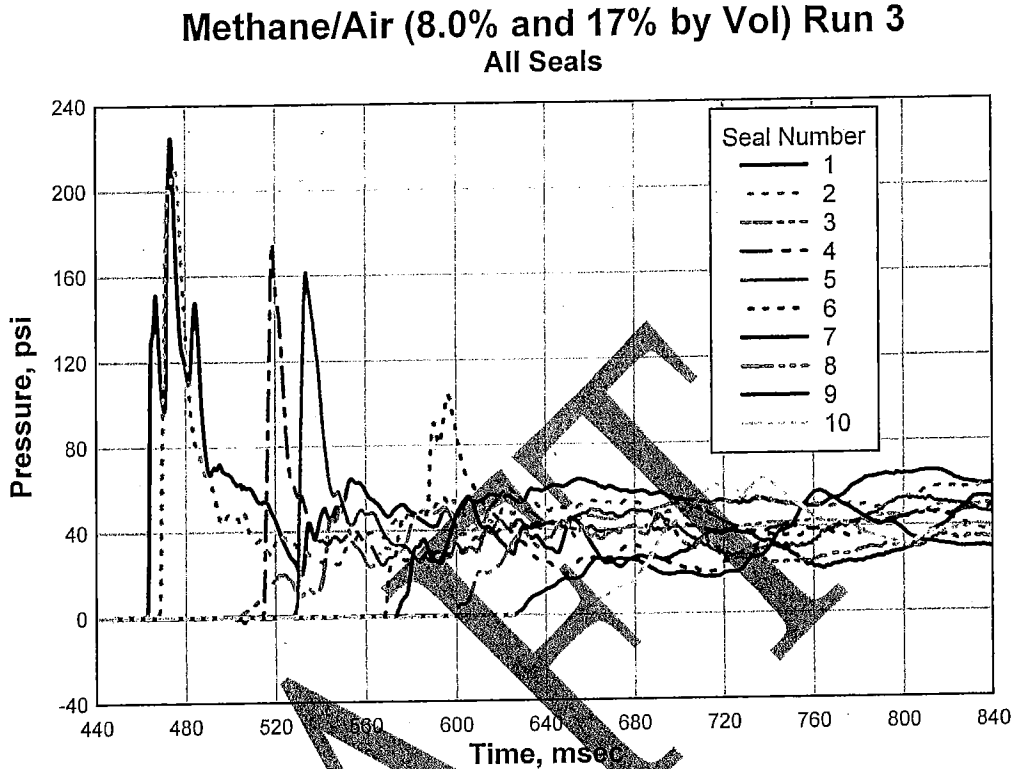

Figure 68. Pressure waveforms at all seals for time 440 to 840 msec.

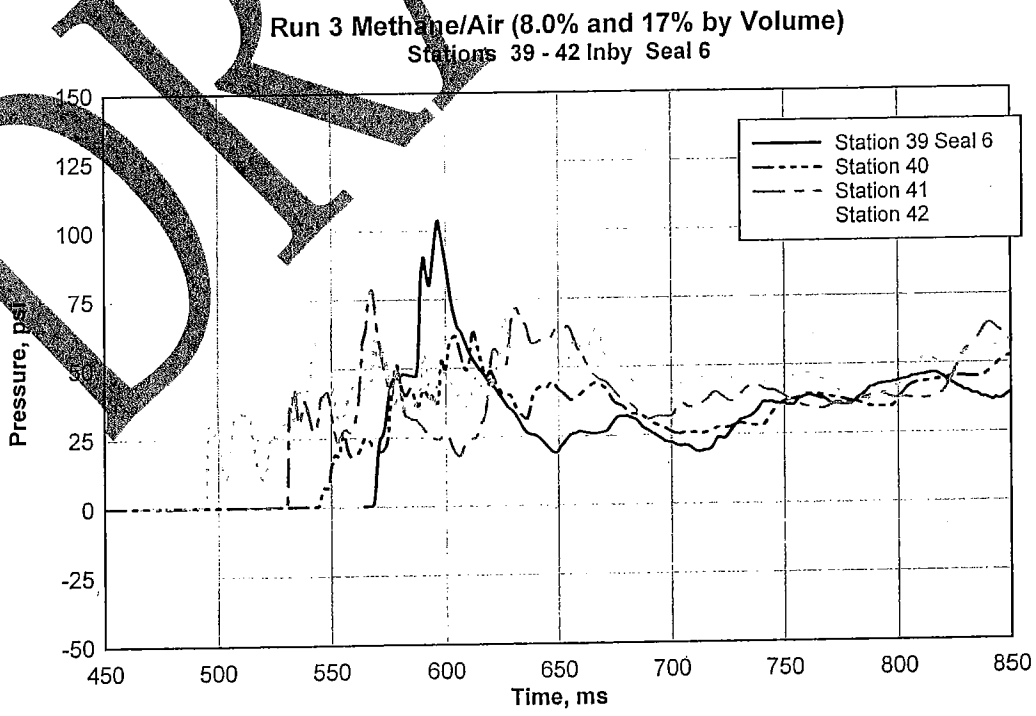

Figure 69. Pressure waveforms at stations 39-42 that lead to seal 6.

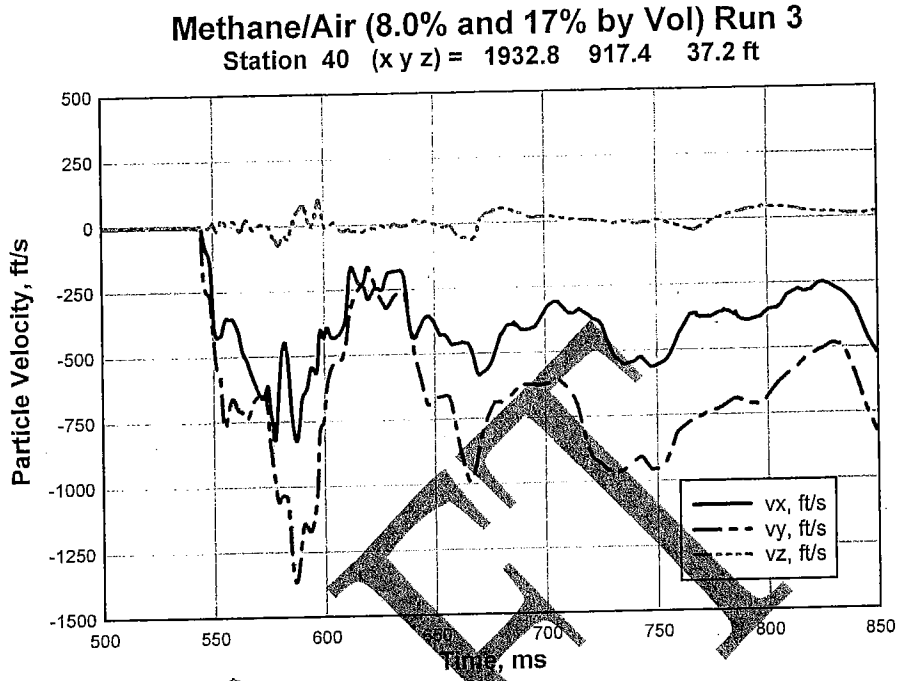

Figure 70. Early time particle velocity at station 40.

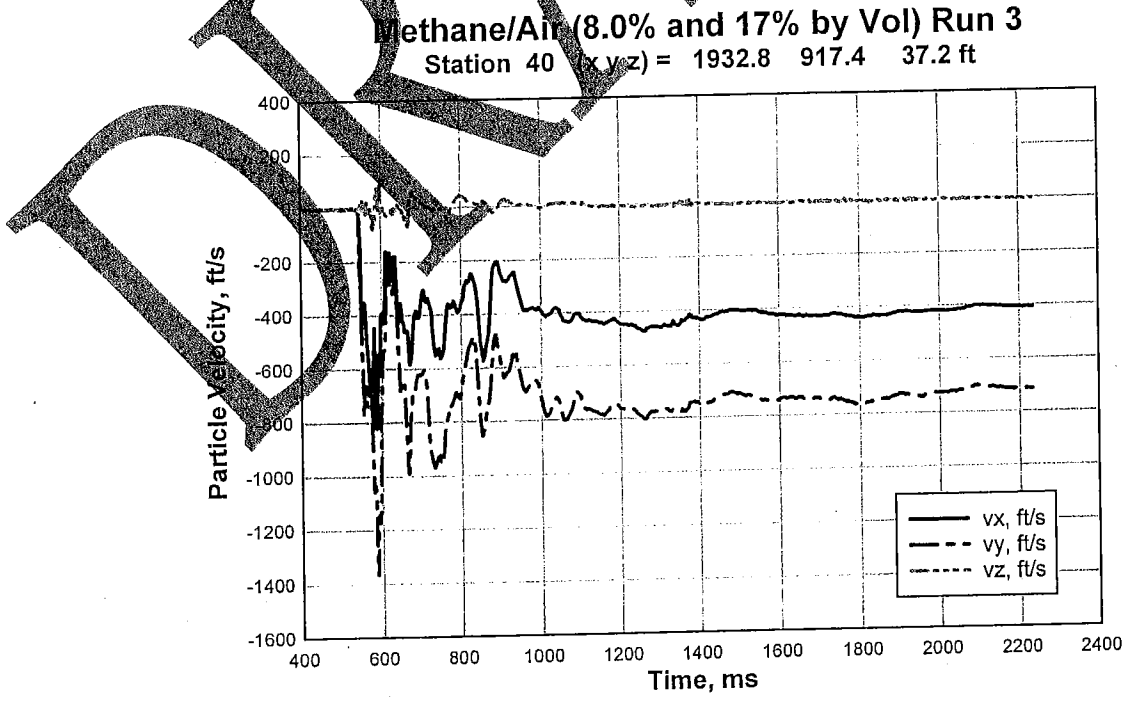

Figure 71. Long duration particle velocity at station 40.

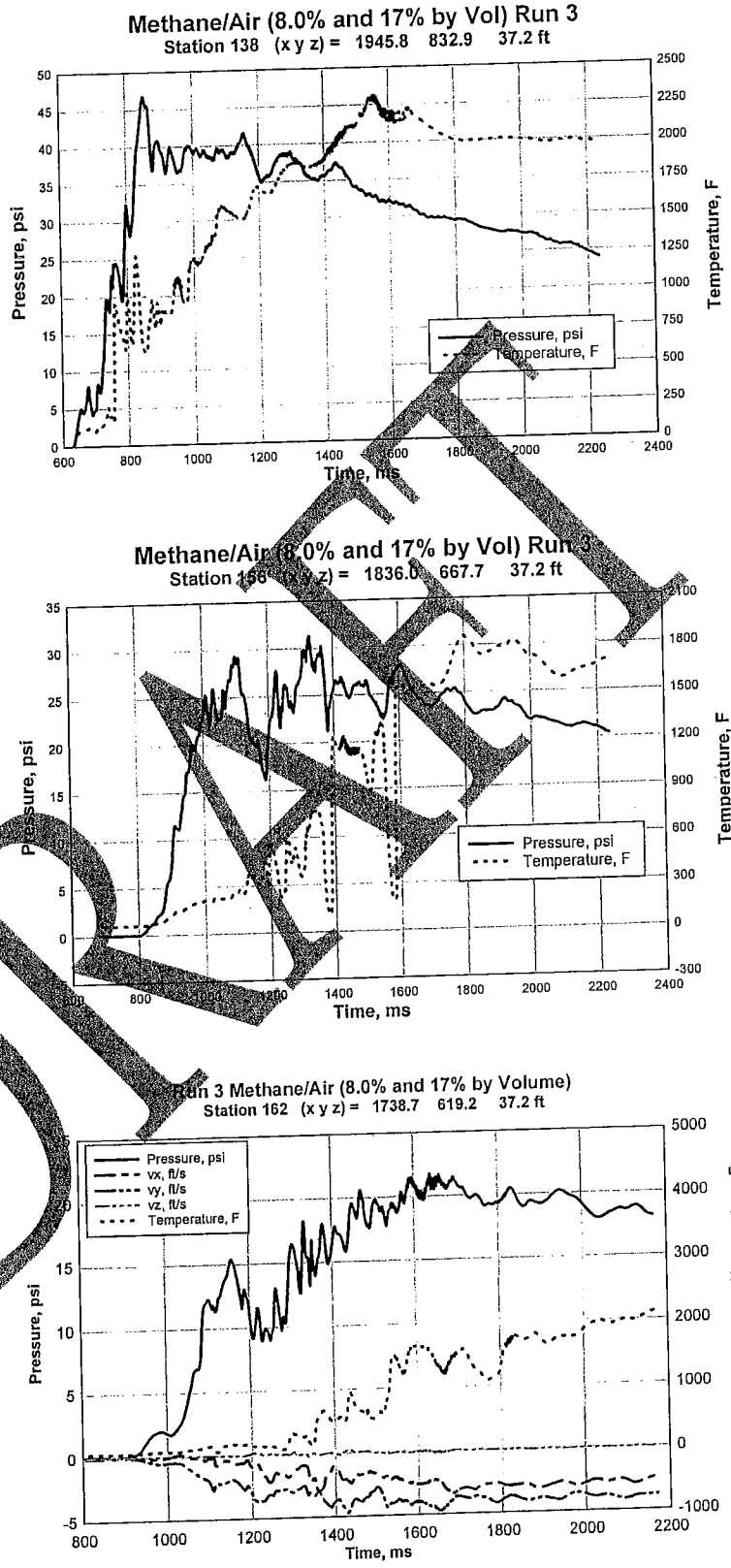

Figure 72. Pressure, velocity, and temperature at stations 138, 156, and 162.

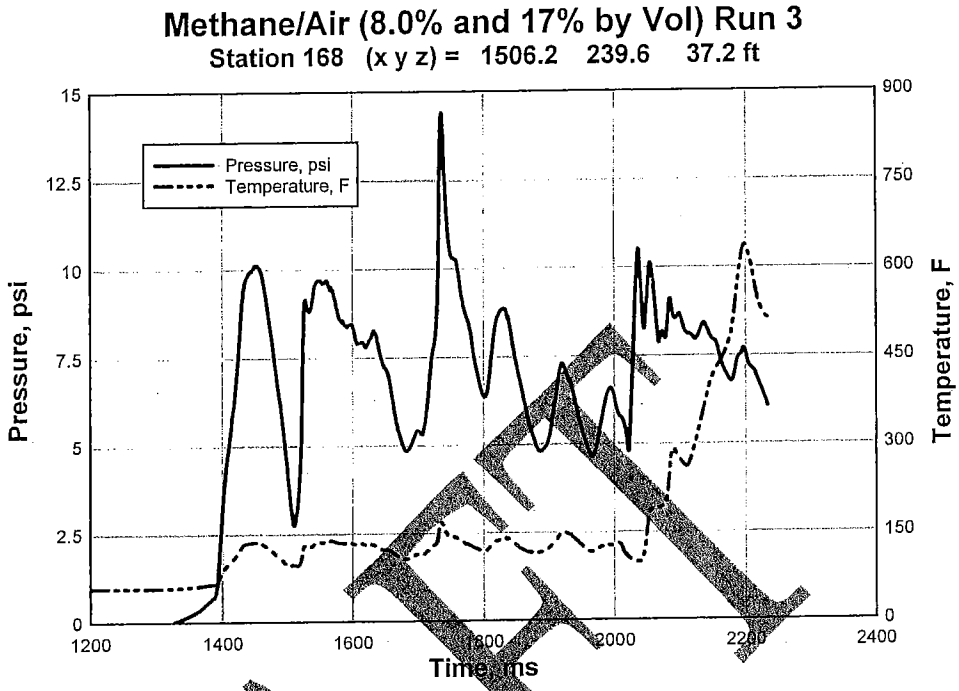

Figure 73. Pressure and temperature at station 168, Run 3.

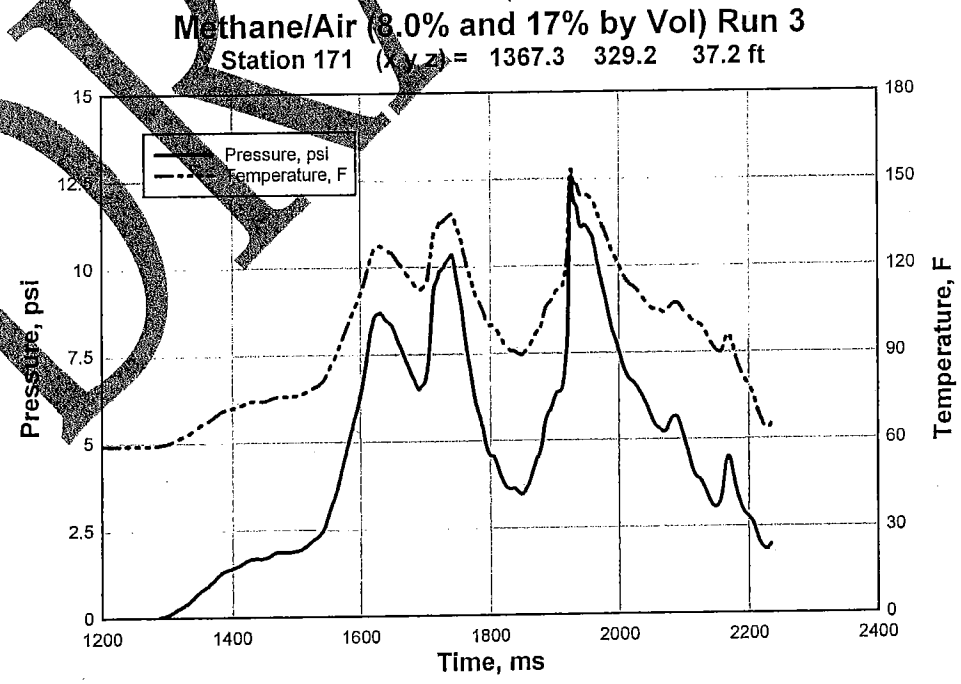

Figure 74. Pressure and temperature at station 171, Run 3.

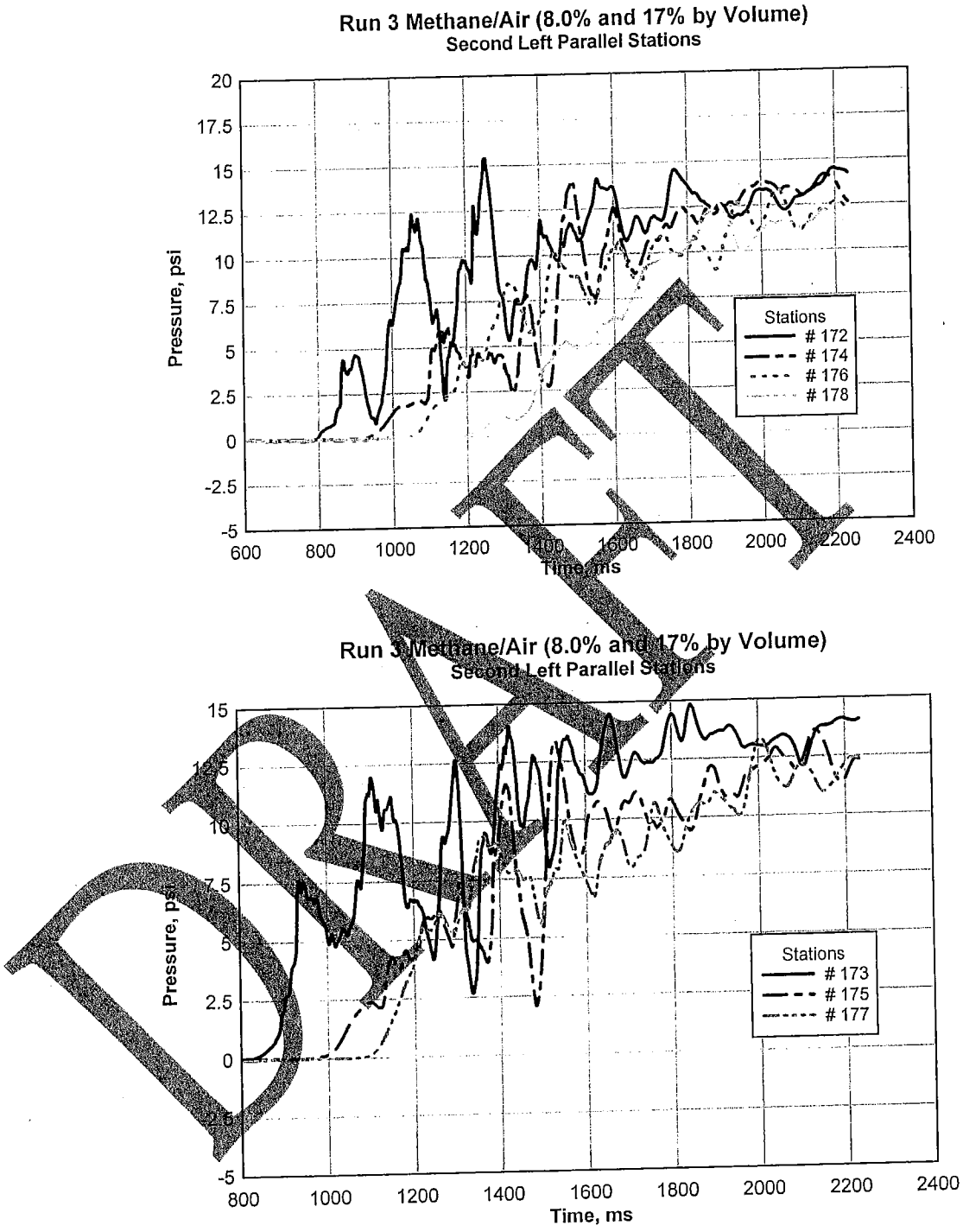

Figure 75. Pressure at stations 172-178 in Second Left Parallel.

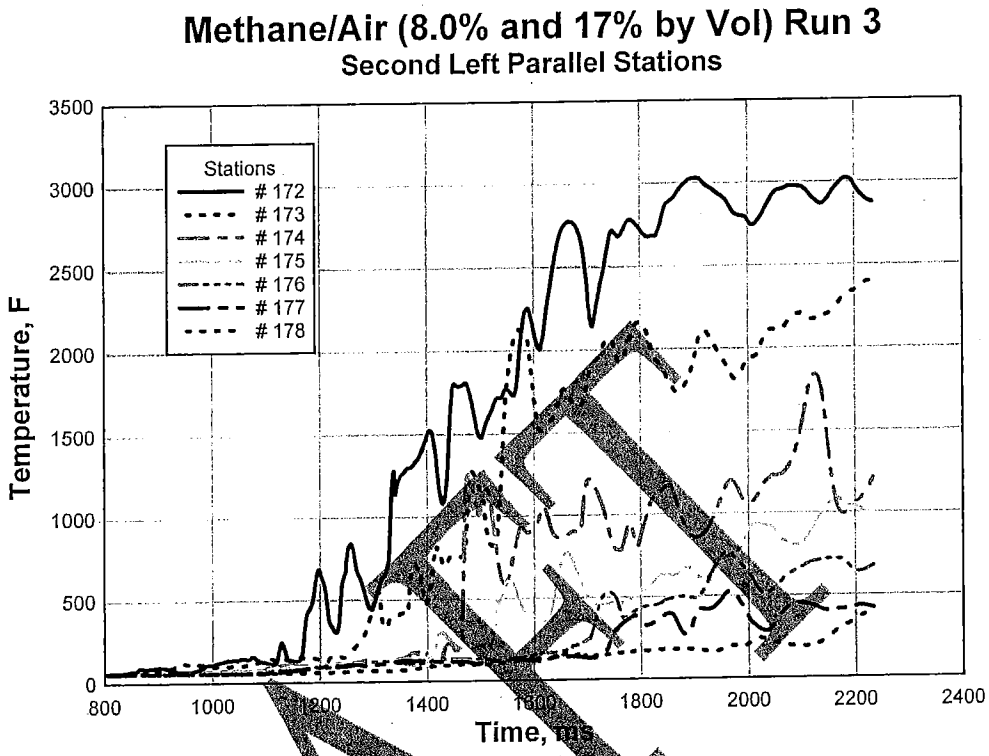

Figure 76. Pressure at stations 172-178 in Second Left Parallel.

Major Findings

Pressures on seals -- Pressures on the seals varied considerably between Runs 1, 2 and 3. In Run 1 with rigid walls at the seal locations, pressures were generally about twice those computed in Run 2 with Omega Block seals that deform and fail. Pressures ranged from 360 to 1300 psi in Run 1, with the lowest pressure at Seal 3 where the blast propagation was side-on, with little reflected component. On all other seals the blast is reflected at normal incidence. In Run 2, peak pressures on the seals ranged from 156 to 629 psi, and the lowest pressure was again at Seal 3. In Run 3 pressures ranged from 51 to 225 psi, with the highest pressures at Seals 1 and 2, which were the seals closest to burning 8% methane/air region. The lowest pressures occurred at Seal 8. In all cases, pressures were at more than the design load (20 psi) of the Omega block walls.

Pressures outby the Seals -- Pressures dropped rapidly outby the seals but at Station 162 were still 50 psi and 21 psi in Runs 2 and 3, respectively. Pressures exiting the calculation region at stations 164-171 dropped to 20 to 25 psi in Run 2, and 12.5 to 14 psi in Run 3. Pressures in Second Left Parallel reached at least 20 psi in Run 2 and 13 psi in Run 3 at Stations 172-178.

Exten of Methane Burn -- In Run 2, burned 9.5% methane/air mixture penetrated most of the Second the Mains at least as far as Station 163, but had not reached Station 164-171 by the end of the calculation. High temperatures were also observed at Stations 172 and 173 in the Second Left Parallel.

In Run 3, burned 8% methane/air mixture penetrated Entries 5-9 as far as Station 163 (at 2092 msec) but not to Stations 168-171. There was no burned gas outby Seals 7-10 in entries 1-4. There was no burned gas inby Seal 10 in entry 1 and at Stations 16-18, 20, 21, and 30. Thus, no burned gas had reached seals 7-10. In the Second Left Parallel, burned gas reached Stations 172-174 but not 175-178. At the end of the calculation, temperatures exceeding 3000 deg F had reached only Stations 140-143, 152, and 172.

4 Structural Damage Calculations

Two types of structural response calculations were performed to correlate the damage levels observed in the Sago Mine accident with applied levels of blast loadings: Single Degree of Freedom (SDOF) analyses, and Finite Element (FE) analyses. Both required very specific and detailed descriptions of the physical properties and characteristic behavior of the materials which comprised the structural elements to be analyzed. This information was developed in the form of "constitutive" models of each material.

This chapter describes the development of the constitutive properties information, and the FE and SDOF model analyses performed to define the response of the structural elements to the postulated loadings produced in the Sago Mine incident.

Constitutive Material Models

All first principal numerical codes require a constitutive model of the materials used in the response calculations. As complicated as some of these models are, they are still a macroscopic approximation of the microscopic mechanics of the material response to external loads. This is the case when developing models of complex, non-homogenous, non-isotropic, elastic, plastic, viscous, visco-plastic materials. The models used for the seal material in these calculations fall into the categories of "hypo-elastic/perfectly plastic in shear", and "hypo-elastic in compression" models. They are represented by a compacting, hysteretic pressure-volume relationship and a shear failure surface. Lacking a complete set of material test data, the models for this study were constructed by scaling known properties data from similar materials.

The data supplied by MSHA (or gleaned from other literature sources) for the Omega Block and the Blocbond Grout (i.e., the mortar) included the unconfined compression strength, tensile strength, direct shear strength, density, and porosity of the materials. While these data provided the basic properties, they were not sufficient for the complete material descriptions required for constitutive models. With this information, however, it was possible to identify both a foamed, light-weight concrete and a high-strength grout in the materials library at ERDC that had properties that closely matched those of the blocks and mortar of the Sago seals. The ERDC laboratory test data for those materials was sufficient to construct representative material models. An average unconfined compression strength was

used for the Omega Block material, since the existing test data showed considerable scatter in the test results.

One of the controlling material properties of both the Omega Block and the Blocbond Grout is the tensile strength. From a material property viewpoint, the mortar is significantly stronger in compression, tension and shear than the foam concrete of the Omega Blocks. This forces the failure of the seal system into the Omega Block material – a result that is borne out in the literature from tests of "beam" elements made from Omega Blocks bonded together with Blocbond Grout (Reference 27).

All of the material properties in the model are for static loads, and do not vary with time. The models do not reflect any rate sensitivity in compression or shear; hence the yield surface does not harden. The pressure-volume curves and failure surfaces representing the material models are presented in Figure 77.

Three key issues of material response can be observed from the material models. First, the non-linear compaction that occurs with hysteretic unloading absorbs energy during the load-unload cycle, particularly for the Omega Block material. The low pressure, non-linear behavior of the pressure-volume relationship is due to the failure and subsequent crushing of the material matrix, and then a locking up as the air is compressed and forced out of the material and the load is carried by the crushed material. For the Omega Block material, this process is irrecoverable; i.e., the strains are not recovered when the material is unloaded. The Blockbond grout material has much less void volume, so it does not show such a collapse, and recovers some portion of the strain.

The second issue is drawn from the yield or failure surface. In Figure 77b and Figure 77d, the second invariant of the deviatoric stress tensor (J_2) is plotted as a function of the mean stress (P). The shear strength component of the stress tensor depends on the hydrostatic compression of the material. This dependence persists with increasing pressure until the shear planes are "oiled" with entrapped water, or with the crushed material itself. This is referred to as the "von Mises Limit", as shown in Figure 77 d. The third item of interest is also demonstrated in the yield surface curves of Figure 77b and Figure 77d. Note that, as the pressure is reduced into the tension domain (negative in the figure plots), the material will lose shear strength. When the negative pressure becomes greater than the material's tensile strength, a tensile fracture will occur and the shear strength will drop to zero.

The material properties for the steel structural items evaluated in the study were provided by MSHA (Reference 28). These were taken from the West Penn Testing Group Report No. 29589-1, and are detailed in Table 4.

Table 4. Steel Material Properties

Component ID	Yield Strength (psi)	Ultimate Strength (psi)	Total Elongation (%)
Belt Hanger	47,140	67,790	37.0
Bearing Plate	46,510	51,970	23.3
Spider Plate	27,370	43,660	43.1
Pie Plate	33,550	51,330	36.3
Rockbolt	59,380	83,570	33.5

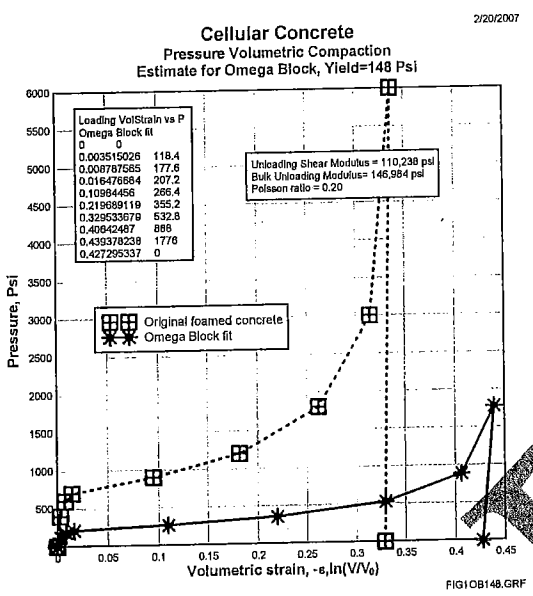

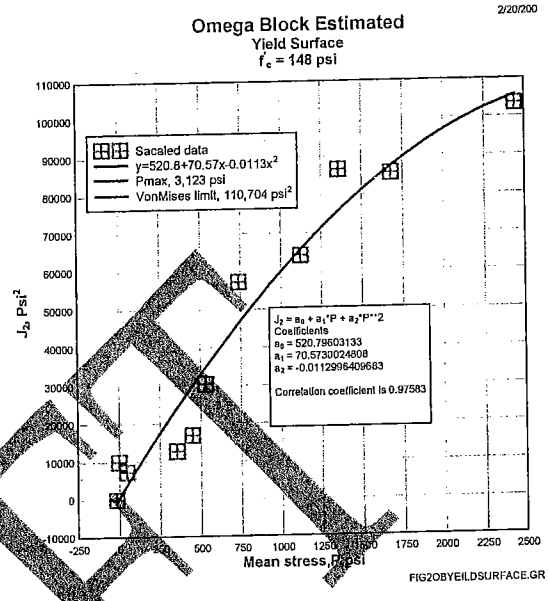

a. P-V curve for Omega Block material

b. Yield surface for Omega Block material

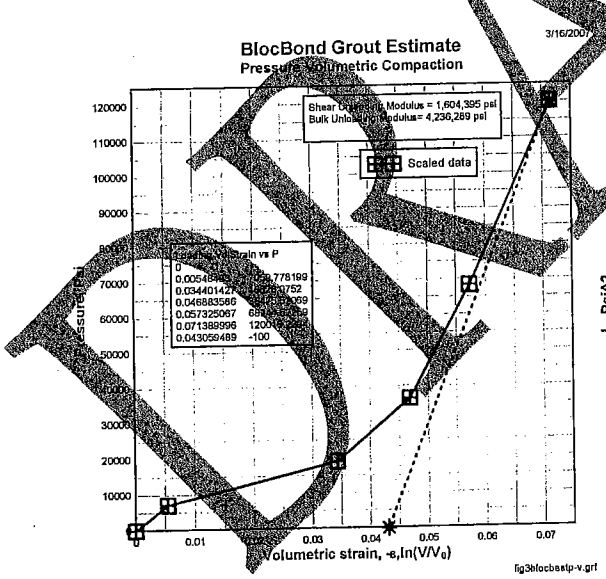

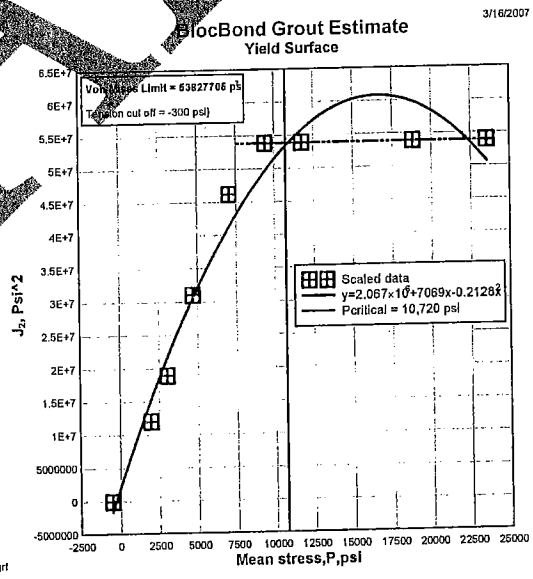

c. P-V curve for Blocbond Grout

d. Yield surface for Blocbond Grout

Figure 77. Pressure-volume curves (left) and fits of yield surfaces (right) for Sago seal materials, estimated from available properties data and failure surfaces for similar materials in the ERDC materials library.

Finite Element Analyses

Procedures

Several advanced computer codes were used in combination to analyze the performance under blast loadings of specific structural items that were damaged or destroyed in the Sago Mine incident. These items included the spider plates and pie pans, the belt hangers, rock bolts, and the mine seals. The results would provide important indications of the explosion environment in the mine that lead to the type and extent of damage observed. Comparisons were made against test data when available (LLEM experiments), but the other components were simulated to determine structural capacity and response to possible blast loads cases.

All of the structural elements were modeled using finite element (FE) formulations; specifically, the codes LS-DYNA (Reference 29) or DYNAN_3d (Reference 30), depending on the loading conditions. LS-DYNA was used when pressure boundary conditions were sufficient to perform the simulation, but when the flow field needed to be coupled to the structural calculation, Dynan_3d was used in conjunction with the Eulerian flow code Gemini, within the suite of codes called DYSMAS (Reference 31). A brief description of LS-DYNA and DYSMAS follows.

LS-DYNA. LS-DYNA is a general purpose, transient dynamic, finite element program capable of simulating complex real world problems. The code was developed specifically to perform analyses of structural response to impact and blast loadings. It is optimized for shared and distributed memory on Unix, Linux, and Windows-based platforms. LS-DYNA has nearly 100 constitutive models to simulate a whole range of engineering materials, from steels to composites and from soft foams to concrete. The new Version 971 features updated models for shell and solid elements, with an extensive element library, including membrane, thin-shell, thick-shell, and solid formulations.

LS-DYNA has many solution procedures to simulate the physical behavior of 3D structures: nonlinear dynamics, thermal, failure, crack propagation, contact, quasi-static, Eulerian, arbitrary Lagrangian-Eulerian (ALE), fluid structure interaction, real-time acoustics, multi-physics coupling, etc. The lower order finite elements in LS-DYNA are accurate, efficient, simple and fast.

DYSMAS. The coupled code DYSMAS was developed by NSWC/Indian Head and the Germans to calculate the response of structures under explosion blast loadings involving fluid-structure interaction (note: air is treated as a compressible fluid in

these problems). DYSMAS is based on the use of three modules: the Eulerian code Gemini, to perform the fluid flow calculations; the Lagrangian code DynaN (a derivative of Dyna3d), to perform the structural response calculations, and a coupler module that interfaces information between the two codes. This enables DYSMAS to execute simulations that include explicit shock fronts, structural fracture, and fluid breakthrough, among other things. Gemini is capable of handling both compressible and incompressible fluids. The Gemini code can be run in parallel on HPC systems to enable the calculation of very large simulations; i.e., with several million elements.

ERDC has used DYSMAS to simulate close-in explosions and fluid-structure interaction problems against a variety of structures. These include dam components (steel gates, gravity sections, powerhouse walls, etc.), large water tanks, bridge structures, blast doors, and similar items.

Computational Resources. The FE calculations were performed on various systems at two of the DOD's Major Shared Resource Centers (MSRC). The primary location for the use of LSDYNA is the SGI Altix 3700 system at the Aeronautical Systems Center (ASC) MSRC (located at Wright-Patterson AFB). DYSMAS can be run on that same SGI Altix, as well as the SGI Origin 3900 machines at ASC and the ERDC MSRC (located in Vicksburg, MS).

The LSDYNA calculations were typically relatively small (<100,000 elements within the model) for the conveyor belt hangers, or in the case of the seal walls, the rectangular construction was not geometrically very complicated. Each conveyor belt hanger response simulation took less than 24 hours on 16 processors. Calculations of the response of the Omega Block seals were larger (300k elements), due to the actual physical size of the seal wall that needed to be modeled, but still took less than 24 hours on 32 processors. Considerable time and effort was used generate the models and post-process the results.

For the DYSMAS calculations, the structural response portion of the rock bolt and surface plate simulations took very little time compared to the calculation of the fluid flow around the structure. These coupled simulations took approximately 24 hours on 28 processors.

Finite Element Model Descriptions

Each modeled structure consisted of finite elements, either four-noded shells – as in the case of the spider and pie plates – or eight-noded solid elements – as were used for the ventilation seal walls, the conveyor belt hangers, and the rock bolts. Loads were applied as pressure boundary conditions to the seals and hangers; i.e., a pressure-time history was applied to the faces of specific element faces to simulate the loadings. The plate loads were generated by the coupled calculations, which directly applied the CFD flow field to the structure.

Two different types of loading were used; a blast loading condition, either idealized or taken from experimental data, or a linearly increasing load that was applied to determine the load capacity of a particular structural element. This load capacity was then used to calculate a load-deflection response curve for that structural element (which could also be used in a simplified analysis, such as the SDOF calculations described later in this chapter). For the steel structures attached to the tunnel ceiling, the loads were applied to the ceiling plates via an interface boundary, which gathered the loads from the calculated pressure flow field and applied them to the elements within the structure model. Boundary conditions were simulated by applying fixity to certain nodes – constraining motion in certain directions – to simulate the restrained edges of a model, including "fixed" walls, ceilings, and symmetry planes.

The material properties used in the models are described in the section on Constitutive Material Models. An elastic-plastic material model was used for the steel of the spider plates, pie pans, belt hangers, and the bearing plates. Each model explicitly defined the yield strength, the elastic (Young's) modulus, Poisson's ratio, a post- yield work-hardening curve, and a failure level for effective plastic strain. When an element reaches that effective plastic strain limit, it is "eroded", or removed from the simulation, approximating failure of the steel at that location within the model. A strain rate enhancement curve taken from the DAHS manual (Reference 32) was used as typical for all the steel models, providing a higher stress level as the strain rates increased within the simulations.

Specific descriptions and pictures of the models for each structural component – ventilation seal walls, conveyor belt hangers, and spider and pie plates – are provided in the following sections.

The following sections describe the application of the FE technique to describe damage response as a function of the applied loads. The response of a structure to

a highly dynamic loading, such as from an explosion, can be represented by a load-deflection curve, defining resistance function for use in simplified analysis. This function can be generated using a Finite Element (FE) model by applying a linearly increasing, uniform pressure to one side of wall from the virgin state to the failed condition.

Characterizing Blast Loads

When a deflagration or detonation event takes place, the pressure field produced has two flow-field components. The first (and most commonly associated with explosions) is the overpressure --- also called the side-on pressure, since it is measured by a gage mounted with the sensing face parallel to the flow. This pressure is generated primarily by the compression of the "fluid" surrounding the event (note that air is also treated as a fluid), and its subsequent decompression. The second component is the dynamic pressure, Q(t), as measured by a gage with the sensing element aimed directly into the flow field. A perfect dynamic pressure gage would cause no disturbance to the fluid flow. In real life, however, the gages do cause some disturbance, causing it to measure some amount of overpressure in combination with the dynamic pressure.

The dynamic pressure is a function of the fluid density and the square of the particle velocity (U) of the fluid in the flow field. One common example of dynamic pressure is the wind in a hurricane or tornado. As the fluid flow field (i.e., the wind) interacts with a structure, the flow stagnates on the upwind side of the structure, thereby creating a force on the structure. This force is usually referred to as the average drag force (Qd) on the structure, and is equal to the dynamic pressure multiplied by a coefficient, Cd. This coefficient is experimentally determined for various geometric configurations of the structure.

The resulting total pressure on a structure exposed to drag loads can be expressed as

$$Qd(t) = Cd * Q(t) = Cd * (0.5 * \rho(t) * U(t)^2) \quad (8)$$

Where, $\rho(t)$ is the fluid density time history, and U(t) is the particle velocity normal to the surface of the structure.

The value of Cd is approximately 2 for both the Sago hangers, and the rockbolts.

The CFD code SAGE generates the complete flow field. Using the fluid density and particle velocity time-histories defined by the code, the complete dynamic pressure

history can then be calculated, along with the drag pressures on the hangers and bolts, as detailed above. These loads were then applied to the hanger and rock bolt FE models.

Roof Support Surface Plates

FE simulations were performed to evaluate the response of two types of rock bolt plates used in the Sago Mine -- spider plates and pie pans -- to the blast flow field in a mine tunnel. Figure 78 shows the 3-D model of the spider plate used in the FE calculations. The edges of the hole where the rockbolt passes through the plate were fixed in space to simulate the rockbolt holding this location completely rigid and fixed.

The structural model contained three parts: the plate itself, a small bearing plate, and a flat section representing the roof of the drift. Each part consisted of shell elements with the correct thicknesses to match the component, and contact was enabled between the parts to ensure that their interactive response was captured. Material properties for all the steel structural components are given in Table 4.

Since the spider plates and pie pans are made of very thin steel and are very flexible, simply applying a pressure boundary condition was not suitable. The flexibility creates a situation where fluid-structure interaction becomes important. Calculating the structural response of the plates in an environment where the initial flows are parallel to the major plane of the structure is not simple, and requires defining the interaction between the structure and the surrounding flow field. As the plate responds, bending changes its profile within the flow field, exposing it to higher loads. The structure responds fast enough to affect the loading upon itself. By coupling the blast environment to the structural model, this interaction can be captured and a more representative response can be calculated.

An important consideration for these calculations was the generation of the flow field at the plate locations. Using the pressure time history recorded at 304 feet from the blast chamber in LLEM Test 506 as a reference base, several methods were used to generate this field. Figure 79 shows an example of the flow field mapped into three-dimensional space and about to strike a spider plate. This figure depicts a cross-section of the flow field, where the change in color represents the boundary between the undisturbed environment and the blast environment, as the blast moves from left to right. Since a properly calibrated growth and ignition model for the methane air mixture was not available within DYSMAS, an equivalent flow field was generated by assuming the detonation of a TNT explosive

charge of a size and standoff distance that would produce the same pressure-time history as recorded at the 304-ft range on LLEM Test 506.

One and two-dimensional analyses were used to generate the initial blast environment calculations and were run out to the point where the flow field was about to reach the plate location. At this point the flow field was mapped into 3-D space and a calculation performed where the flow field moved across the plate. The starting point for this 3-dimensional calculation is shown in Figure 79.

The initial interaction between the flow field and the spider plate can be seen in the cross cut of pressure plotted with the structure in Figure 80. The areas of higher pressure, indicated in pink, are where reflections come off the ridge of the plate, and a stagnation area of lower pressure, indicated by yellow and green, occurs behind the ridge. Initially, the plate is pushed up into the roof, as shown in Figure 81, where the red coloring shows the areas of greatest vertical upward deflection (at this point in the simulation that equals less than 0.10 inch).

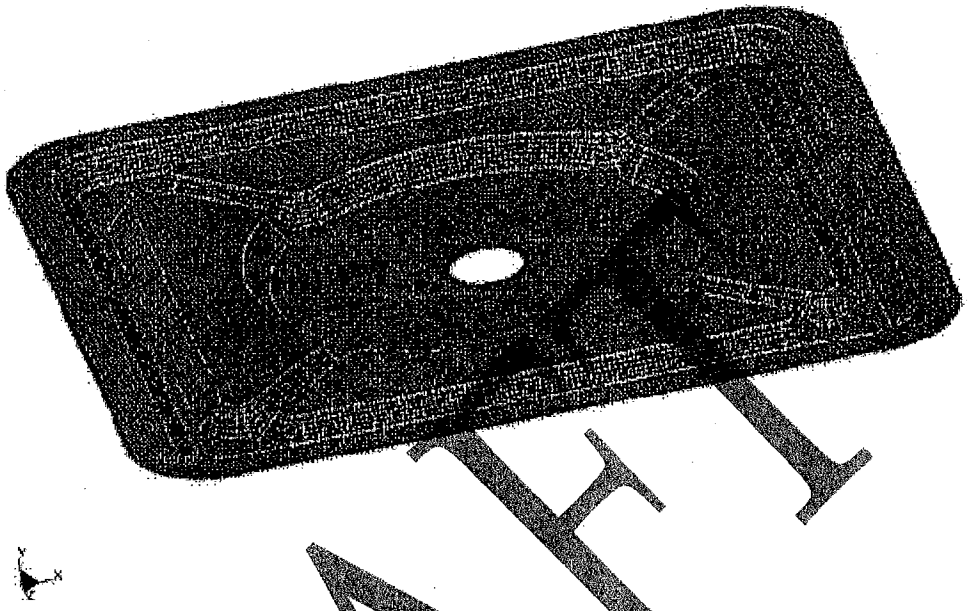

Figure 78. DYSMAS Spider Plate Model

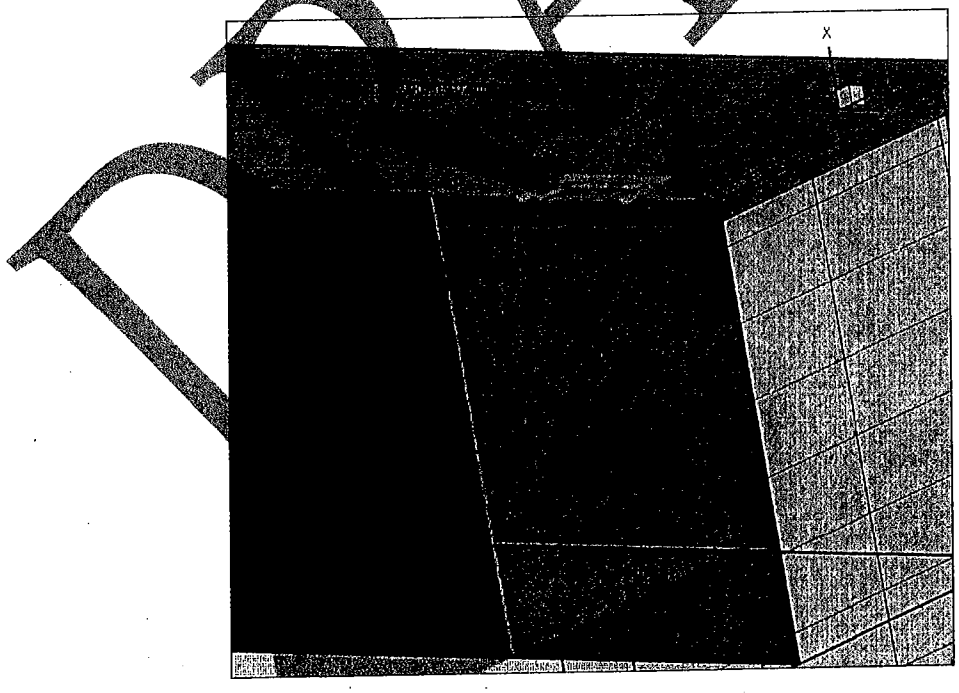

Figure 79. DYSMAS 3-D representation of blast wave approaching a spider plate.

Multiple iterations of these calculations were performed in an attempt to model the response over a longer time period; i.e., until the initial blast wave has passed the plate location and its reflection is coming back from the seal. However, numerical problems only allowed the simulations to be carried out to approximately 15 msec after the blast wave first strikes the plate. The calculated plate deformation at that point in time is shown in Figure 82. The velocity of the plate deformation had not dropped to zero in the simulation at the point shown in Figure 82, so the final configuration of the plate deformation could not be exactly determined. However, the calculated deformation shown in Figure 82 closely resembles that observed in LLEM Test 506, as shown in Figure 83. The pie pan calculations were done in a similar manner as the spider plates. The driving flow field was the same as was used for the spider plates, and the plate configuration was developed in a manner similar to that in the spider plate calculations. The calculated pie pan deformation is shown in Figure 84. The portion toward the blast is bent over before the calculation was prematurely stopped. As can be seen in Figure 84b, the bearing plate is bent, which is similar to the deformation seen in LLEM Test 506 (see Figure 85). Again, since the calculation was prematurely stopped before the velocities dropped to zero, it cannot be concluded that the simulation captured the entire response, but the calculated damage to that point in time certainly resembles the experimental case results.

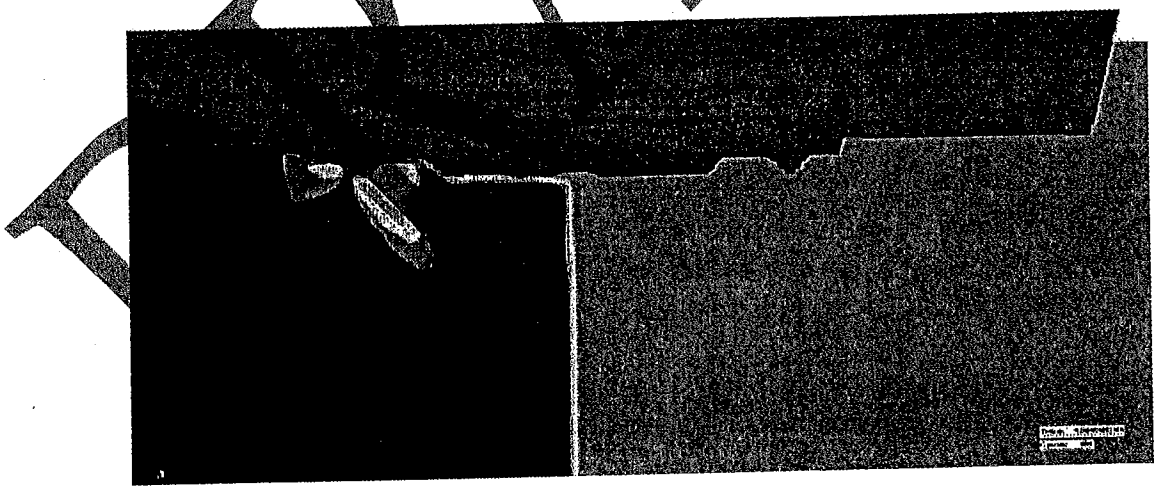

Figure 80. Early-time flow field as the blast wave (in red) moves from left to right across a spider plate. Note the turbulence at the leading edge of the plate.

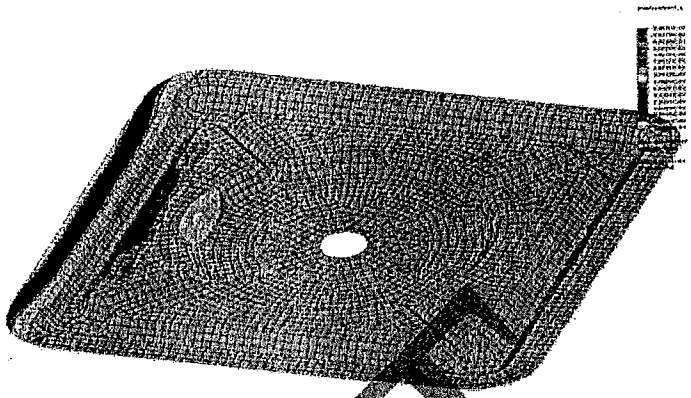

Figure 81. Early-time deflection of the spider plate.

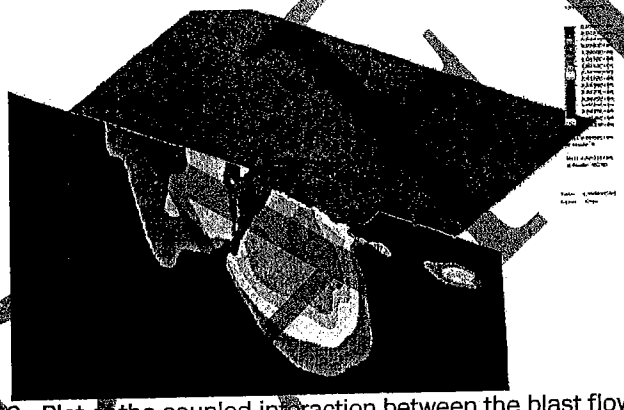

Figure 82. Plot of the coupled interaction between the blast flow field and the plate.

Figure 83. Spider plate deformation on LLEM Test 506, at the 304-ft range.

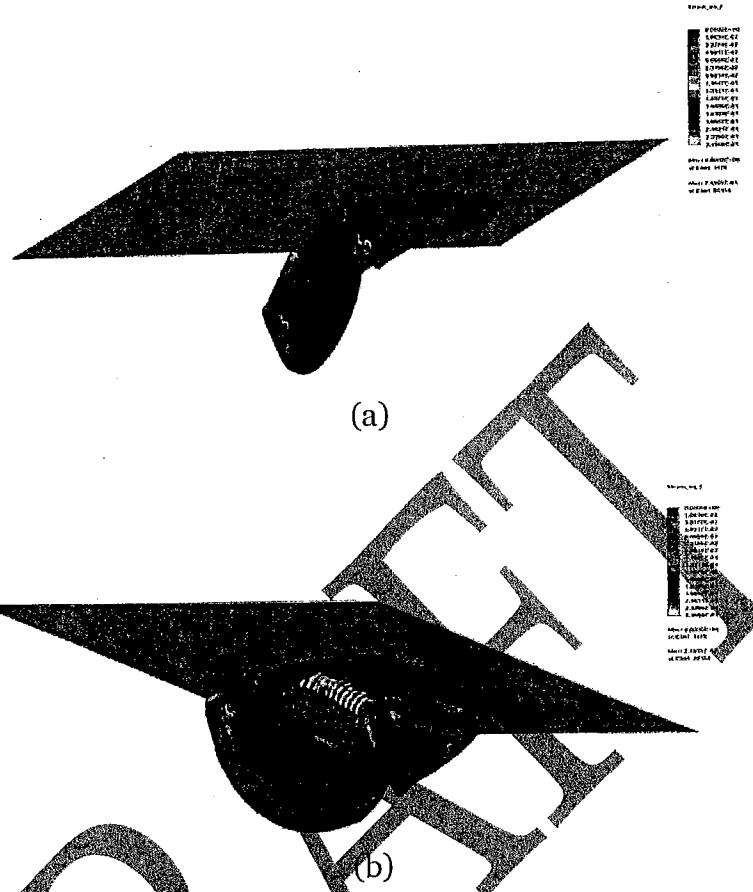

Figure 84. Loaded side (a) and opposite side (b) of the calculated pie pan deformation

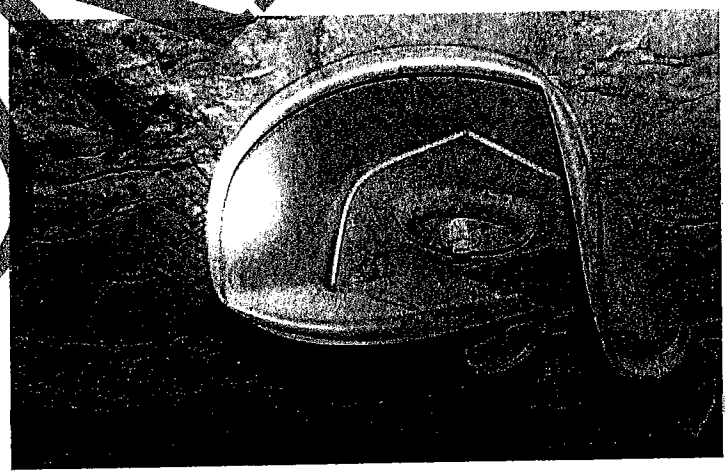

Figure 85. Pie pan deformation observed in LLEM Test 506, from measured blast pressures equivalent to those assumed in the FE simulation.

Belt hangers

Conveyor belt hangers are steel angles 4 inches wide and 0.25 inches thick. They are normally held against the tunnel ceiling by rock bolts 0.75 inches in diameter that are grouted into the tunnel ceiling. When an area is being mined, conveyor belts are hung from the belt hangers by a cable. After the belts are removed, the hangers are left in place. In areas where coal was later excavated from the tunnel crown, some of the rock bolts to which the belt hangers were attached were left exposed over a length of one to five feet above the hanger. A typical hanger is shown in Figure 86.

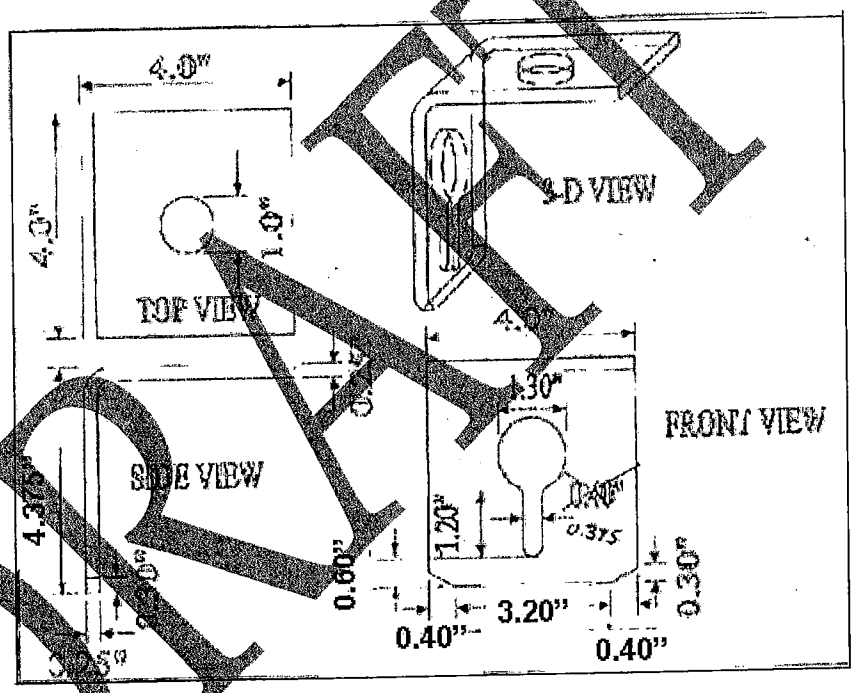

Figure 86. Dimensions and of a the conveyor belt hanger used in the analysis.

LSDYNA was used to perform dynamic analyses to determine the structural response of the conveyor belt hangers under several loading conditions. From an original flat plate, the hanger was first numerically "formed" into its finished shape in order to retain the strains generated by the forming process. Figure 87a shows the initial configuration of the belt hanger before the forming process. Included here are the tool and the form, and the process used by Broene (Reference 33) and Maker (Reference 34) was replicated here by imparting a defined displacement to the tool to push down and bend the hanger plate against the form to get the final configuration shown in Figure 87b. The form was rigid and fixed in space, while the tool was rigid and confined to only move along the vertical forming line. Each of these parts consisted of shell elements, while the belt hanger was constructed of solid elements to better capture the response as it deformed. After the plate was

bent to a 90-degree angle, the tool and form were removed, a representation of the ceiling was added, and the plate was fixed to the tunnel ceiling at the hole to represent the complete belt hanger (Figure 87c).

The hanger plate was subjected to linearly increasing levels of loadings to develop a resistance function, which allowed the generation of a load-displacement plot for the belt hanger and roughly determine the load levels required to produce various levels of response. The horizontal load was put on the hanger structure at a linearly-increasing rate of 100 psi per 0.1 second. Figure 88 shows an intermediate stage and the final deflection of the hanger. The load-deflection curve and the loading time history are shown in Figure 89.

Figure 90a shows a dynamic pressure time history from Run 1 (Station 32) of the CFD calculation applied as a pressure boundary condition to the belt hanger. This dynamic pressure is the quantity acting down the entry, normal to the face of the belt hanger and is derived from the adding the vector components of the x-and y-particle velocity time histories and the density time history as described above.

Figure 90b shows the resulting deflection-time history of the belt hanger from the FE calculation. Since the dynamic pressure loading does not exceed the yield load of about 150 psi, the response of the hanger is essentially elastic.

After observing the resulting behavior of an actual hanger that bends flat against the roof, several observations can be made. First, the top of the hanger (the portion against the roof) is more constrained than reality, and that affects the global response more than is actually seen in the test. A second point is that the loads applied here are follower forces on the front face of the hanger. This means the force stays normal to the plate regardless of its orientation. So in this simulation, the increasing load continues to be applied perpendicular to the plate as it is failing, further deforming the plate and causing the separation between the two legs of the hanger.

The load deflection response indicates that significant plastic strain exists in the plate before the blast loading (as is known from the forming process). This was determined due to the low amount of deformation followed by sudden extreme deflection and failure. Since the plate had already been work-hardened by the formation process, it had an increased stress level before going into further plastic deformation, but the capacity of plastic work remaining was diminished, leading to the observation that the load-deflection behavior was indicative of the stress states within the hanger. This response resulted in a capacity of approximately 200 psi in the hanger before it failed.

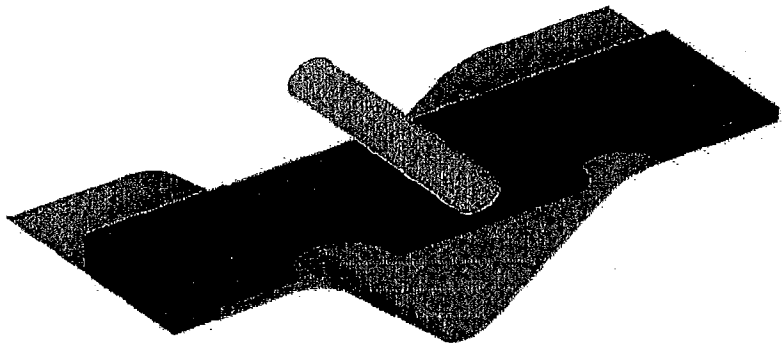

a. Simulation of the initial plate shape before bending.

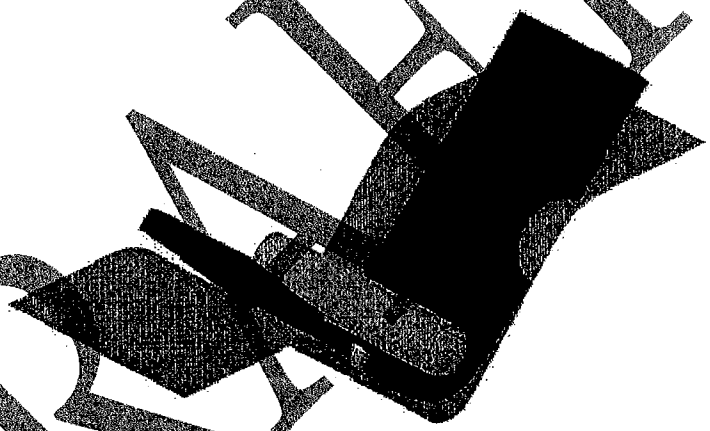

b. Belt hanger after bending into final shape.

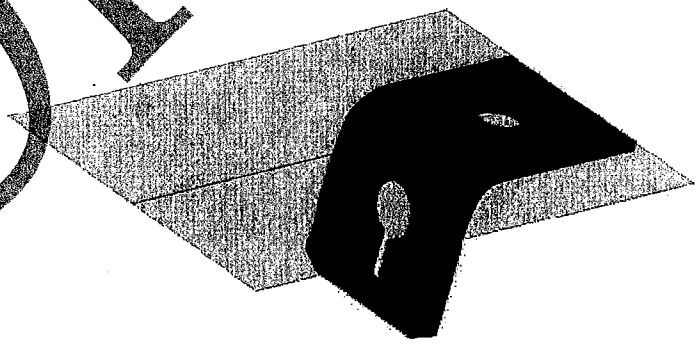

c. Belt hanger in position on tunnel ceiling before blast load was applied.

Figure 87. Numerical development of belt hanger configuration for analysis.

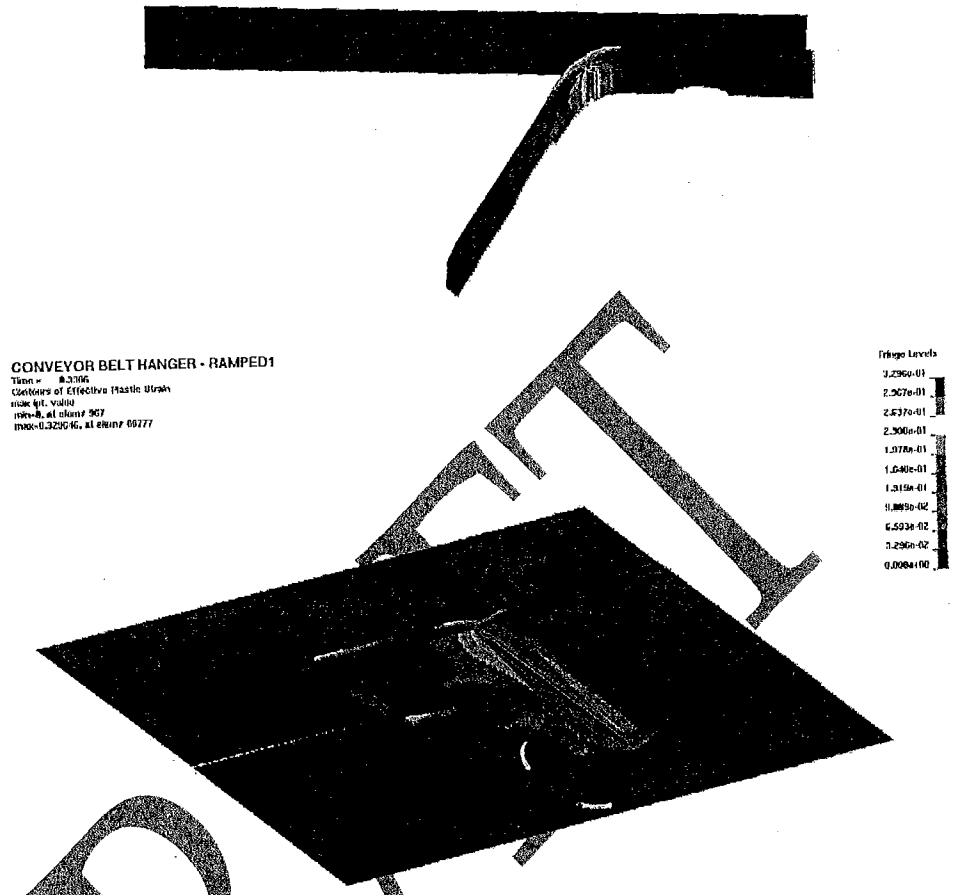

Figure 88. Intermediate (top) and final deflected shape of the belt hanger.

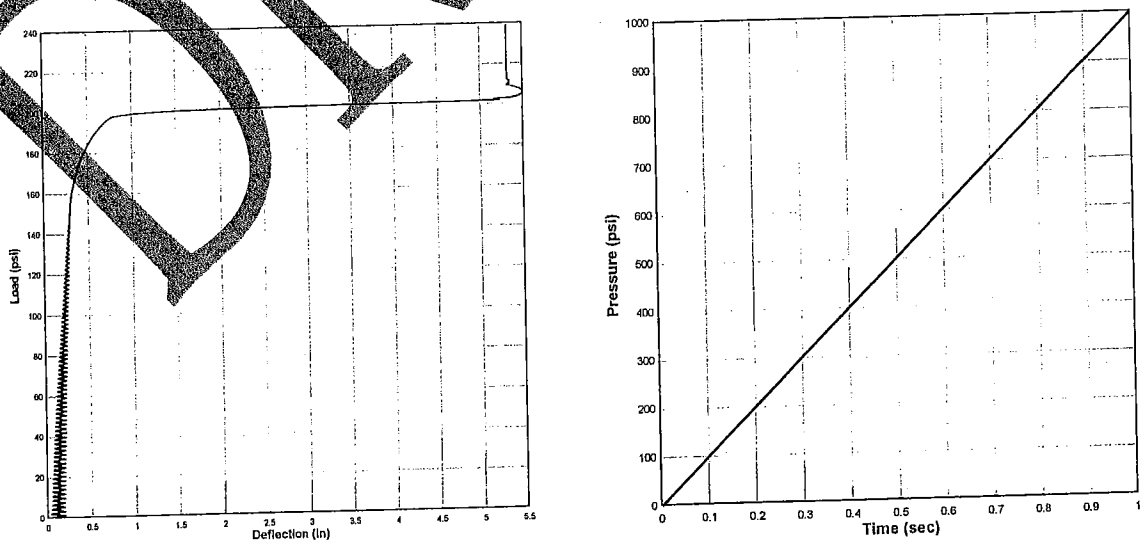

Figure 89. Load-deflection (left) and loading-time history (right) applied to belt hanger.

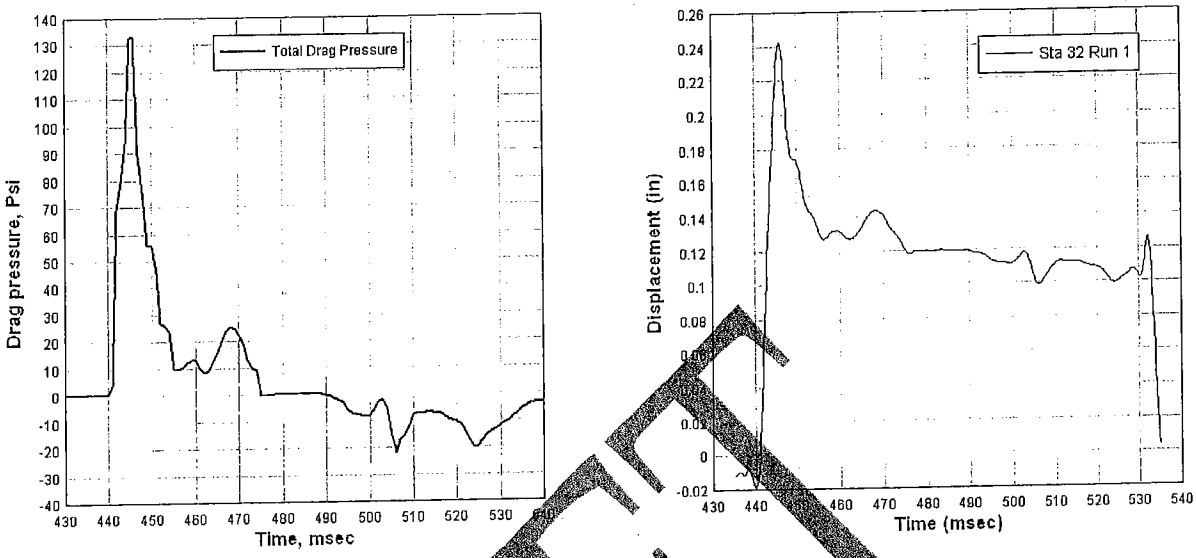

(a) (b)

Figure 90. Dynamic pressure loading applied to belt hanger from Run 1 CFD Sta 32 (1 cross cut back from seal number 7) (a) and the corresponding displacement time history from the FE analysis (b)

Rockbolts

Calculations were also performed for rockbolts that extended from the tunnel ceiling, with the extended length being exposed to the blast environment. A belt hanger was attached to the end of the rockbolt to provide the correct amount of drag. The portion of the rockbolt above the ceiling was numerically fixed and held rigid.

When the dynamic blast load generated by the CFD calculations was applied to the exposed portion of the rockbolt, significant bending was seen in the response. The initial and final positions of the rockbolt are shown in Figure 91a, along with the corresponding displacement time history (horizontal deflection for the end of the rockbolt) Figure 91b. Although the bolt experienced some plastic strain, the levels did not approach those necessary to cause failure beyond the bending deformation.

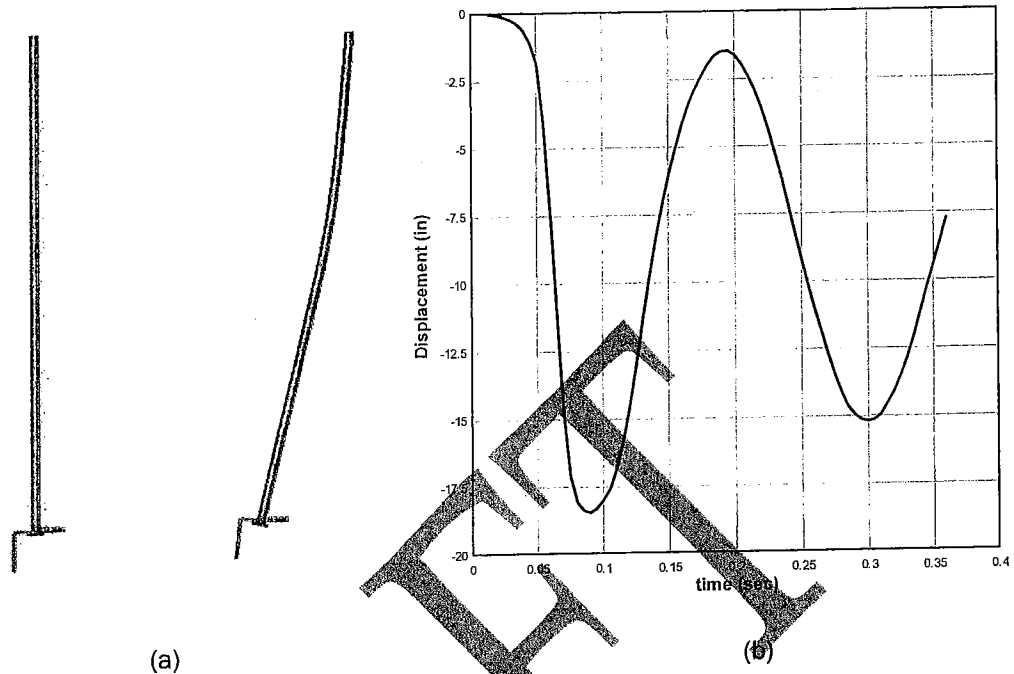

Figure 91. **Initial and final position of the extended portion of the rockbolt (a), and the horizontal displacement of the bolt and a function of time (b), under the applied blast loading.**

Mine Seals

Figure 92 shows the numerical representation for the FE model of an Omega block seal. The blocks are stacked exactly as they would be in a real seal, with alternating layers of a row of blocks placed longwise in front of a row placed shortwise, and vice versa. There is a 0.25-inch thick layer of Blocbond mortar explicitly modeled between each Omega block. The model also includes a 0.25-inch layer of BlocBond on all the faces of the wall.

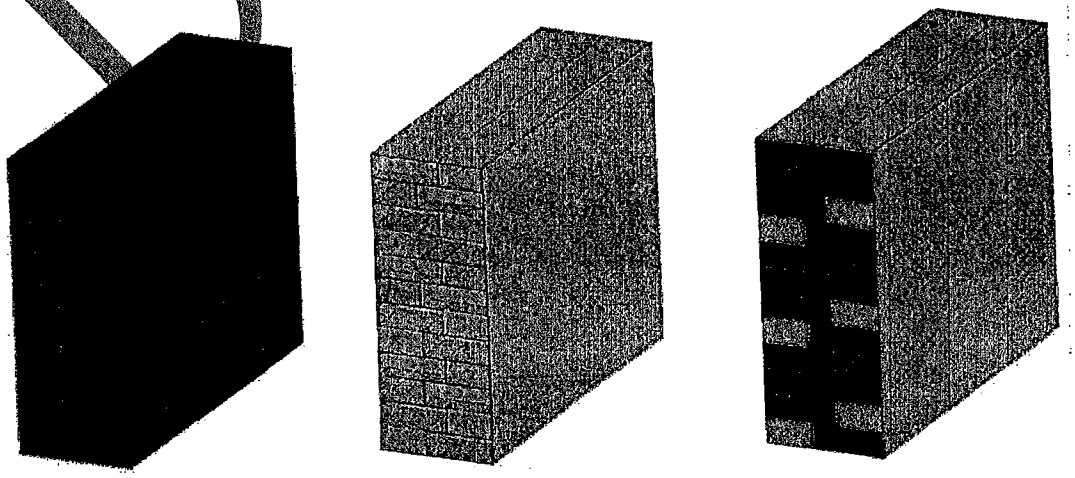

Figure 92. Omega blocks (left) and Blocbond mortar (center) components used to construct the Finite Element model of a complete mine seal (right).

Each block was composed of 325 solid elements. Each layer of BlocBond mortar was a single element thick, with the layout of the mortar elements coincident with that in the adjacent block. Each block and the surrounding BlocBond were numerically tied to the surrounding blocks, so any failure of the wall system was constrained to a failure within the models of the Omega and BlocBond materials. A failure criterion of 75 percent strain was added in later calculations for visualization purposes, and to allow the seal to fail and separate as it actually did in the NIOSH experiments at the LLEM. The material properties of the blocks and mortar are given at the beginning of this chapter, under *Constitutive Material Models.*

Three sets of FE simulations of the response of the Omega block seals to the methane blast loads were performed. The first two calculations were designed to validate the FE simulations against full-scale LLEM tests; Test 504, in which the seal survived, and Test 506, in which the seal was destroyed. Once the FE method was shown to compare well with the LLEM test results, a third simulation was run using the blast load developed by the CFD calculations for the Sago Mine incident.

Simulation of LLEM Test 504: For the simulation of Test 504, the loads placed on the FE model were the same as the time history recorded at the inby face of the seal on the LLEM experiment. These were measured directly in front of the seal, and accurately depict the reflected pressure load seen by the seal. This load was taken to be uniform over the entire cross section of the seal. Figure 93 shows the measured pressure-time history that was applied to the face of the seal in the simulation.

Figure 94 depicts the deformed shape of the seal as it responded to this loading, with the displacements magnified by a factor of 100. This shows a view looking at the symmetry plane down the middle of the seal, on the left half of the picture, with the wall of the drift being the fixed portion of the mesh, on the right side and away from the viewer. The parts that look like they're pulling out of the wall are just realizations of the areas where elements have failed and no longer have any strength, thus allowing some spurious motion of their nodes. This is not consequential to the overall response of the seal described herein. It can be seen in Figure 94 that arching action is not present in the vertical direction but, while it is not clearly seen, some horizontal arching is present across the width of the seal.

In Figure 95 the displacement at the center of the seal in the simulation is compared with the measured displacement at a corresponding location in Test 504. Two versions of the simulation were performed to represent the bounding cases for the fixity of the top of the seal. The wood slats that are usually wedged between the

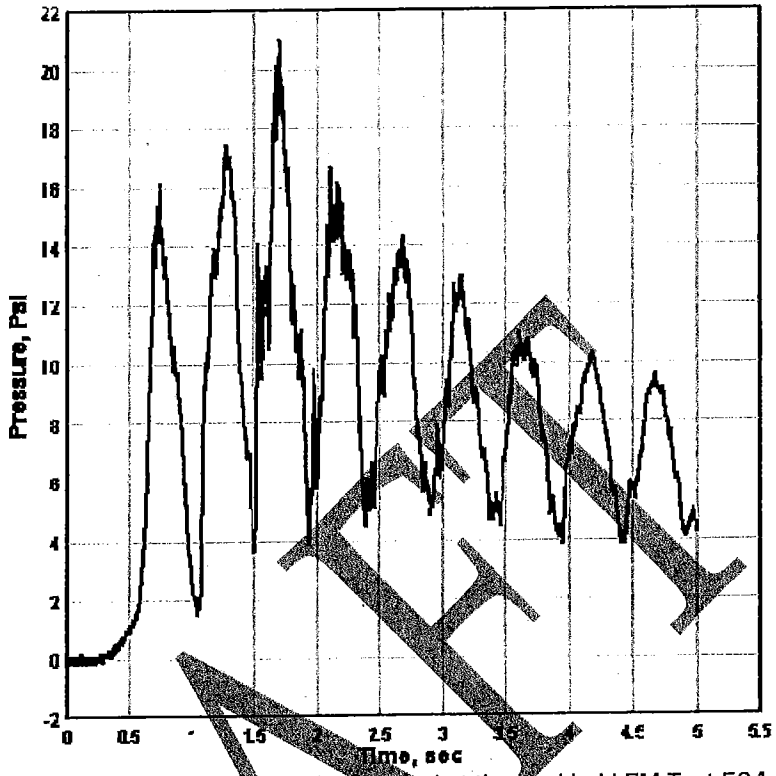

Figure 93. Pressure record measured at the seal in LLEM Test 504.

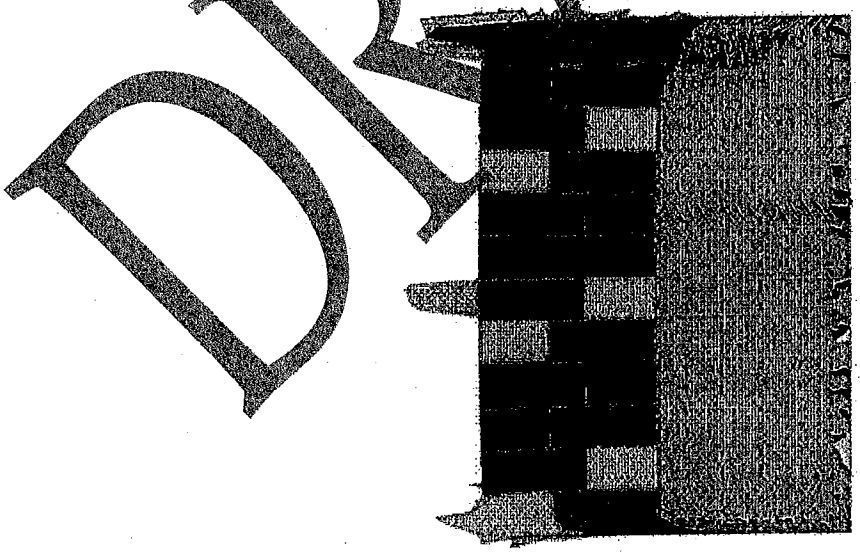

Figure 94. Simulation of seal response in LLEM Test 504, with deflection scaled up 100 times.

seal and the roof of the drift were not modeled. The cases modeled had either the nodes on the top of the wall free to move (unconstrained) or completely fixed in space (constrained). The unconstrained case resulted in unrealistically large deflections, while the corresponding peaks in the constrained case matched the measured results fairly well. Both simulation cases qualitatively track the excursions in the experiment record, with the constrained case showing an excellent match to the track of the experiment displacement pattern. Note that the displacement records all follow the oscillations of the measured pressure applied to the wall Figure 93.

Figure 96 shows the discrepancy between the numerical and experimental cases can clearly be seen at about 0.6 sec where there is a jump in the response of the simulations. It can be seen that quite a bit of failure has occurred around the edges of the wall (represented by element pressure being set to exactly zero in the "after" picture). This clearly shows the difference between reality, where the wall failure is more gradual, and the simulation, where element failure happens in a single time step and can lead to more brittle global failures, as shown in this comparison.

Overall, the simulation results compared well with the measured data, closely tracking the response with only slightly larger peak deflections. Globally speaking, the seal survived the simulation as it did during the experiment. The failure of the Omega block material in the simulation resulted in the 0.10 inches of permanent displacement, compared to the measured permanent displacement of about 0.05 inches.

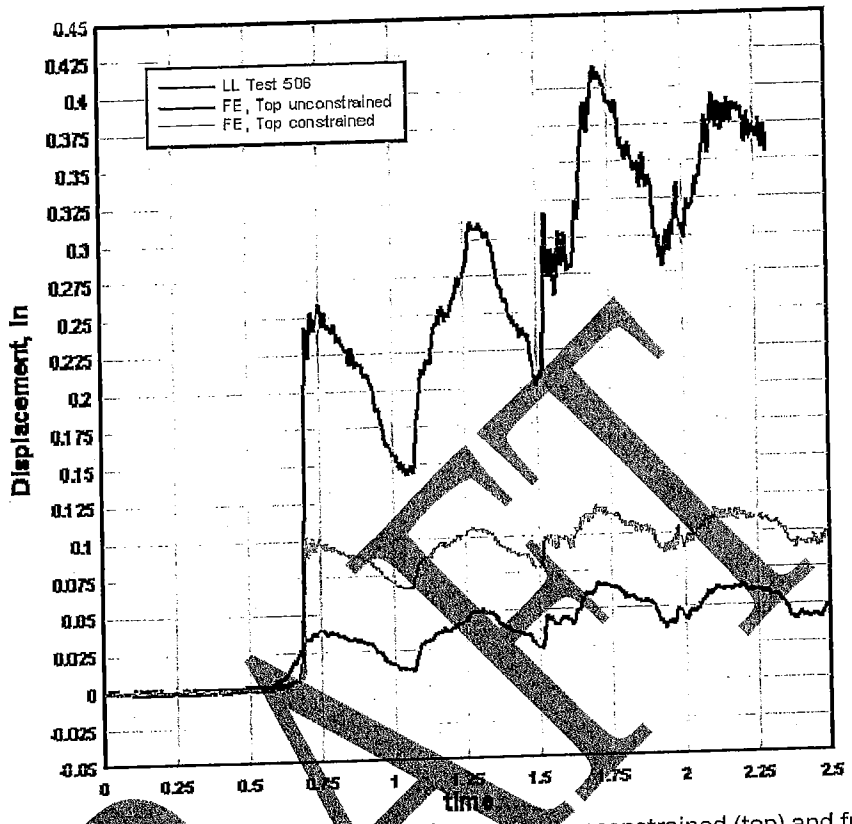

Figure 95. FE calculated displacements with the seal wall unconstrained (top) and fully constrained (center), compared to the measured record (bottom) from LLEM Test 504.

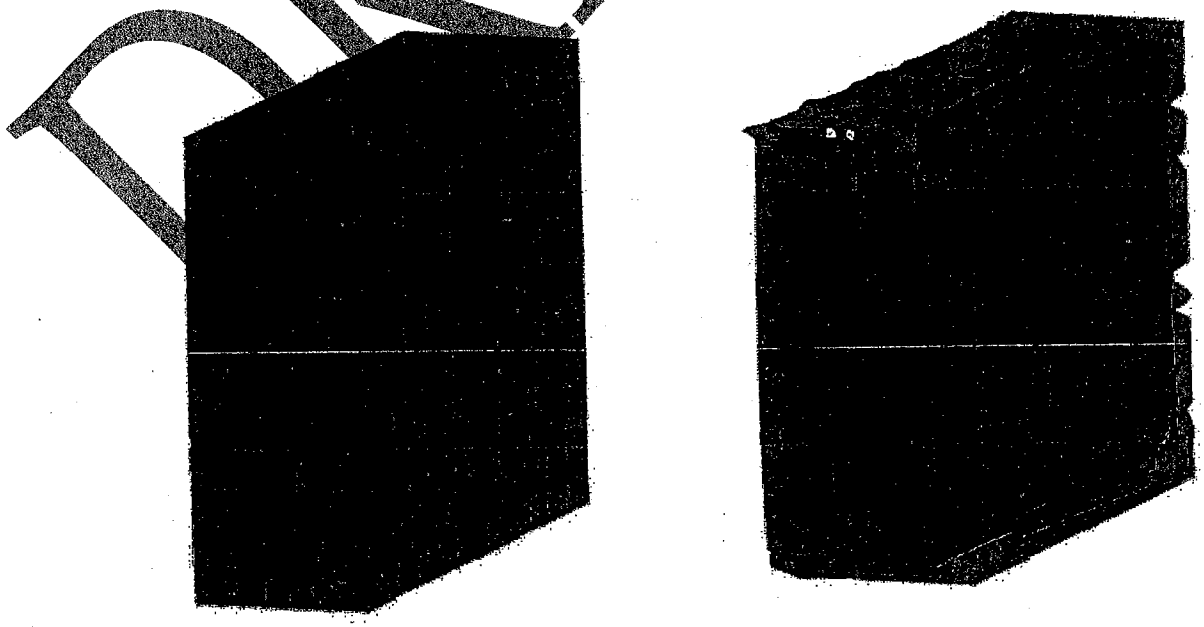

(a) (b)

Figure 96. Simulated Lake Lynn Test 504 (a) before deflection jump, (b) after deflection jump

Simulation of LLEM Test 506. The FE simulation of LLEM Test 506 was performed in order to compare the calculated response with the measured response for the case where a seal fails completely. Figure 97a shows the measured pressure and impulse loads from Test 506, which were also applied in the FE model to the simulated seal.

Figure 97b shows the calculated displacement at the center of the back of the seal, compared to the measurement obtained in the experiment at the same location. Unfortunately, the LVDT gage used in the experiment could only measure a maximum of six inches of displacement, so the test record is not valid beyond that point. For the FE calculations, only the case with the constrained top of the seal is shown in Figure 97b, but the case with the top unconstrained produced very similar results. If the measured record is projected past the point of gage failure, it can be seen that the simulation gives a very close approximation of the actual displacement of the seal, as it fails under the loading.

To provide a better understanding of what happens to the Omega block seal under the loading of Test 506, breakup of the structure was included in the FE simulation. Two criteria were used. First, the failure condition for the crushable foam material model was used with the same limits; a 15.0-psi tensile strength for the Omega blocks, and 300-psi tensile strength for the BlocBond. A strain erosion criterion of 75% within each element was also inserted to better visualize the results. This resulted in the seal response shown in Figures 98a and 98b, at times of 20 and 80 msec, respectively, after arrival of the loading wave. The wall initially arches in a similar fashion to Test 504, but then quickly begins to breakup. The Omega blocks fail first, followed by the BlocBond mortar, until the wall is broken into hundreds of pieces which would be propelled down the tunnel (which is not modeled). This qualitatively compares well with the debris field produced by Test 506. However, it is difficult to quantitatively compare these without explicitly modeling the tunnel as well as the seal, which would show some of the interaction between the seal debris and the tunnel boundaries. The difficulty of doing so did not seem justified by the value of the information that would be gained.

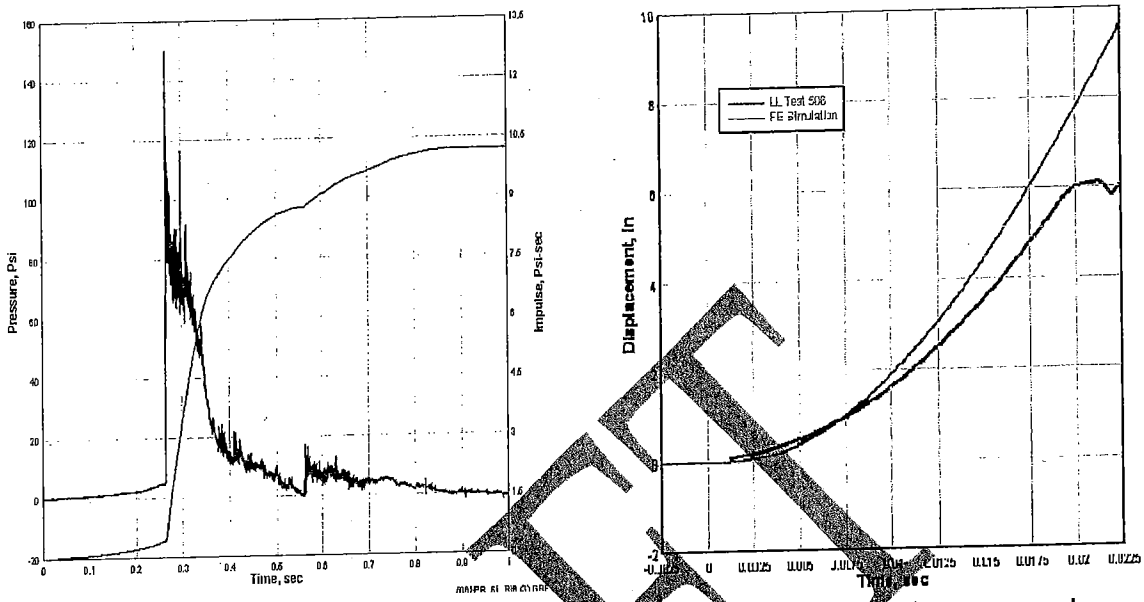

a. Measured pressure (spiked curve) impulse (smooth curve).

b. Calculated (top curve) versus and measured (lower curve) displacements

Figure 97. Loading conditions (left) and comparison of calculated and measured displacement response (right) of Omega seal in C drift for LLEM Test 506.

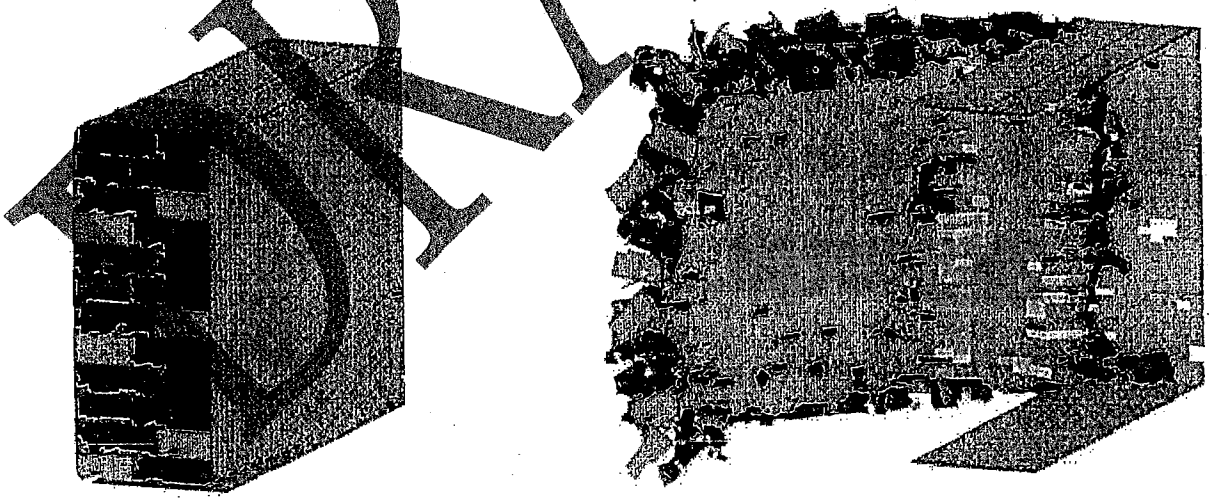

a. Deflections at 20 msec.

b. Deflections at 80 msec.

Figure 98. FE simulation of Omega seal breakup in LLEM Test 506.

Effect of the Loading Derived from the CFD Calculation. A pressure time history was generated by the Sago Mine CFD calculation at Seal 1 from Run2 (shown in Figure 99). This time history was then applied to the seal model to demonstrate the response that would occur from that loading level. The response was similar to that seen in Test 506, in that the seal failed (Figure 100) and the debris was propelled at high velocities down the tunnel (Figure 101).

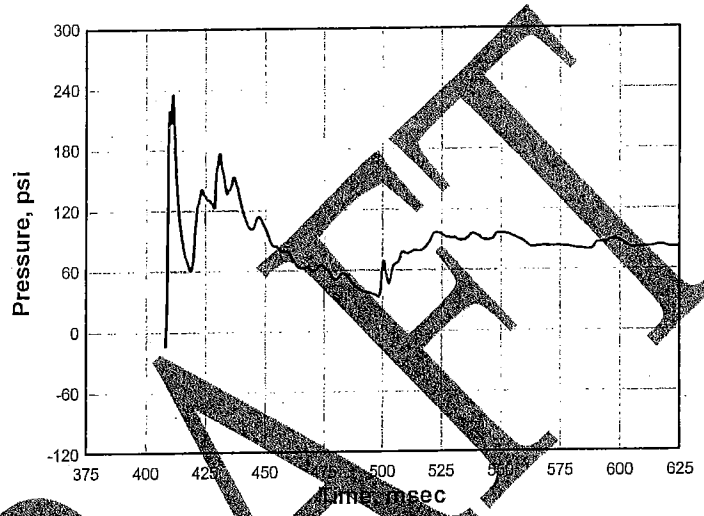

Figure 99. Load on Seal No. 1, from the SAGE CFD calculation, Run 2.

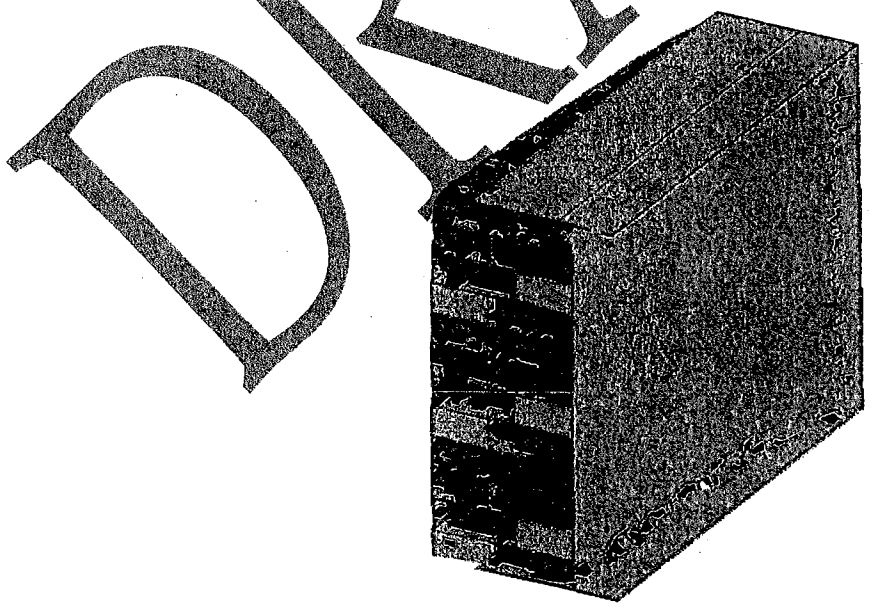

Figure 100. Early time response of Seal No. 1 to loading from SAGE Run 2.

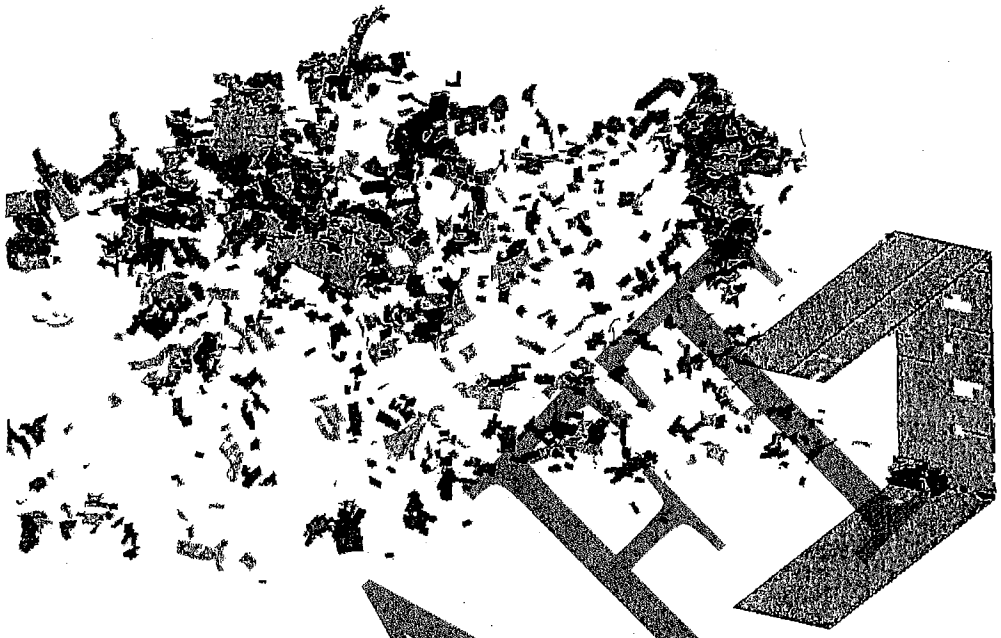

Figure 101. Late-time response of Seal No. 1 to the loading from SAGE Run 2.

Significant Findings from the FE Analysis:

- Seal Calculations were able to capture the failure mode of the Sago Seals, which was predominately a shear failure around the seal perimeter.

- Belt hanger calculations show the load required to initiate bending of the belt hangers was about 150 psi.

- A resistance function for use in SDOF analysis was generated for the belt hangers

- Spider plate and Pie pan calculations provided insight into the failure mechanism, time of response, and directionality of damage.

- Rock bolt calculations captured responses similar to those documented in damage surveys

- Specific correlation of FE results with the responses seen in Sago is difficult since the exact loading on each structural component within the mine is unknown and the pre-incident state of these components is also unknown (bent before incident?).

- Seal calculations compared well against LLEM tests 504 and 506.

- General failure of the seal seemed to be captured well by the models

- CFD loads produced extreme failure and propelled the debris at high velocities away from the original seal location.

SDOF Analysis of Mine Structures

Mine Seals

The results of the FE calculations have shown that the dominant response of the Sago seals is shear, as opposed to bending, of the block material around the perimeter of the seal. By definition, a single-degree-of-freedom (SDOF) model can approximate only on mode of response, therefore, a shear model was chosen.

In the development of any single-degree-of-freedom (SDOF) model, it should be remembered that we are trying to approximate the complex behavior of a multi-dimension structural response with a model that is only one-dimensional. The SDOF has two specific parameters, the mobilized mass and the system stiffness. The mobilized mass for the shear approximation can be taken as the entire mass of the section undergoing shear displacement. In a bending analysis, the mode shape being approximated is used to determine the "mass factor", whereas in the shear mode, the entire mass is moving. This same approach is used to determine the load factor for a bending analysis, but again, for the shear response the entire area is assumed to be loaded. In an SDOF bending analysis, the mass factor and the load factor are usually combined into a "mass-load" factor. In the shear SDOF analysis that follows, however, the mass-load factor is simply taken to be 1.0, since there is no contribution from the shape factors of the bending modes.

The second parameter is the system stiffness; i.e., the apparent spring response of the system as defined by the load-displacement curve. For the shear SDOF, the shear modulus, G, is needed along with an estimate of the shear strength, f_s, of the structural material in order to construct the "elastic" portion of the load-displacement function. By dividing the shear modulus into the strength (f_s / G), we can compute the shearing strain at "yield". Knowing this strain and the thickness of the material in the shear plane, we can calculate the displacement, d_e, at yield. Data from direct shear test are needed to establish the ultimate shearing strain. Knowing the ultimate shearing strain and the thickness, we can compute the ultimate displacement, d_u, for the system.

We are left with only one more displacement point to construct for our load-displacement curve. Since the shearing strain occur across the entire shear plane, the shearing forces result in a failure mode that is very abrupt, and we must choose a value of displacement where the load capacity of our model is zero. To minimized numerical instabilities during the solution of the SDOF, this point may be taken to be equal to the "elastic" yield point plus the ultimate displacement (d_e + d_u). The purposed construct will generate design-conservative results for external loads that are sufficient to cause a shear failure.

The final step is to establish the loads on the system that are to be paired with the system displacement points derived above. Since we know the yield strength of the material, f_s, and the available shear area, A_s, we can calculate the shear capacity of the system, F_s, as f_s times A_s. Using the external loaded area, A_l, the external load, P_y, required to cause yield is equal to F_s/A_l. This is also the load to be paired with d_u. The resulting load-displacement curve determined through the above process is shown in Figure 102.

To demonstrate the Shear SDOF, two calculations with time-varying loads were performed. Shown in Figure 103 is the displacement-time history result of the Shear SDOF using the pressure loading history of LLEM Test 504. The calculated history is compared with the LVDT data recorded on the same test for the seal located in the C drift, as an evaluation of the "elastic" part of the model. The agreement is quite good. It is interesting to note that the LVDT-measured response does not follow the decay in the pressure loading at late times, whereas the SDOF model does. If the LVDT data can be considered accurate, then the seal is exhibiting a softening in cyclic shear response at loads below the shear strength. This complex behavior is not represented by the model, however.

A second calculation was performed using exactly the same model of the Shear SDOF, but with the loading from LLEM Test 505. A comparison of the SDOF-calculated response and the LVDT data from the Test 505 (seal located in C-drift) is presented in Figure 104. The comparison can be made only up to a displacement of approximately 6 inches, at which time the LVDT is stroke-limited. Also shown in this figure is a comparison of the initial velocity of the seal up to the same 6-inch displacement. Again, the comparison is quite good. Note that the SDOF appears to slightly over-predict the displacement and velocity at the end of the LVDT stroke.

To demonstrate the Shear SDOF model as a rapid assessment tool, the model was used to generate pressure-impulse (PI) curves and to compare the calculated response with data from the LLEM Tests 504, 505, and 506. Figure 105 presents the comparative results in PI format. The two criteria chosen for the PI's are the "yield" displacement(0.16 inch), to segregate the elastic response region from initiation of shear damage, and the "ultimate" displacement (0.86 inch), which represents the displacement from which the system cannot recover, and brittle failure is imminent. The PI curve was generated using the WAC code (Reference 35). WAC iterates on a wide range of open air charge weights, calculating free-air pressure and impulse pairs to drive the SDOF computation, and determining the P-I pair that matches the response level desired. Strictly speaking, the P-I curves generated should only be used for free-air pressure pulses where the wave-shape

exponentially decays from the peak to ambient pressure over the duration of the pressur pulse. However, the wave shapes measured in the LLEM experiments closely approximate this shape. Therefore, plotting the results of the LLEM Sago wall results against the calculated P-I curves for the Sago walls gives us some insight into the response of these walls.

Firstly, we see that the tests in which the Sago walls did not fail fall to the left of the "yield" curve, indicating that the SDOF shear model would have predicted that they remained elastic. Secondly, All but one test in which the walls failed fall to the right of the "ultimate" curve indicting that the SDOF shear model would have predicted that the walls would have failed. One the test between the "yield" and "ultimate" curves is close to the failed line, and was shown to fail from the pressure pulse that reflected off of the seal in drift 3, so it was essentially loaded twice.

The other observation we can make from the LLEM Sago wall data compared to the PI curve is the relative position of the P-I pairs. They are all up on the "static pressure" side of the P-I curves. This is to say that the loads the seals experienced are of sufficient duration that they are responding to the peak pressure applied.

Lastly, the P-I presentation demonstrates that the SDOF shear model provides reasonable estimates of Sago wall design failures.

The Omega block wall constructed in X-cut 2, which survived experiments 501 through 506 and experienced pressure loadings from 23-, 22-, 15-, 26-, and 51-psi was constructed as a "proper" Omega wall. The differences in a Sago wall and a proper wall are in the construction process, namely the Sago wall used a dry mortar bed to start the first course, and in the Proper wall, much more attention to detail was used in wedging and mortaring the top of the wall. Using the SDOF shear analysis described above, the result would have been failure of the wall for tests wher the pressure was above about 20 psi. Possible explanation of why this wall did not fail include, better construction practices, the Omega blocks used had a higher average strength, stronger bloc bond material, increased thickness of bloc bond mortar beds, increased thickness of block bond face coatings, and more attention to wedging in the top of the wall and applying the block bond at the top of the wall. Further analysis of these parameters would be required to definitively answer why the "Proper" was significantly stronger than the "Sago" wall.

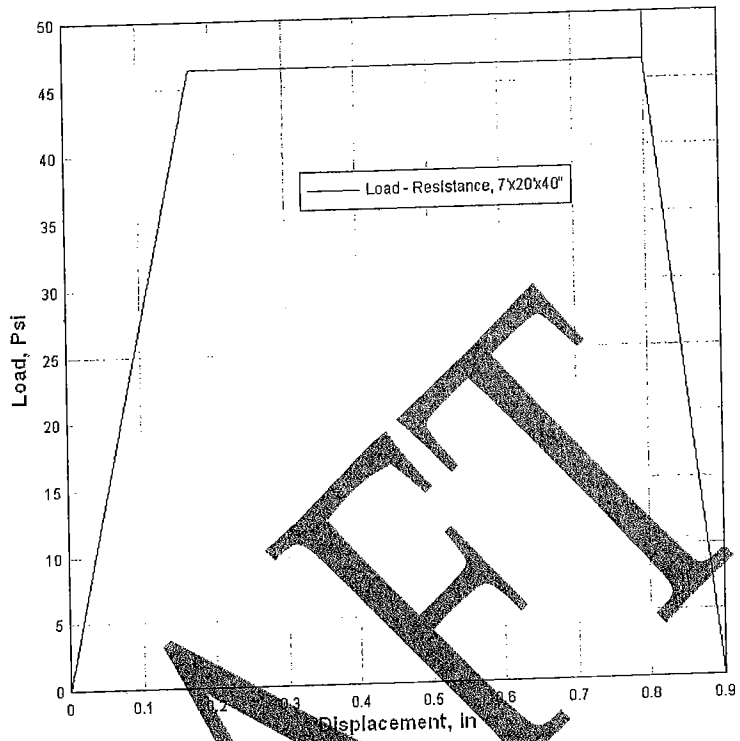

Figure 102. Shear SDOF load-displacement curve for an Omega Block Seal

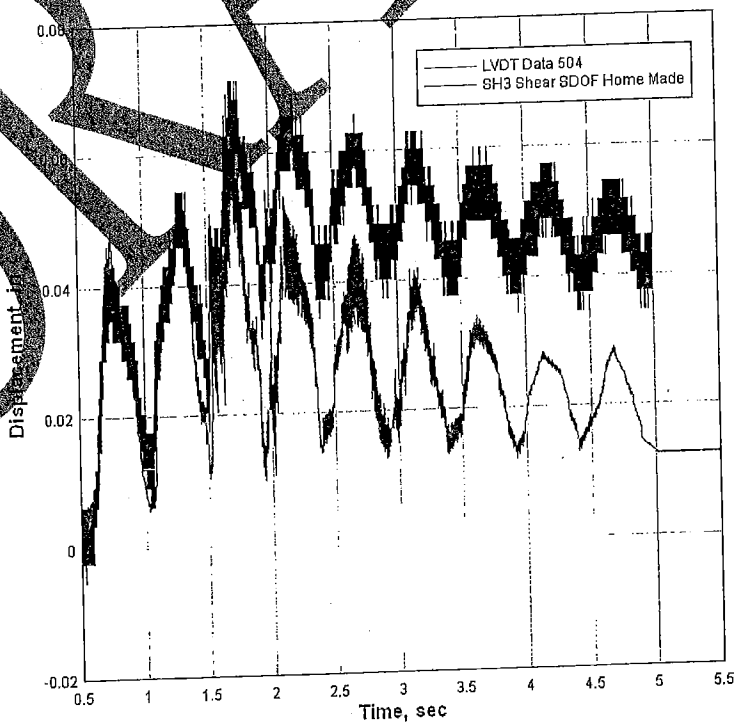

Figure 103. SDOF shear displacement compared to LVDT-recorded displacement, for LL Test 504

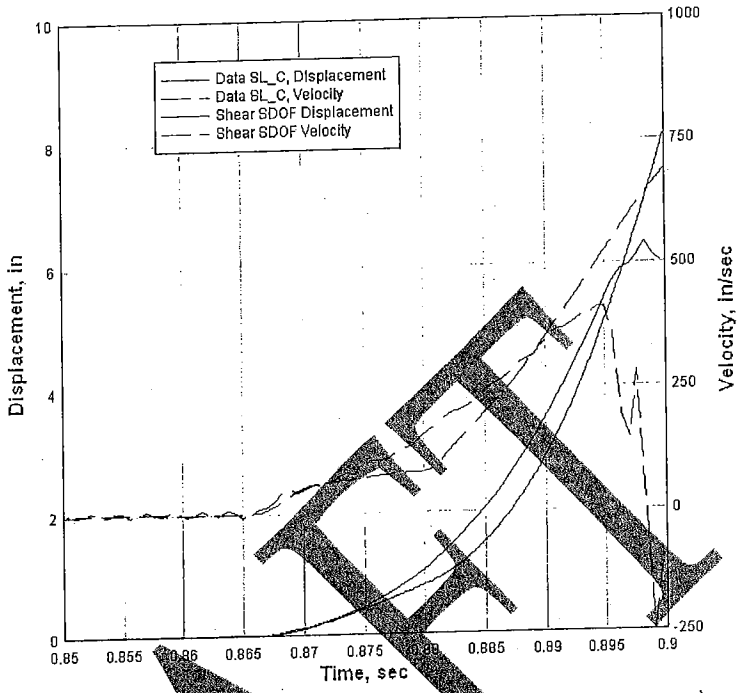

Figure 104. SDOF-calculated shear displacement and velocity (lower curves) compared to those recorded on LLEM Test 505 (upper curves).

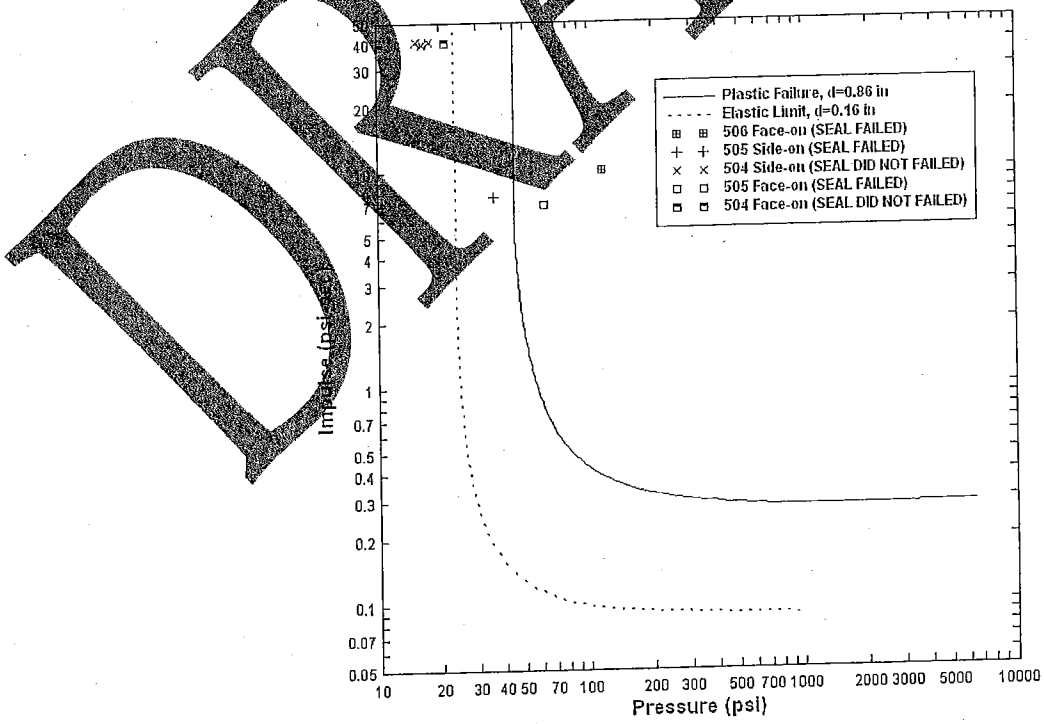

Figure 105. PI curves calculated by the SDOF model compared with those from measurements on LLEM Tests 504 - 506.

Belt Hangers and Rock Bolts

Many of the belt hangers and exposed bolts in the Second Left Mains were bent by the force of the methane explosion. It would first appear that the direction and degree of bending would indicate the direction and force of the blast wave as it passed down the tunnel. The bending of a hanger or a bolt requires a large differential between the pressure on one side of the hanger and that on the opposite side. But the thickness of these items is so small, and the blast wave moves so fast, that they are quickly engulfed by the blast wave, causing the pressures on all sides to be essentially equalized.

However, the exploion and burning of the methane produces a strong gas expansion, which rushes down the tunnel passages behind the blast front. This is the "dynamic" pressure that behaves more or less like an intense wind. Unlike the pressure immediately behind the blast front, the load produced by the dynamic pressure is highly directional, with the belt hangers and bolts being loaded only on the "upwind" side. If the dynamic pressure is great enough, it can bend them in the manner observed in the Second Left Mains. And if a relationship can be established between the applied force and the degree of bending deflection, then the bending damage to the hangers and bolts in the Second Left Mains can be used to indicate the dynamic pressure that occurred at their locations. The SDOF analysis described here was performed for that purpose.

SDOF Analysis. To supplement the detailed 3D Finite Element (FE) analyses and to provide tools for further analysis, SDOF models of the belt hanger and rock bolt structures were developed. Since the procedures for both structures are similar, they were treated together and any differences are noted. The hanger resembles a flat plate and the bolt is a simple right circular rod, but both can be treated as a cantilever beam. These structures were exposed to the drag forces generated by Sago event, and their deformations were recorded during the post-event damage survey as forensic evidence. While the hangers are a very uniform structure, their observed deformations yield inconclusive information. The bolts, on the other hand, vary significantly in length, yielding a large range of frequency response samples.

Belt Hangers. By assuming a uniform loading in the simple cantilever beam formulas, a load-resistance curve for the belt hangers can be approximated. The loading is the drag load from the explosion blast wave, and it can be constructed as previously discussed. The SDOF calculation was performed using the simple cantilever beam resistance function, and also using the FE derived load displacement curve (numerically produce resistance function). Both resistance

functions are shown in Figure 106. A comparison of the results of the three calculations is presented in Figure 107 for representative dynamic pressure loading. The deflection is measured at the tip of the belt hanger and is measured on a radial arch, where a displacement of 6.9 inches represents a belt hanger bent flat (180 degrees). As can be seen, there is an acceptable agreement with the first and more simple model, resulting in a conservative estimate of the displacement of the belt hanger.

The SDOF model developed in this analysis represents a useful tool for further analysis of belt hanger response to dynamic pressure loads.

Rock Bolts. Again using the simple cantilever beam formulas for a uniform load, a load-resistance curve for a bolt can be approximated. Since the bolts used in the Sago mine have uniform material and geometric properties, their variable lengths provide a variable frequency "gage". The following analysis is based on the frequency of the fundamental bending mode of the bolt-cantilever. The objective is to construct an estimate of the drag forces required to deform the bolts to the degree observed in the damage survey. Figure 108 shows the reference location of the cross-cuts through the belt hanger entry.

Figure 109 shows the "raw" bolt deformations that were measured in the damage survey (Reference 36), shown as the residual angle from the vertical, and plotted against a locator number that indicates the distance of the bolt location from the explosion source, in a direction away from the seals and toward the working face (see Figure 108). Note that there is an order of magnitude spread in the residual angles of deformations that were observed.

The frequency of the first bending mode for each bolt was calculated from its material properties and its length. The distribution of these frequencies is shown in Figure 110. It can be seen that there is a two orders-of-magnitude spread in the frequencies. To collapse this data into a reasonable and systematic measure of the estimated drag loads, the frequency of our "bolt-gage" must be taken into account. Returning to the cantilever model of the bolt, the plastic moment can be calculated and used with the residual angle of deformation to obtain an estimate of the plastic work absorbed by each bolt. This plastic work is presented in Figure 111. Note that the plastic work value has an average excursion of about six units about the mean curve at any locator point. This plastic work and the ideal cantilever model give an estimate of the ductility experienced by the bolts.

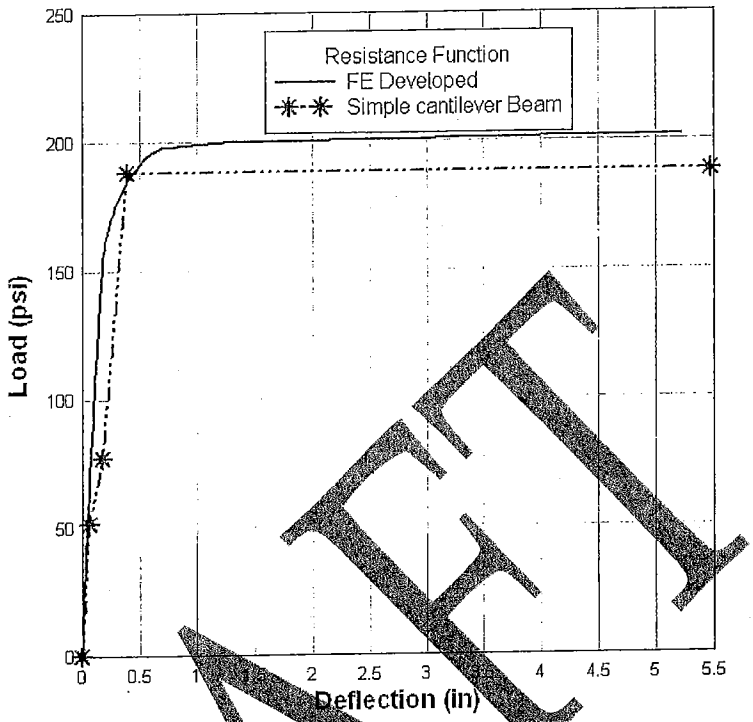

Figure 106. Resisance functions used in SDOF analysis of belt hangers

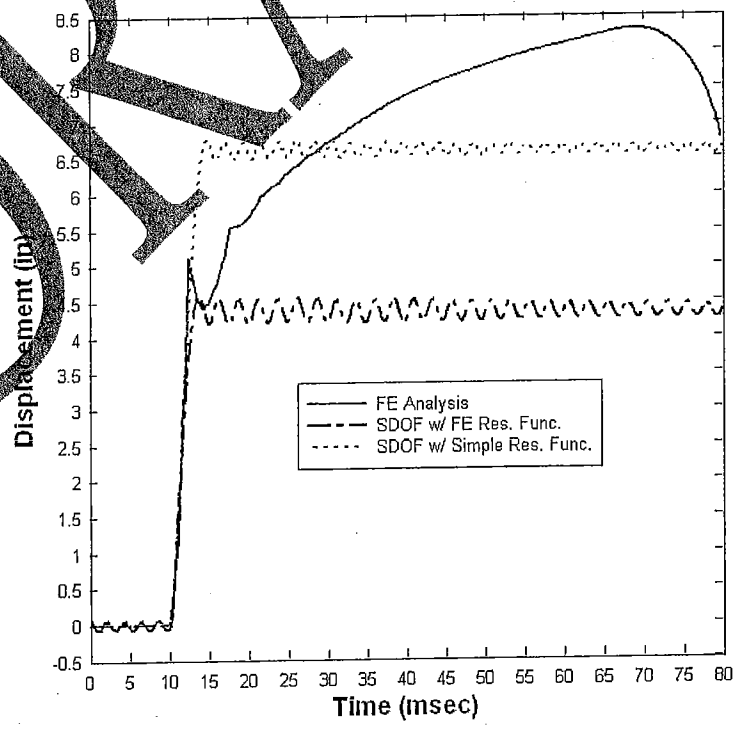

Figure 107. SDOF results compared to 3D FE calculation and SDOF with FE generated resistance function .

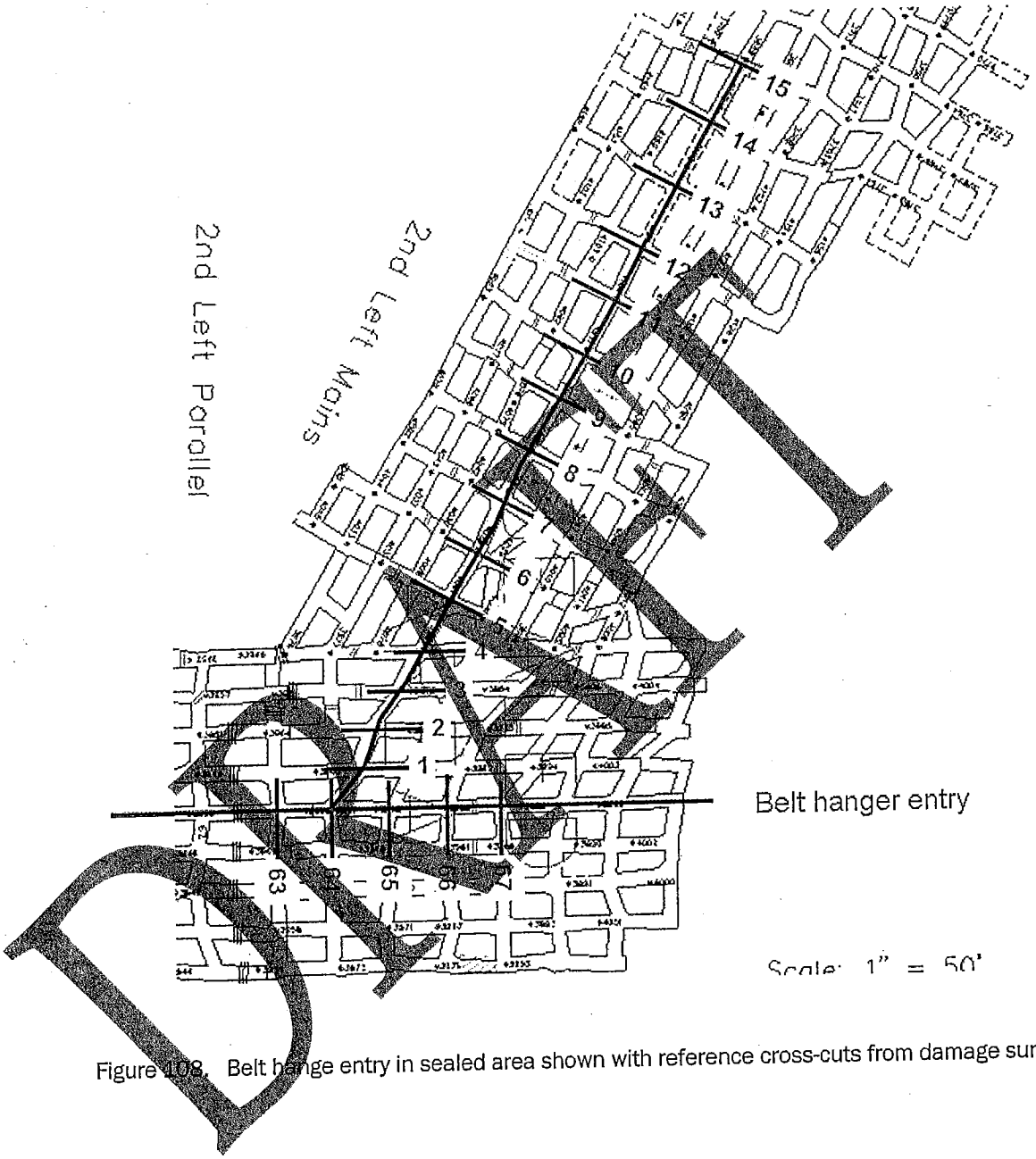

Figure 108. Belt hanger entry in sealed area shown with reference cross-cuts from damage survey.

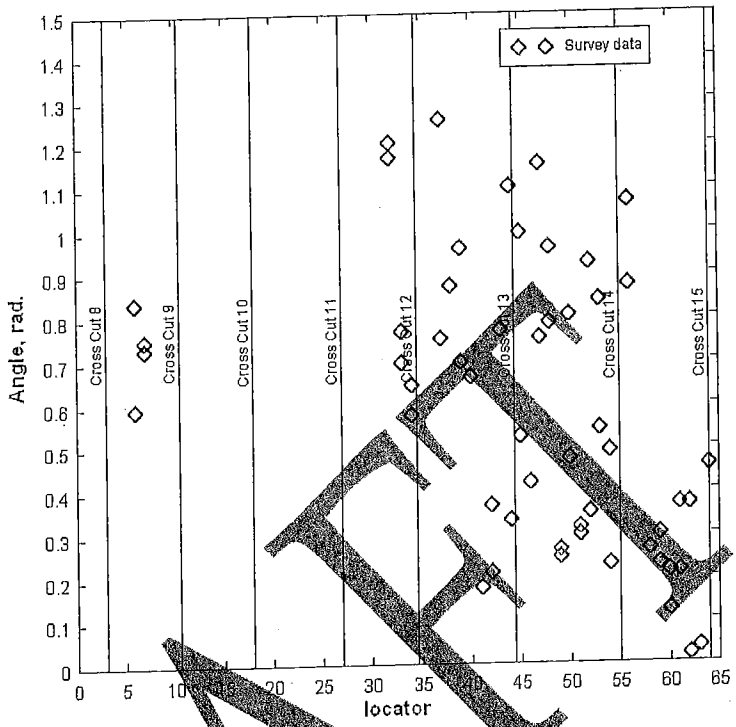

Figure 109. Recorded bolt angle versus distance from ingnition source

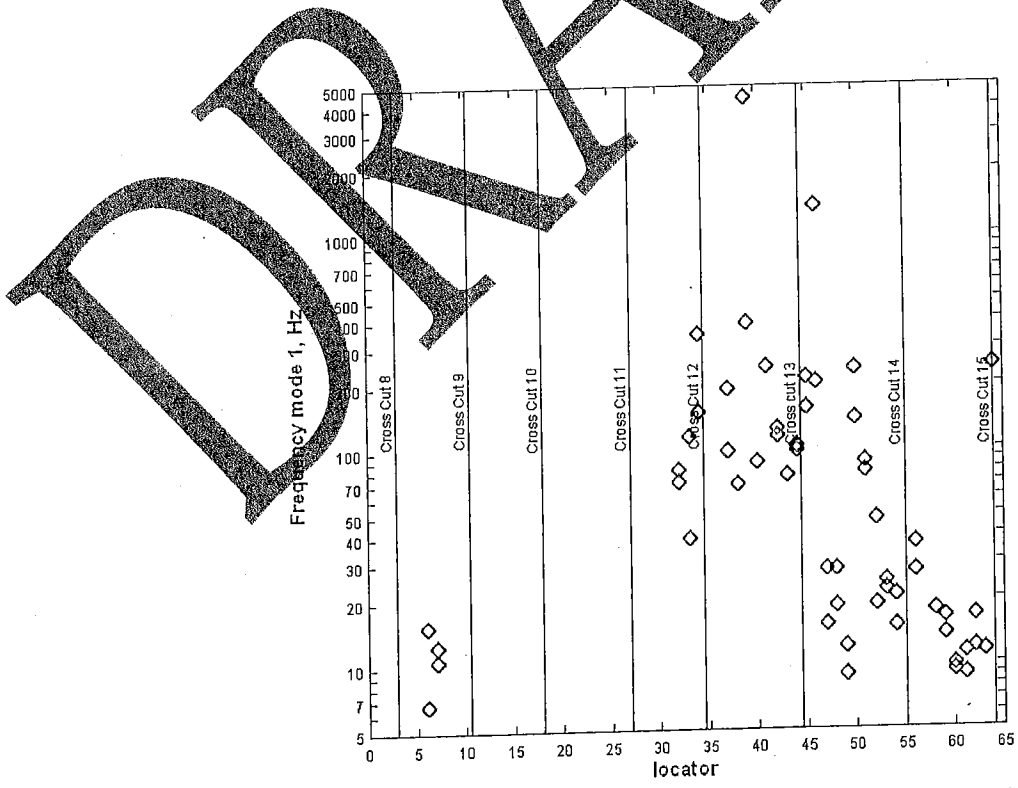

Figure 110. Primary mode frequency of bolts versus bolt distance from explosion source.

To construct an estimate of the loading required to deform the bolts as observed, it is necessary to assume a load-time history shape. Based on the SAGE calculations reported in the previous chapter, a triangular loading with a duration of 20 msec is appropriate. This loading would have an impulse (I) equal to $0.5*Q_o*0.02$. Now if we tacitly assume that the bolts are impulse sensitive, the following expression gives the impulse necessary to develop a specific ductility or plastic response:

$$I^2 = [R_u^2/(2*pi*f)^2]*(2*d-1) \quad (9)$$

Where

R_u = the ultimate resistance at the plastic moment,

f = the frequency of the model (i.e., the cantilever bolt)

d = the ductility of the resulting deformation caused be the impulse,

and I = the loading impulse

Since we know all of the parameters on the right hand side of the equation, if we substitute the formula for the impulse of the triangular load given above, we can solve for the one unknown, Q_o. And since the peak drag load is the dynamic pressure multiplied by a drag coefficient, which in this case is 1.0, we can also estimate the peak overpressure that was necessary to create the drag force. The peak overpressure may be derived by introducing appropriate Rankine-Hugoniot conditions based on mass, energy, and momentum conservation (Reference 37) and ideal air as:

$$P_{so} - C_1*P_{so} - C_2 = 0 \quad (10)$$

$$C_1 = 2/5*Q \quad (11)$$

$$C_2 = 14/5*Q*Po \quad (12)$$

Where P_{so} = Peak Overpressure

Q = Peak Dynamic Pressure

Po = Atmospheric Pressure

However, this overpressure is not necessarily the peak overpressure in the drift.

The results of the above analysis are presented in Figure 112. Note that there is still a spread in the data, but it has been significantly reduced from the frequency plot. Based on the results shown in Figure 112, it can be seen that the calculated dynamic pressures that it took to deform the bolts are lowest between cross cuts 8 and 9. This is consistent with the CFD calculated dynamic pressures in this area being lower than further up the entry where the flow is more in line with the entry. The highest dynamic pressures are seen between entries 12 and 13, beyond which the the pressure drops off slightly.

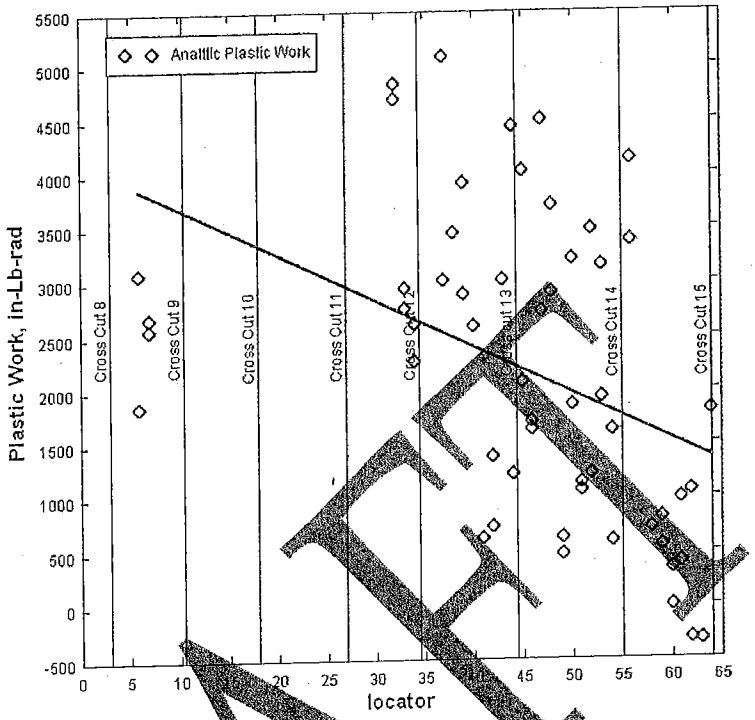

Figure 111. Plastic work required to produce measured bolt displacement angle

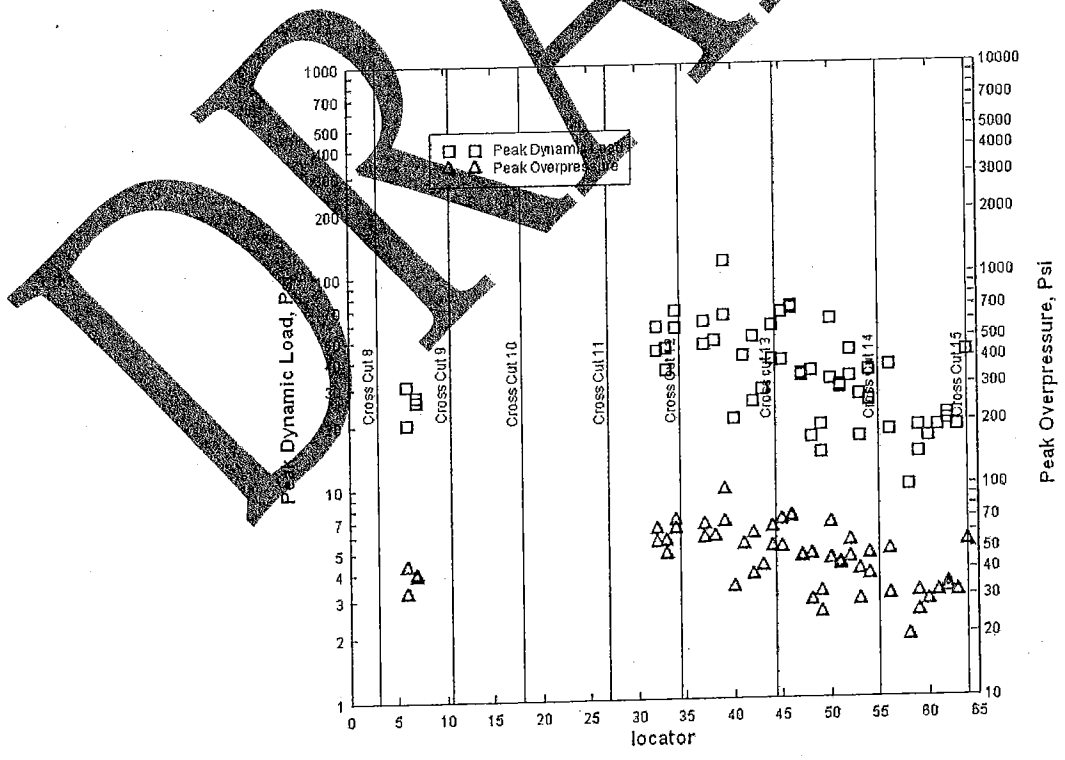

Figure 112. SDOF calculated peak dynamic load required to produce the recorded bending displacement, based on a triangular 20 msec blast pulse.

5 Conclusions

A complicated, fully three-dimensional computational fluid dynamics (CFD) model of the Sago Mine was generated and several possible event scenarios were simulated within that model. The validity of this model was based on good comparisons of data for similar calculations performed of LLEM tests. Structural finite element analysis was performed for several components that are contained within the mine system, including Omega wall seals, conveyor belt hangers, rock bolts, and spider and pie plate support systems. Simplified methods were also developed for several of these components both through analytical methods and using the high fidelity finite element results.

The CFD study provided significant insight into the effects of the methane explosion in Sago Mine. Using the 3-dimensional model and the SAGE code, the study was able to demonstrate the highly complex propagation of the burning methane. It clearly shows the multiple pressure waves interacting from multiple directions to form higher pressure regions as the burning methane front expands in a radial direction through the entries and cross-cuts.

The results of the CDF simulations provide not only the spatial plots of pressure, but complete time histories of the field variables in the calculation at up to 191 locations within the sealed area and outby of the seals. These field variables include overpressure, temperature, particle velocities, and density in the x-, y- and z-directions. These time-history data are analogous to an experiment where measurements were recorded at 191 locations, but at each location all of the field variable "data" are available. While many of these time histories have been analyzed in this study, it is outside of the scope of this study to analyze it all. These time history data will be provided to MSHA for future analysis.

Also available from the CFD simulations are the "snap shots in time" of the complete grid that are used to generate computer movies. Several of these frames are shown in the report to illustrate the development of the explosion. For example, for Run 3 there are 452 frames available at about 4 ms increments. In each of these frames there is the complete information of the physical state, material distribution, and other information of each of over 30 million cells (locations) in the mine model.

The theoretical worst case scenario of the sealed area of the 2nd Left Mains in Sago mine completely filled with methane provides an upper bound of seal loading for

non-failing rigid (Run 1) and failing seals (Run 2). These bounding cases demonstrate the very high loads on perfectly rigid seals (Run 1) compared to seals constructed of foam concrete and having realistic material properties and finite failure times (Run 2). However, as Run 2 shows, if the sealed area had been filled with a 9.5% methane-air mixture and initiated near the location defined by MSHA, the loads on the Sage seals could have ranged from 629 psi on Seal 8 to 156 psi at seal 3. The constant volume pressure calculated within the sealed area from Run1 reached the theoretical maximum value of 120 psi for a 9.5% mixture of methane/air.

Run 3 represented what can be considered a lower bound case in terms of loads on the seals. It is a lower bound because the 8% methane – air mixture volume is located away from the seals, is a less-than optimum concentration of methane, and had to propagate through an inert mixture of 17% methane-air in order to reach the seals. For this case, the loads on the seals ranged from 51 psi at seal 8 to 225 psi at seal 2.

The load on each of the seals are influenced by many factors, including, but not limited to the distance to the initiation source, whether or not a burnable concentration of methane was against the seals, the interactions of the multiple burn fronts and pressure fronts arriving at each seal at different times, and the orientation of the seal with respect to the primary direction of flow. There is no clear indication that the bottom mining contributed to increased loads on the seals. In Runs 1 and 2 the CFD calculations showed the 9.5% methane air mixture transitioned to detonation both inby and outby the ignition point. In Run 3 the 8% methane air mixture did not detonate between the initiation point and the seals. However, as the analysis shows significant pressures can still be developed in the reacting methane air mixture as well as in the pressure wave that propagated through the unburned 17% methane.

Once the seals failed in Runs 2 and 3, the pressures generated dropped quickly as one moved outby of the seals. In the case of Run 2 this is primarily due to the fact that the fuel stopped at the seals. In Run 3 the seals had the effect of reflecting the short duration "shock" pressures back into the sealed area. As the seals failed and were displaced, they are driven by the remaining gas pressures from the expanding burned methane. This pressure build up in the sealed area can only be relieved by expanding outby through the failed seals. The venting generates a significant velocity of air and burned and unburned methane that lasts for a considerable amount of time. Run 3 was stopped at 2233 ms (2.233 seconds) and the gas pressure at each of the seals was still about 30 psi.

Based on the LLEM tests of Sago seals and confirmed by the structural analysis, the Sago seals have the capacity to resist about a 20psi load before they start to fail. The failure mechanism is dominated by shear response around the perimeter of the wall. Since the Sago walls were unreinforced and constructed of individual blocks, once failure occurs there is an abrupt loss of strength and complete failure, as is commonly seen in other articulated wall systems. Failure of the Sago walls occurs at perimeter displacements of about 0.2 inches. For a 90 psi load such as measured on LLEM test 506 the wall has displaced 6 inches in about 20 msec. At this point the wall is broken up and is in free flight. Due to the different strength materials used within the seals (Omega block and BlocBond) it appears that the Omega material fails prior to the higher strength BlocBond material. Very complicated failure conditions exist within these structures due to the nature of both materials and the disparity between their failure behavior.

The analysis of the spider plates and pie pan roof support plates was affected by limitations of the coupled code. The response of the roof support plates is affected by many variables, including the roughness of the tunnel ceiling, the orientation of the plates, the amount of gap between the plate and the roof, and the direction of the pressure wave exerting load on the plates. However, the analysis did provide important insight into the response of these systems. It was determined that dynamic pressure is the predominate load affecting response of the plates. LLEM tests showed that the plates are deformed when subjected to overpressures above about 30 psi. Overpressure exerts a side-on load on the pans, and if there is no or a small gap, this load will force the pan against the roof. If there is a slight gap, displacement from the overpressure, or a tilt to the pan, the dynamic pressure, which acts in the direction of the pressure propagation, can exert a force causing the pan to deflect. As the pan deflects, more area is exposed for loading, resulting in more deflection, necessitating the use of coupled codes to analyze these components under these loading conditions. The calculations showed the response time for a spider plate to be completely bent, using loads measured in LLEM test 506 at station 304 ft. is about 15 msec. This short response time and low overpressure value partially explain the many instances in the mine where roof support plates are bent in multiple directions. As the CFD calculations show, the intersecting entries and cross-cuts produce complex pressure waves with components bouncing around and coming from many directions.

The analysis of the conveyor belt hangers and the bolts extending from the roof provide insight on the loadings required to damage these items. The FE analysis showed that it would take a dynamic pressure of about 150 psi to begin to permanently deform a belt hanger. However, this dynamic pressure must act in a direction normal to the face of the belt hanger. Loads are highest on a belt hanger

when the pressure wave is traveling directly down the conveyor entry. Based on the FE modeling a resistance function was developed for in a SDOF model of the belt hangers. It was shown that the SDOF model provides results comparable with the FEM calculations.

Analysis was performed for the conveyor belt hangers under several loading conditions and included numerically cold forming the hanger. This analysis predicted the behavior of the hangers for those multiple loading conditions, but these analyses have not been validated against experimental data, especially the case of a cold formed hanger subjected to a load that would permanently deform the hanger. Both the FE and SDOF analysis use loads applied on the hanger as a boundary condition. The load acts as a "force follower" in that as the face of the hanger deflects, the force remains normal to that face. In effect as the hanger deflects, the dynamic load continues to act horizontally, so under large deformations, the load can be significantly decreased.

The analysis of the rock bolts supporting belt hangers showed that the bolts can be permanently bent by much lower pressures than the belt hangers attached directly to the roof. The SDOF analysis of the rock bolts showed the peak dynamic pressure required to permanently displace the bolts to their observed level was calculated to be between 10 and 120 psi, depending on the length of the bolt.

6 Recommendations

The conditions under which a combustible concentration of methane-air can transition to a detonation are not well understood. A series of experiments in a simulated or actual mine should be conducted in order to further understand these phenomena. A much larger region of the methane mixture than previously used in LLEM should be used to allow the burn rate to accelerate toward detonation levels. Additional experiments should be conducted with concentrations of methane ranging the explosive limits. These experiments would also provide data for improvement of and validation for further CFD studies, increasing the confidence in the results of future CFD studies.

Seal design tests should be conducted in the same proposed mine in order to validate whether candidate seal designs can withstand the maximum design loads. This work requires a facility where a large volume of methane can be ignited in entries that are hundreds of feet long. The case of the methane cloud against the seals and various ignition locations within the entry should also be investigated.

As a result of this study a very detailed 3-dimensional model of the Sago Mine was created. Only two of many plausible methane distribution scenarios were computed in this study. Others scenarios that investigate various methane – air concentrations and distributions within the sealed area of Sago Mine should be accomplished. Calculations should also investigate the impact of the simplifying assumption used in the CFD calculations. For example, calculations could determine whether heat conduction to the walls of the mine is a significant factor and whether mixing and burning of mixtures, such as the 17% methane of Run 3, is important.

Material Properties should be better characterized for the materials used in seal construction if advanced finite element or other structural calculations are to be used to analyze these structures.

Alternate seal designs should be investigated that incorporate shear reinforcing and materials other than foam concrete. This research should include numerical analysis of candidate designs in order to understand failure modes and focus on the most promising designs, experiments in a simulated mine environment under realistic loading conditions, and material properties testing in order to better develop design specifications.

Validation data are needed for the belt hangers and rock bolt components. This includes experiments where the loads are known and the response has been documented. The process by which the hangers were numerically cold formed also should be confirmed and validated in order to ensure the hangers contain the correct stress/strain pre-event state. Load deflection tests to determine the resistance of the cold formed belt hanger should also be done for comparison to the analytically generated resistance functions.

The effect of bottom mining on the seals was not definitively established. A CFD study should be performed on a single entry with and without bottom mining, for several methane concentrations and explosion volumes. This would demonstrate the whether bottom mining and the "pressure piling" effect is a significant factor in seal loads.

7 References

1. "Focus on Coal Mining: Safety Hazards, Health Hazards, and Mine Rescue"; Bulletin of the National Institute for Occupational Safety and Health; March 2006.

2. Sapko, Weiss, Trackemas, and Stephan; "Designs for Rapid In-Situ Sealing"; 2004; National Institute for Occupational Safety and Health, U.S. Department of Health and Human Services; NIOSH Publication No. ____(?).

3. Interagency Agreement between the U.S. Army Corps of Engineers and the Mine Safety and Health Administration; MSHA Interagency Agreement No. IA-AR600012, signed July 2006.

4. MSHA memo entitled "Information involved in determination of Methane removal from the 2 Left Mains Sealed Area of Sago Mine";

5. Data package supplied by MSHA, ACAD file of Sago Mine sealed area contours, 15 November, 2007.

6. John E. Carpetta, et al, Report of Laboratory Investigation, "Comparison of the Uniaxial Compressive Strength of Burrell "Omega" Blocks from Various Sources Under Wet and Dry Conditions", Roof Control Division, Pittsburgh Safety and Health Technology Center, MSHA Technical Support, July 11, 2006.

7. "Research Evaluation of the Omega 384 and Superblock Low Density Masonry Units Subjected to Out-of-Plane Loading", National Concrete Masonary Association, Research and Development Laboratory, Project No. 99-292, August, 1999.

8. Lake Lynn Experimental Mine Experiment Results for Tests 501-506, supplied by MSHA, 3 November, 2007.

9. Specification of Omega Block walls constructed in Sago Mine, ICG, supplied by MSHA.

10. "The Sago Mine Disaster"; a preliminary report to Governor Joe Manchin III, July 2006; J Davitt McAteer and Associates, Sheperdstown, WV.

11. U.S. Department of the Army TM5-1300, "Design of Structures to Resist the Effects of Accidental Explosions", Washington, D.C., 1990

12. Allwes, Richard, "CH4 Volume and Concentration Computation", Email attachment, 2 February, 2007.

13. Gittings, M., et al., 2005, "SAGE Users Manual," LA-UR-04-2959, Los Alamos National Laboratory.

14. Godunov, S. K., 1959, "A Difference Scheme for Numerical Computation of Discontinuous Solutions of Equations of Fluid Dynamics," Mat. Sb. 47, 271-306.

15. Collela, P., and Woodward, P. R., 1984, "The Numerical Simulation of Two-dimensional Fluid Flow with Strong Shocks," Journal of Computational Physics, vol. 54, pp. 115-173.

16. Lee, E. L. and Tarver, C. M., Phys. Fluids, V 23, No 12, 1980

17. Mader, C. L. and Forest, C., "Two-Dimensional Homogeneous and Heterogeneous Detonation Wave Phenomena," Los Alamos Scientific Laboratory Report LA-6259, 1976.

18. Fried, L. E., et al., Cheetah 3.0 User's Manual Energetic materials Center at Lawrence Livermore National Laboratory , 2001.

19. Fried, L. E., et al., Cheetah 4.0 User's Manual Energetic materials Center at Lawrence Livermore National Laboratory , 2005.

20. M. Cowperthwaite and W. H. Zwisler. *TIGER Computer Program Documentation*, 1973. SRI Publication No. Z106.

21. Lemmon, E. W., et al., REFPROP Reference Fluid Thermodynamics and Transport Properties, NIST Standard Reference Database 23, Version 7.0, Physical and Chemical Properties Division, National Institute of Standards and Technology, 2002.

22. Harlow, F. H. and Amsden, A. A., "Fluid Dynamics: an Introductory Text," Alamos Scientific Laboratory Report LA-4700, 1971.

23. M. Kuznetsov, et al., "DDT in Methane-Air Mixtures," Shock Waves (2002) 12: 215-220.

24. Mader, C. L., *Numerical Modeling of Explosives and Propellants*, 2nd ed., CRC Press, New York, 1997.

25. M. Sapko, et al., "Experimental Mine and Laboratory Dust Explosion Research at NIOSH," *Journal of Loss Prevention in the Process Industries*, 13 (2000) 229-242.

26. Blast Tube Facility Staff, "Information Summary of Blast Patterns in Tunnels and Chambers (Second Edition)," DASA Report 1273, Ballistic Research Laboratories, Aberdeen Proving Ground, MD, 1962.

27. Beam Element Shear Tests, data supplied by MSHA.

28. West Penn Testing, Material Properties Testing Data of Steel components, supplied by MSHA, 11 October 2006

29. LSTC (2006), LS-DYNA User's Manual Version 971, Livermore Software Technology Corporation.

30. Whirley, R.G., and Engelmann, B.E., "DYNA3D - A Nonlinear, Explicit, Three-Dimensional Finite Element Code for Solid and Structural Mechanics - User's Manual," UCRL-MA-107254 Rev. 1, 1993.

31. McKeown, R., Dengel, O., Harris, G., Diekhoff, H-J., et.al., "Development and Evaluation of DYSMAS Hydrocode for Predicting Underwater Explosion Effects, Volume I: Executive Summary", IHTR 2492, 13 February 2004, Naval Surface Warfare Center (NSWC), Indian Head, MD.

32. Department of the Army, TM5-855, "Design and Analysis of Hardened Structures to Conventional Weapons Effects", Washington, D.C., 1998.

33. Broene,W., "Improving Crash Analysis through the Estimation of Residual Strains Brought About by Forming Metal", 7th International LS-DYNA Users Conference, Dearborn, Michigan, May 19-21, 2002.

34. Maker, B., and Zhu, X., Input Parameters for Metal Forming Simulation using LS-DYNA, 2000

35. Thomas R. Slawson, "Wall Response to Airblast Loads: The Wall Analysis Code (WAC)", ARA TR-5208, Applied Research Associates, Inc., November 10, 1995, Applied Research Associates, Inc.

36. Drawings of belt hanger and rock bolt damage survey, supplied by MSHA, 1 Jan, 2007.

37. Crawford, R.E., et al, "The Air Force Manual for Design and Analysis of Hardened Structures", AFWL-TR-74-102, October, 1974